(40)

A Diagnosis of Quasi-Stationary Eddy Transports

by

Christopher R Winkler

B.S., Physics (1995)

Iowa State University

Submitted to the Department of
Earth, Atmospheric, and Planetary Sciences
in partial fulfillment of the requirements for the degree of

Master of Science in Meteorology

at the

Massachusetts Institute of Technology

September 1997

Signature of Author _____

Center for Meteorology and Physical Oceanography
Department of Earth, Atmospheric and Planetary Sciences
1 September 1997

Certified by _____

Peter H. Stone
Professor of Meteorology
Thesis Supervisor

Accepted by _____

Professor Thomas H. Jordan
Department Head

A Diagnosis of Quasi-Stationary Eddy Transports

by

Christopher R Winkler

Submitted to the Department of Earth, Atmospheric and Planetary Sciences
on 1 September 1997, in partial fulfillment of the requirements for the degree of
Master of Science in Meteorology

ABSTRACT

The purpose of this thesis is to clarify the variability and scales of motion of the quasi-stationary eddy transports of sensible heat, momentum, and latent heat from 13 years (1982–1994) of data from the NCEP/NCAR Reanalysis. A climatological record of the transport and it's interannual variation is presented in zonal mean and latitude-longitude maps. The variation of transports in the tropical atmosphere is compared to the El Niño oscillation. Spectral decomposition of the fluxes is performed for wavenumbers 1, 2, and 3 for select pressure levels. In the northern hemisphere in January $[\bar{v}^*\bar{T}^*]$ is composed primarily of wavenumbers 2 and 3 (1 and 2) at 850 hPa (200 hPa) and $[\bar{u}^*\bar{v}^*]$ at 200 hPa is mostly due to wavenumbers 1 and 3. Diagrams of the Eliassen-Palm flux for January, July, and the annual cycle in wavenumbers 1–3 are presented. The July cross-section suggests diabatic heating is responsible for much of the eddy propagation.

Thesis Supervisor: Peter H. Stone
Title: Professor of Meteorology

Acknowledgments

A list of the people who have contributed to the completion of this thesis is too lengthy to delineate in this space, but I would like to thank a few individuals for their generous support.

Helpful discussions with Rick Rosen and Yuanlong Hu clarified aspects of this work, particularly those relating to interactions in the tropics. Yuanlong Hu made the NCEP/NCAR Reanalysis CD-ROM available for use, and Amy Solomon kindly provided access to the ECMWF data. Bill Gutowski at Iowa State nurtured my initial forays into meteorology with sound advice and a helpful hand. I would especially like to thank my advisor, Peter Stone, for his ceaseless encouragement and interest in this work. Working with him over the last year has truly been a pleasure.

The support of my family and friends has been unconditional and essential. My parents, Kirk and Arlene, developed and encouraged my interest in science and have provided love and guidance throughout. My wife Amy has patiently stood by me during my time at MIT. Her faith and love have been a constant source of inspiration, for which I am forever grateful.

This research was supported by the Global Atmospheric Modeling and Analysis Program of the National Aeronautics and Space Administration under Grant NAG5-2490.

CRW

Cambridge, Massachusetts
1 September 1997

Contents

List of Figures

Chapter 1

Introduction

The atmospheric general circulation is a complex non-linear system possessing a range of temporal and spatial scales and no comprehensive theory or numerical model has as of yet successfully explained or simulated all of it. Insight has been achieved, however, by compiling statistics of the atmospheric field variables and examining their large-scale, time-averaged budgets. Analysis of these statistics has shown that the time-averaged zonal asymmetries, usually referred to as the quasi-stationary eddies, are of major importance for the northern hemisphere's energy budget, especially in winter (Oort and Peixoto, 1974; Holopainen, 1970; Oort and Peixoto, 1983).

1.1 Motivation

Detailed knowledge of the generation mechanisms, propagation characteristics, modes of variability, and scales of motion of the quasi-stationary eddies is needed if a theory of these disturbances is to be validated. Numerous investigators have studied the generation (e.g., Charney and Eliassen, 1949; Smagorinsky, 1953; Held,

1983) and propagation (Charney and Drazin, 1961; Plumb, 1985) of the stationary waves. Quasi-stationary eddies are not strictly stationary waves, however. Any semi-permanent, spatially varying feature of the atmosphere will contribute to the quasi-stationary statistics. Moreover, the quasi-stationary eddies are sensitive to the time averaging period; any phenomena whose time variation occurs on time scales longer than the averaging period will appear stationary. These caveats aside, a significant fraction of the quasi-stationary eddy field can be described by wave dynamics.

The large body of work devoted to the wave-like behavior of the quasi-stationary eddies has not been complemented by a similar volume of research on quantifying eddy variability. Much of our understanding of eddy transport and it's variability is due to Oort (1977; Oort and Rasmusson, 1971). In his work the interannual variability of various atmospheric circulation statistics, including the quasi-stationary eddy sensible heat, momentum, and moisture transports, were computed from mostly northern hemisphere radiosonde data. Oort found that during northern winter the maximum quasi-stationary eddy sensible heat flux occured at 50°N with a roughly 30% standard deviation. The wintertime momentum flux of these eddies had extrema of opposite sign at 35°N (poleward) and 65°N (equatorward).

Speth and Frenzen (1982; hereafter SF) performed an independent analysis of the northern hemisphere quasi-stationary meridional transports of sensible heat and momentum, though unlike Oort's work only the geostrophic component of the meridional wind was used. An annual cycle for the zonal and vertical mean transports was derived complete with standard deviations and compared with Oort's analyses. SF used data from 15°N–80°N while Oort considered 10°S–75°N.

Interestingly, significant differences exist between these two studies. In SF the quasi-stationary meridional sensible heat transport was 25% weaker than Oort's value at 50°N in January. Furthermore, the momentum transports in SF were 38% stronger than Oort's at 35°N and 42% weaker at 65°N. Perhaps the most interesting differences occured in the standard deviations of these transports. SF showed mid-latitude quasi-stationary sensible heat flux standard deviations as much as 50% larger (40% weaker) in January (July) than in Oort (1977), while the mid-latitude momentum flux standard deviations in January (July) were 85% (138%) larger in SF than Oort and Rasmusson (1971).

The quasi-stationary eddy transports have been the focus of other research as well. A time series of the quasi-stationary eddy sensible heat flux at 700 hPa from 1949–1978 has been presented (van Loon, 1979) and the geographic variability of this flux analyzed (van Loon and Williams, 1980). Stratospheric analyses of the quasi-stationary sensible heat and momentum transports have also been performed (Geller et al., 1983; Mechoso et al., 1985).

The significant differences between SF and Oort's results suggest the need for further work. In light of the variability in van Loon's (1979) 29 year time series, a more extended examination of the quasi-stationary eddy fluxes is needed than Oort (5 years of data) or SF (10 years) have provided. The advent of satellite technology has presented another source of data unavailable to these authors. The objective analyses used by SF were also hampered by the lack of high-quality data assimilation. Indeed, only within the last 15 years have numerical models produced credible two day forecasts. Investigation with a modern dataset including coverage of the boundary layer and stratosphere would be a good next step.

A complete theory or numerical model of the quasi-stationary eddies must

also account for the dominant scales of motion in these disturbances. Kao and Sagendorf (1968) generated co-spectra of the stationary and non-stationary sensible heat transport in the winter and summer of 1964 at 850, 500, 200, and 100 hPa. This study found that for the stationary eddy sensible heat flux in mid-latitudes zonal wavenumbers 2 and 3 were dominant and poleward at 850 hPa during winter, wavenumber 1 was the major component of the transport at 100 hPa in both seasons, and in summer the 850 hPa transport was equatorward. Speth and Osthaus (1980) found similar results for the quasi-stationary sensible heat flux. These authors further studied the momentum transport and found zonal wave 2 produced equatorward transport in winter while during July waves 4 and higher were more important for the transport. Additional research has shown the importance of zonal waves 1–3 for the quasi-stationary eddies in numerical models (Pratt, 1979) and the real atmosphere (Speth and Kirk, 1981; Randel and Held, 1991; Fraedrich and Böttger, 1978).

As with the questions surrounding the work on quasi-stationary eddy variability, investigations of the scales of motion in these eddies suffer from the lack of a geographically extensive, high resolution time series of the transport. Kao and Sagendorf (1968) analyze only one year's data, and only for the sensible heat flux. Speth and Osthaus (1980) use a longer time series (10 years), but utilize only the geostrophic component of the wind field. Their 850 hPa results may be inaccurate since near the earth's surface friction introduces deviations from geostrophy in the wind field.

The lack of high-quality data has been a major detriment to previous studies. Recently, however, the National Centers for Environmental Prediction (NCEP) and the National Center for Atmospheric Research (NCAR) have released a 13

year global dataset of the atmospheric field variables at 17 vertical levels, including improved resolution in the boundary layer and stratosphere (Kalnay et al., 1996). The first part of this thesis utilizes the NCEP/NCAR dataset to perform a more comprehensive analysis of the variability and scales of motion of the quasi-stationary eddy northward transports of sensible heat, momentum, and latent heat. In the second part of the thesis I will attempt to clarify the dynamical mechanisms responsible for the observed quasi-stationary eddies.

1.2 Notation

In this thesis a quasi-stationary atmospheric statistic, $\bar{A}^*$, is defined as

$$\bar{A}^* = \bar{A} - [\bar{A}]$$

where the overbar refers to a monthly mean, the brackets to a zonal mean, and A is any atmospheric state variable. In this manner the local contributions to the zonal mean northward transport of heat $\bar{v}^*\bar{T}^*$, momentum $\bar{u}^*\bar{v}^*$, and moisture $\bar{v}^*\bar{q}^*$ by quasi-stationary eddies may be determined from a space-time decomposition of the total field.

Vertical integrals of the transports are useful when discussing the atmospheric heat balance. As such, the transport of sensible heat around a latitude circle is computed as

$$2\pi a \cos\phi \int_{p_{sfc}}^{p_{top}} c_p \left[\bar{v}^*\bar{T}^*\right] \frac{dp}{g}$$

where a is the earth's mean radius, ϕ is latitude, c_p is the specific heat capacity of air at constant pressure, and g is gravity. The monthly mean surface pressure, p_{sfc},

is provided in the NCEP/NCAR reanalysis, and p_{top} is taken as 5 hPa. Simple finite differences are used in the integration.

As with the sensible heat transport, the latent heat transport is computed as

$$2\pi a \cos\phi \int_{p_{sfc}}^{p_{top}} L_v \left[\bar{v}^* \bar{q}^*\right] \frac{dp}{g}$$

where q is the specific humidity and L_v is the latent heat of vaporization.

Chapter 2

Data Overview

The length and resolution of the NCEP/NCAR Reanalysis data is such that it may be of use in diagnosing quasi-stationary eddy transports. The reanalysis will also be extended to 40 years of data (1957–1996) in the near future, all produced with a frozen data assimilation scheme. This seeks to insure that improvements in data assimilation techniques do not alter the data output in such a way as to give rise to a spurious climatic change. The data used in this thesis include 13 years of analyses beginning January 1982 and ending December 1994. Because of it's relative newness, I will provide a brief review of the NCEP/NCAR Reanalysis data in this chapter.

2.1 Data Sources

A full range of data sources have been used in compiling the NCEP/NCAR Reanalysis dataset (Kalnay et al., 1996). Rawindsonde data has been gathered from South Africa, Australia, Canada, Argentina, Brazil, the United Kingdom, France and the United States. The Comprehensive Ocean Atmosphere Marine Dataset,

including data from ships, fixed buoys, drifting buoys, pack ice buoys, and near surface ocean stations, has been used as a data source over the oceans. Aircraft and piloted balloon (pibal) data in both hemispheres has been incorporated into the reanalysis, as well as satellite data. The satellite data consist of remote measurements of the atmospheric state variables and estimates of cloud drift wind speed.

The impact of satellite data on the NCEP/NCAR Reanalysis has been examined in some detail (Mo et al., 1995; Kanamitsu et al., 1997). The impact studies have found that the use of satellite data in the reanalysis is important, particularly in the Indian and southeastern Pacific oceans where direct measurements are scarce. Also, analyses using satellite data tend to have increased tropical precipitation near 120°W, weaker tropical easterlies, a weaker Pacific westerly jet, and a warmer southern stratosphere than analyses where satellite data is not used. The satellite bias in the wind data may have lessened over the past 10 years or so as the instrumentation has improved (Kanamitsu et al., 1997). The biases present in daily observations might also be less of a factor in this thesis since monthly means are used throughout.

Due to the volume of information incorporated into this dataset, preprocessing has been performed on the atmospheric data as well as certain boundary fields[1] in order to eliminate errors or inaccuracies in the raw observations. The rawindsonde data is put through a complex quality control process to search for errors, and all data is subject to an optimal interpolation quality control routine.

---

[1]Sea-surface temperatures, snow cover, sea ice, surface albedo, soil wetness, roughness length, and vegetative resistance.

The data is then used as a general circulation model's initial guess field, whereby a global dataset is generated.

2.2 Model Formulation and Output

The model used in the NCEP/NCAR reanalyses is a T62 global spectral model with 28 vertical levels. Notably, 5 of the vertical levels are in the planetary boundary layer and 7 are above 100 hPa. The model's vertical levels extend from 5 hPa above the surface to 3 hPa. Parameterizations of many important processes (e.g., convection, boundary layer physics, and surface hydrology) are incorporated in the model (Kalnay et al., 1996). Furthermore, much of the model has been changed and/or improved since Gleckler et al. (1995) exposed some serious deficiencies. These additions include expanded vertical and horizontal resolution, new cloud and convective parameterizations, and an updated soil model.

Model output is interpolated to 17 vertical levels: 1000, 925, 850, 700, 600, 500, 400, 300, 250, 200, 150, 100, 70, 50, 30, 20, and 10 hPa. The geographic coverage has 144 points zonally and 73 meridionally (2.5° by 2.5° resolution). The wind and temperature data used in this thesis are classified as "A" data by Kalnay et al. (1996), meaning they are less dependent on the model formulation. The specific humidity is classified as "B" data, thus more model dependent. It should be noted, however, that the quadratic transport quantities examined herein will be more sensitive to the model dependencies than the individual fields themselves.

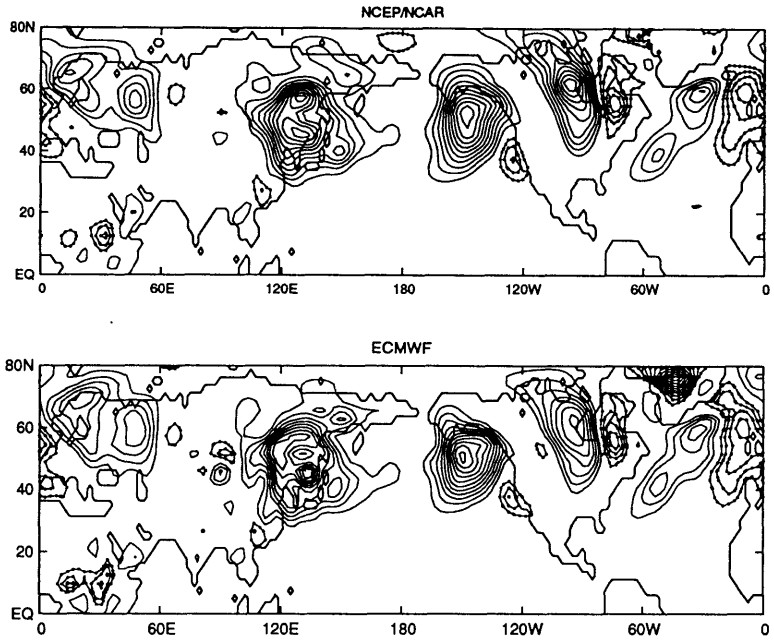

Figure 2.1: Local contribution to $[\bar{v}^*\bar{T}^*]$ at 850 hPa for February of 1989. Top (bottom) figure is from the NCEP/NCAR (ECMWF) data. Contour interval is 10 °C m s^{-1} . Negative contours are dotted.

A comparison of the NCEP/NCAR Reanalysis with an analysis from the European Center for Medium Range Forecasting (ECMWF)[2] has been performed. Plots of the sensible heat transport by quasi-stationary eddies were constructed for the six winter months of 1987-88 and 1988-89 at both 850 hPa and 200 hPa. Very similar results were obtained for all winter months between the analyses. Figure 2.1 presents the local contribution to the quasi-stationary eddy sensible heat flux in the northern hemisphere at 850 hPa for February of 1988. As can be seen in the figure the qualitative and quantitative agreement is quite good. The main dif-

[2]The ECMWF data is computed from uninitialized global analyses from the ECMWF WCRP/TOGA model with horizontal resolution T106 at 15 pressure levels and made available by NCAR. For further details consult Trenberth (1992).

ferences are over Greenland and the Tibetan plateau where the ECMWF analyses include heat transports for isobars lying below the surface and the NCEP/NCAR plot does not.

Furthermore, plots of $[\bar{v}^*\bar{T}^*]$ and $[\bar{u}^*\bar{v}^*]$ averaged over the three Januarys from 1987–1989 from the NCEP/NCAR dataset have been compared with similar fields from ECMWF analyses (Trenberth, 1992). Both analyses show similar agreement in the zonal mean up to roughly 100 hPa. A latitude-longitude map of the local contribution to $[\bar{u}^*\bar{v}^*]$, however, reveals very significant differences between the analyses. The NCEP/NCAR transports are more than double the ECMWF transports over central Europe, Arabia, the north Atlantic, and the eastern Pacific. Also, the southern hemisphere transports are stronger in the NCEP/NCAR Reanalysis. Despite the tremendous differences between the NCEP/NCAR and ECMWF analyses in $\bar{u}^*\bar{v}^*$ for the Januarys of 1987–1989, the 13 year average field in the NCEP/NCAR data bears a close qualitative and quantitative resemblance to the ECMWF atlas (compare Figure A.20 to Figure A38 in Trenberth (1992)). The strong qualitative and quantitative agreement of the NCEP/NCAR Reanalysis and ECMWF analysis suggests that the results of this thesis are robust in the troposphere.

The general agreement of these analyses in the troposphere does not hold in the stratosphere. At 10 hPa, for example, $[\bar{v}^*\bar{T}^*]$ and $[\bar{u}^*\bar{v}^*]$ are 233% and 155% stronger, respectively, in the NCEP/NCAR Reanalysis than in Trenberth (1992). In a study of a 31 level GCM built by the Goddard Institute for Space Studies the quasi-stationary transports showed a pronounced sensitivity to the gravity wave drag parameterization (Winkler, unpublished), perhaps accounting for the marked differences between the NCEP/NCAR and ECMWF analyses there. The results

of this thesis in the stratosphere should thus be regarded as tentative. Further comparison with reliable stratospheric data is warranted, as well as a study of the influence of gravity wave drag parameterizations on general circulation statistics.

Chapter 3

Transport Climatology and Variability

In this chapter I will detail and quantify the quasi-stationary eddy northward transports of sensible heat, momentum, and moisture from the NCEP/NCAR Reanalysis data. Also, the transport variability will be assessed. In this manner I hope to shed light on the nature of the transport and provide an observational climatology with which to validate quasi-stationary eddy theories and models. The vertical transports, while not presented in detail, were investigated and found to be of the same order of magnitude as those presented by Oort (1983). The weak quasi-stationary vertical fluxes thus suggest that the majority of the vertical eddy transport deduced by Hantel (1976) is due to transient disturbances.

3.1 Northward Transport of Sensible Heat

The northward transport of sensible heat by quasi-stationary eddies has long been viewed as an important component of the northern hemisphere winter circulation (e.g., Lau, 1979). Stratospheric analyses have also pointed to the importance of

this flux in the middle atmosphere. A coherent picture of the quasi-stationary eddy sensible heat flux has not arisen, however, and would represent a significant insight into the real atmosphere, as well as the possible shortcomings of today's general circulation models.

In Figure A.1[1] the annual cycle in the total sensible heat transport by quasi-stationary eddies is presented. Northern mid- and high-latitudes show considerable transport from November to March, as also documented by Oort (1983) and SF, weak poleward transport in April and October, and virtually no flux from May to September. Conversely, southern latitudes show little sensible heat transport in all months. A minimum in the sensible heat transport in the northern tropics exhibits an annual cycle that follows the position of the inter-tropical convergence zone (ITCZ). Furthermore, the interannual variability of the quasi-stationary eddy sensible heat transport is significant in northern mid-latitudes during winter (approaching 1 PW in February), and compares well with Oort (1977). In fact, the quasi-stationary eddy sensible heat transport is comparable in magnitude to the transient flux in northern mid- to high-latitudes during the winter season (Peixoto and Oort, 1992; Trenberth and Solomon, 1994).

The high degree of stratospheric resolution in the NCEP/NCAR data allows a comparison of the relative contributions of tropospheric and stratospheric motions to the heat transport. At 50°N the stratosphere accounts for roughly one-fifth of the entire quasi-stationary transport, while at 60°N the ratio increases to one-third. Inadequate stratospheric resolution may thus explain why the mean transport in January of Figure A.1 is 1 PW greater than that computed by SF and

[1]All figures for this chapter are presented in Appendix A.

0.75 PW greater than in Oort and Peixoto (1983). A very rough estimate of the quasi-stationary transport[2] from the ECMWF analysis (Trenberth and Solomon, 1994) gives about a 0.5 PW difference with Figure A.1. The vastly stronger stratospheric transports in the NCEP/NCAR Reanalysis outlined in Chapter 2 are the most likely cause of this difference. Climate models have typically overestimated the atmospheric energy transport (Gleckler et al., 1995). If the NCEP/NCAR transports in the stratosphere are real, and if the climate models have similar magnitude stratospheric transports, the models may be less inaccurate than previously thought.

Zonal mean cross-sections of the sensible heat transport reveal much stronger stratospheric wintertime fluxes than found by Geller et al. (1983) for the northern hemisphere in December and February (Figure A.2), consistent with the differences with Oort's work outlined above. Also, the tropospheric transports of SF are weaker than in the NCEP/NCAR data near 50°N for December through February, especially at 850 hPa. As mentioned previously, the use of the geostrophic wind rather than the full field may explain this discrepancy, though the inadequate resolution and data assimilation of that study are also potential sources for error. Oort (1983) compares more favorably with Figure A.2, for his wintertime maxima at 850 and 200 hPa are only about 4 °C m s^{-1} different than presented here. The southern hemisphere sensible heat transport occurs predominantly in the stratosphere from August to October, and a brief mid-winter lull is evident at 10 hPa in July, a feature absent in other studies (Mechoso et al., 1985).

The standard deviations of the zonal mean tropospheric transport (Fig-

[2]Calculated from 1000–10 hPa, not just in the stratosphere.

ure A.3) reveal that the northern hemisphere wintertime maxima at 850 and 200 hPa typically vary by up to 40%. During January and February the upper tropospheric variations can be greater, approaching two-thirds the zonal mean value. Both SF and Oort (1977) found a lower tropospheric maximum standard deviation in January of 4–6 °C m s^{-1} north of 55°N, in good agreement with Figure A.3. Also, Oort (1977) found a strong variation at 50 hPa in high northern latitudes during winter, and SF computed an upper tropospheric maximum of 4–6 °C m s^{-1} between 60°N–80°N, both of which are evident in Figure A.3.

The southern hemisphere shows little interannual variability, except in the upper troposphere and lower stratosphere during September and August when the transport is strongest. In the stratosphere, however, the deviations are much larger (Figure A.4), though still 40–50% of the transport's magnitude, and active from August to November. The northern hemisphere stratosphere also shows significant interannual variations, consistent with Geller et al. (1984).

The zonal mean transports discussed above are useful tools for determining the atmospheric levels that contribute to the total northward transport of heat by quasi-stationary eddies, and by extension some of the processes that may be at work. For example, the large hemispheric asymmetries in the tropospheric transports point to the role of the land-sea contrast in sustaining this flux. The zonal mean view does not, however, reveal the geographic areas over which the flux occurs. Latitude-longitude maps of the transport do provide such information and are another means by which to quantify and clarify the eddy transport.

3.1.1 Northern Hemisphere

In Figures A.5–A.7 latitude-longitude maps of the sensible heat transport are presented for 850 hPa. These maps point to four main regions that contribute to the zonal mean quasi-stationary heat transport during winter: east Asia, the Gulf of Alaska, northern Canada, and the north Atlantic. The east Asia maximum has the largest heat transport by far, with almost double the flux of the other regions from December to February. Moreover, the east Asia center has a significant transport from November to March. Clearly this is the principal region of heat transport in the lower troposphere during winter and is most likely associated with the airflow around and over the Tibetan plateau, though Figures A.5–A.7 cannot prove this assertion. During the spring and summer months an intense region of equatorward transport develops over the Arabian peninsula because of strong southward flow out of the region and into the monsoonal circulation over India. Also, a small region of poleward transport exists over continental North America during the summer months, a consequence of the strong boundary layer flow that penetrates off the Gulf of Mexico at this time.

The standard deviation of the 850 hPa maps are shown in Figures A.8–A.10. During winter the east Asia region, despite being double the strength of the other prominent regions, is not the locale of strongest variability, as was also found by van Loon and Williams (1980). The lack of interannual variability in this feature in the atmosphere presents a strong challenge to any theory or model of the quasi-stationary eddies. The largest deviations instead occur in the north Atlantic and Gulf of Alaska with values ranging from 30–40 °C m s^{-1}. The north Atlantic, however, shows strong standard deviations for longer periods of time than does the Gulf of Alaska region. Furthermore, the standard deviations in the Atlantic

extend well into western Europe and Scandinavia. During the summer months the largest standard deviations are located near the Indian subcontinent and over the North American plains, though the Gulf of Alaska still shows some interannual variation.

The east Asia maximum, presumably associated with orographic forcing from the Tibetan plateau, is thus the dominant contributor to the northern hemisphere transport of sensible heat by quasi-stationary eddies. This region is not, however, the prime contributor to the interannual variability of the flux. The north Atlantic sensible heat flux center is located at the tail end of the Atlantic storm track, a region of strong diabatic heating and transient wave activity. Indeed, the diabatic heating associated with the storm track may be the major forcing of the quasi-stationary eddies in this region (Yang and Gutowski, 1994) though the relationship between the storm tracks and quasi-stationary eddies is still an open question (Branstator 1995; Whitaker and Dole, 1995). A study of the relative importance of thermal and orographic forcing for the quasi-stationary eddies could be performed by relating monthly and yearly changes in the low-level zonal wind and diabatic heating fields to the various transports. Such an in-depth look at the forcing mechanisms is beyond the scope of this thesis, however.

The 200 hPa sensible heat flux maximum also shows an interesting distribution (Figures A.11–A.13). The northern winter mid- to high-latitudes have extrema over central Asia, the extreme north Pacific, western Europe, and northern Canada. The extremum in Canada exhibits equatorward transport at 200 hPa, in contrast to the poleward transport at 850 hPa. The central Asian center is due to a westward tilt with height of the 850 hPa east Asian center, while that over the north Pacific is related to the low-level maximum in the Gulf of Alaska.

During summer a pattern of northward and southward heat fluxes is evident over southern Asia, with the most pronounced flux near Greece. The interannual standard deviations (Figures A.14–A.16) of the sensible heat flux at 200 hPa show several mid-latitude centers, though none particularly stands out. In February a large standard deviation exists near the Bering strait, though on closer inspection much of this variability is due to one abnormally strong year.

3.1.2 Southern Hemisphere

Despite the weak total transport in the southern hemisphere shown in Figure A.1, the zonal mean cross-sections revealed a noticeable stratospheric transport of sensible heat. Latitude-longitude maps of the sensible heat transport at 70 hPa are presented in Figure A.17 for August to November. In these months the sensible heat transport by quasi-stationary eddies occurs most prominently south of Tierra del Fuego and south of Australia on the Antarctic continent. The Antarctic flux center is stronger than that off Tierra del Fuego, and both centers show comparable variability (Figure A.18). In October and November a small region of positive flux does occur between the two main centers.

The discrepancies between the NCEP/NCAR Reanalysis and ECMWF WCRP/TOGA climatology imply that the southern hemisphere transports might be in error. Also, at high southern latitudes the state of the atmosphere is observed almost entirely by satellites, so that the biases outlined in Chapter 2 should be taken into consideration. Nonetheless, other investigators (e.g., Quintanar et al., 1985) have found similar zonal mean transports in the southern hemisphere, lending credence to these results.

3.2 Northward Transport of Westerly Momentum

Previous studies of the northward transport of westerly momentum have shown that the quasi-stationary eddies are an important contributor to the atmosphere's momentum budget, especially in northern mid-latitudes during winter (Oort, 1983; Starr et al., 1970), thus providing a source for interesting comparison with the NCEP/NCAR Reanalyses.

The annual cycle in the zonal and vertical mean quasi-stationary westerly momentum transport is presented in Figure A.19, and several interesting features are worth mentioning. First, the westerly momentum transport by the quasi-stationary eddies exhibits a pronounced annual cycle in the northern hemisphere and almost no cycle in the southern hemisphere. The northern hemisphere transport is most active from October to March with fluxes in excess of 5 $m^2\ s^{-2}$ in mid-latitudes. From April to September the transport of momentum in the northern hemisphere is weak but typically poleward at mid-latitudes. Also, high northern latitudes show equatorward transport from October to May with the strongest and most variable transport occuring in December and January. The southern hemisphere transport of westerly momentum is extremely weak, generally poleward, and most variable during winter.

The northern hemisphere wintertime (December, January, February) transport is decidedly stronger in the NCEP/NCAR Reanalyses than in Oort and Peixoto (1983) and Oort (1977), who found a poleward transport by quasi-stationary eddies (there defined as a seasonal mean) of less than 10 $m^2\ s^{-2}$. SF, on the other hand, found a wintertime maximum in the momentum transport of

17 $m^2\ s^{-2}$ at 40°N in December, a dip in the January transport to 11 $m^2\ s^{-2}$, and an increase in February to 14 $m^2\ s^{-2}$ though moved to 45°N. SF's cycle for the northern hemisphere momentum transport is not evident in Figure A.19, but the standard deviation in the December transport does not rule out the possibility of values as large as SF. The equatorward polar flux of roughly 5 $m^2\ s^{-2}$ in Figure A.19 is consistent with Oort (1983) and smaller than in SF. The relative absence of summertime transport by the eddies is also consistent with both of these studies.

A closer examination of the momentum transport distribution should illuminate the discrepancies between my analysis and those of Oort (1983) and SF, as well as elucidate some of the physical mechanisms responsible for the transport. A natural means of investigating the transport distribution is through the use of zonal mean cross-sections and latitude-longitude maps.

3.2.1 Northern Hemisphere

Figures A.20 and A.21 show zonal mean cross-sections of the northward flux of westerly momentum by quasi-stationary eddies and their interannual standard deviation. The dominant northern winter flux of Figure A.19 is thus seen to arise from a strong center of poleward transport (greater than 50 $m^2\ s^{-2}$ in December and January) centered at 30°N and 200 hPa. Indeed, the annual cycle observed in Figure A.19 seems directly due to the variation in this 30°N cell. To be sure, the stratospheric transport is strong, with values approaching 60 $m^2\ s^{-2}$ from November to February, but contains considerably less mass than in the troposphere. The validity of the stratospheric transports in the NCEP/NCAR Reanalysis has not

been determined, however. Furthermore, high polar latitudes transport momentum equatorward at about 10–15 $m^2\ s^{-2}$ in the troposphere and lower stratosphere during winter.

The interannual standard deviations during the active phase of the momentum transport have maxima at polar latitudes in the troposphere (60°N, 300 hPa) and stratosphere (70°N, 10 hPa). The variations in the strong tropospheric cell at 30°N are significantly weaker than these two regions.

From April to September the northern hemisphere momentum transport is relatively weak, with both polar latitudes and the stratosphere dormant. The strongest transport in the northern hemisphere is again at 30°N, 200 hPa and typically 15 $m^2\ s^{-2}$ in magnitude. Little interannual variation is present in the northern hemisphere zonal mean from April to September.

Several other studies have investigated the northern hemisphere northward transport of westerly momentum by the quasi-stationary eddies. Oort (1983) found a winter maximum of 36 $m^2\ s^{-2}$ at 30°N and 200 hPa, about 20 $m^2\ s^{-2}$ weaker than in Figure A.20. An equatorward transport from the middle troposphere to lower stratosphere was also observed by Oort north of 50°N and is in good agreement with that shown in Figure A.20, despite the small number of radiosonde stations at this latitude in Oort's data. Oort's analysis also produced summertime momentum transport maxima at 30°N, 200 hPa and 10°N, 1000 hPa. The NCEP/NCAR Reanalyses contain both of these summer features, though with larger magnitudes. The use of seasonal means by Oort may explain this difference, since in general a shorter averaging period generates a more prominent quasi-stationary response (Peixoto and Oort, 1974). The stratospheric transports show weaker winter values than other studies (Geller et al. 1983, 1984)

as well as the absence of any tropical transport.

The analyses of SF show quite a few differences with this thesis. The strong poleward transport of momentum at 200 hPa observed in the NCEP/NCAR Reanalyses is 20–40 $m^2\ s^{-2}$ weaker from November to February in SF and located at 40°N. The equatorward transport at polar latitudes in winter is also a bit weaker. In summer the analyses of SF are in closer agreement with this thesis, showing a poleward maxima at 30°N and 200 hPa of 5–10 $m^2\ s^{-2}$. The limitations of SF's dataset outlined in Chapter 1 are perhaps the cause of the differences between these works. Since the NCEP/NCAR Reanalyses cover 1982–1994 and SF used data from 1967–1976, one cannot rule out the possibility that the differences are due to a change in the atmosphere's behavior. The similarities with Oort's work, however, do suggest that this is not the case.

The interannual variability in Oort (1977) and SF are in fair agreement with the NCEP/NCAR Reanalyses. Both of these studies found that the strongest northern hemisphere variability occurs during winter. Oort (1977) found maximum January variability in excess of 10 $m^2\ s^{-2}$ from 40–65°N at 300 hPa, while SF found a maximum of 15 $m^2\ s^{-2}$ at 50°N. Figure A.21 shows deviations of 15–25 $m^2\ s^{-2}$ during wintertime, though centered further north than in SF. During summer both Oort and SF show weaker and less extensive interannual deviations than in Figure A.21. The analyses of Geller et al. (1984) show a tendency for the stratospheric maximum to be located further south than in Figure A.21 and more variable in December and February than in January, though data from only 4 winters was used in that study.

A geographic map of the momentum flux further helps to elucidate the physical mechanisms producing the northern hemisphere transports. Also, the longitu-

dinal pattern of the transport imposes important constraints on quasi-stationary eddy theory since a successful theory or model should describe more than the zonal mean state.

Figures A.22, A.23, and A.24 present the annual cycle in the northern hemisphere 200 hPa quasi-stationary momentum flux. The principal region of momentum transport is centered over Japan and extends almost 60° in longitude from October to February. This region of flux lies at the exit of the Pacific storm track, and a similar, though weaker, flux region is present at the end of the Atlantic storm track. Also, a region of strong momentum transport exists off the northwest coast of Africa. At high latitudes an equatorward flux is present over northern Canada and Siberia during winter. Smaller scale features include a dipolar structure in the central Pacific and a weak poleward transport in western North America.

Analysis of the asymmetric vector wind[3] reveals that the strength and northward extension of the Pacific jet produce the large momentum flux at 45°N, 140°E. The poleward transports of momentum in the Atlantic are produced by high pressure in the mid-latitude Atlantic. The southern arm of this high is particularly strong. The polar latitude minima in the transport over Canada is due to a pronounced northerly flow out of the Arctic which results from the polar front setting up in a trough position over North America during the winter. Also, the Aleutian low and Siberian high[4] produce the momentum transport maximum in the eastern Pacific and minimum in the northwestern Pacific, respectively.

---

[3]The asymmetric wind is that part of the wind field left after subtraction of the zonal mean.

[4]The Aleutian low and Siberian high are surface features. The circulation at 200 hPa is in the opposite sense.

Oort (1983) has also constructed a map of the northward transport of westerly momentum by the quasi-stationary eddies at 200 hPa. The maximum wintertime transport regions in his analysis are near the exit region of the Pacific storm track and the northwest coast of Africa. A comparison of Figures A.22 and A.24 with Oort's analysis shows his values to be 60–80 $m^2\ s^{-2}$ weaker. Also, the momentum fluxes in the Atlantic storm track are 100 $m^2\ s^{-2}$ weaker in Oort (1983) than in the winter fluxes of Figures A.22 and A.24. This difference might again be due to the difference in averaging period between the two datasets. The wintertime blocking circulation common to the north Atlantic and Pacific atmospheres constitutes an important contributor to the quasi-stationary energy (DaCamara et al., 1992) on monthly time scales and hence would contribute to Figures A.22–A.24. The central Pacific momentum flux dipole and North American poleward flux are common between the two sets, though stronger in the NCEP/NCAR Reanalyses. Also, the equatorward fluxes over northeastern Siberia and northern Canada are present in Oort (1983) and the NCEP/NCAR data, though again with stronger values in the reanalyses. A noticeable difference between the datasets occurs in the cross-equatorial transport of momentum in the central Pacific—the Oort observations lack any such feature. This point will be returned to in section 3.2.3.

The most prominent features of the northern hemisphere summer are similar in position and magnitude between Oort (1983) and the NCEP/NCAR Reanalyses: a poleward transport of momentum by the quasi-stationary eddies above the eastern Mediterranean, an equatorward flux over China, and weak equatorward transport over Arabia. The magnitude of the quasi-stationary momentum flux over the eastern Mediterranean is slightly stronger in Figure A.23 than in Oort's data. The asymmetric wind shows that a strong southwesterly flow at

200 hPa from Africa into southeast Asia is responsible for the Arabian maxima, a consequence of an upper-level anti-cyclonic circulation associated with the Indian monsoon.

The standard deviations of the westerly momentum transport by the quasi-stationary eddies (Figures A.25, A.26, and A.27) suggest that variations in the time-averaged Pacific storm track are primarily responsible for the interannual variability of the wintertime eddies, though the Atlantic sector also shows tremendous interannual variation. Changes in the position of the time-averaged polar front undoubtedly contribute to the variations over the eastern Pacific ocean, North America, and north Atlantic ocean. Central Asia is noticeably devoid of interannual variation, suggesting that the Siberian high is very persistent from year to year. The summertime variations are mostly due to changes in the intensity of the eastern Mediterranean momentum flux.

3.2.2 Southern Hemisphere

The annual cycle of quasi-stationary momentum transport in the southern hemisphere is noticeably different than in the northern hemisphere. Foremost among these differences is the complete lack of the mid-latitude tropospheric transport so important in the northern hemisphere (Figure A.20). During austral winter an equatorward transport of momentum is evident in the southern hemisphere tropics[5], but mid-latitude and polar tropospheric regions are devoid of any significant transport. From September to June a weak region of poleward momentum

[5]See section 3.2.3 for further details.

transport is in evidence at 30°S, 200 hPa. The southern hemisphere jet is predominantly zonal in character (figure not shown, see Oort (1983)) and hence the quasi-stationary eddy momentum flux is not very strong. The relative lack of land in the southern hemisphere, and the concomitant longitudinal contrasts in diabatic heating and orography, are the root of this hemispheric asymmetry in the momentum transport.

The polar stratospheric quasi-stationary momentum transports also exhibit a different annual cycle than their northern hemisphere counterparts. The southern stratospheric momentum transport is a maximum during spring, rather than winter, at about 60°S, 10 hPa. Moreover, the southern stratosphere shows a mid-winter lull in the quasi-stationary momentum transport absent in previous work (Mechoso et al., 1985). A mid-winter minima in the amplitude of planetary waves in the southern stratosphere is present in observations (Mechoso et al., 1985), however, and may be due to the linear nature of these waves (Plumb, 1989). This point will be returned to in Chapter 5.

Oort's (1983) analysis does not reveal the weak 30°S momentum transport of Figure A.20. Furthermore, his latitude-longitude map of the momentum flux reveals almost no transport whatsoever south of 30°S at 200 hPa. Likewise, the NCEP/NCAR data show minimal transport at 200 hPa in the southern hemisphere mid- to high-latitudes.

3.2.3 Tropics

The tropical atmosphere shows an interesting annual cycle in the zonal mean cross-sections of Figures A.20 and A.21. During northern winter a strong center of

equatorward transport of westerly momentum is present just north of the equator at 150 hPa. This flux is robust (notice the weak interannual standard deviations) and unexplained (R. Rosen, personal communication). Previous studies (Starr et al., 1970; Rosen et al., 1985) have also observed this feature of the tropical atmosphere. During northern summer the tropical, quasi-stationary transport of momentum is still equatorward, but now shifted to approximately 10°S. This flux is very strong in August with minor interannual variation relative to that of the northern hemisphere. The near surface atmosphere also shows a poleward momentum transport at 10°N during summer.

Latitude-longitude maps of the tropical momentum transport at 150 hPa are presented in Figures A.28, A.29, and A.30. The transport of momentum toward the south during northern winter is primarily achieved over southeast Asia and the central Pacific with roughly equal magnitude. In fact, the central Pacific yields a significant cross-equatorial transport of momentum. Also during northern winter, the quasi-stationary momentum transports over the equatorial Atlantic are southward at about half the intensity of the other two regions. By May these cells are absent from the tropical atmosphere and an intense northward transport of momentum begins developing over the Indian Ocean. Also during summer, a small region of southward transport is observed over northeast Africa.

The latitude-longitude maps of Oort (1983) at 200 hPa are quite different than those presented here. During northern winter the momentum transports by quasi-stationary eddies over the equatorial Pacific and Atlantic are completely absent in Oort's data, and the southeast Asia region transports are present but 80 $m^2\ s^{-2}$ weaker than the NCEP/NCAR winter fields. During summer the transports of momentum over the Indian Ocean and Africa are 50–80% weaker in Oort's

data. These significant differences between the analyses might again be due to the lack of radiosonde stations in this part of the globe. Also, the vertical resolution in the NCEP/NCAR Reanalysis is much greater than that of the radiosonde data because of the use of a numerical model.

The strong cross-equatorial transport of momentum by the quasi-stationary eddies during northern winter is due to a tendency for the tropical winds at 150 hPa to be weakly westward or even eastward in association with the basin-scale, three-dimensional Walker circulation. The southward momentum transport over southeast Asia, however, is due to the presence of southeasterly anomalous winds wrapping around a high in the eastern Pacific. In the equatorial Atlantic, subtropical lows off the African and Brazilian coast are responsible for the pattern of momentum flux. During summer the Indian monsoonal circulation produces strong momentum transports over the Indian Ocean. The low level easterly wind pushes onshore at this time to feed the monsoonal rains (Findlater, 1969), and is also responsible for the lower tropospheric, quasi-stationary momentum transport seen in Figure A.20. The strong rising motion over the Indian surface necessitates a divergent flow aloft, which in turn produces a northward transport of momentum as the northeasterlies push over the Indian Ocean. As the tropical easterly jet affiliated with this anti-cyclone impinges on the mountain ranges prevalent in east Africa, the winds turn meridionally. Consequently, in northeast Africa westerly momentum is transported northward while in southeast Africa westerly momentum is transported southward. The tropical easterly jet has also been shown to vary interannually in conjunction with the quasi-stationary eddies (Chen and Yen, 1993).

The interannual standard deviations of the northward transport of momen-

tum by quasi-stationary eddies in the tropics do not provide much insight to the variation of the quasi-stationary momentum fluxes, other than suggesting that the variations are greater during northern winter than summer (Figures A.45–A.47). The primary interannual variation of the tropical atmosphere is the El Niño/Southern Oscillation (ENSO), having an average period of 2 to 7 years and typified by above average sea-surface temperatures in the central Pacific. Since the primary region of cross-equatorial transport is located in the so-called Niño 3 region, it is not unreasonable to ask how the quasi-stationary momentum transport varies with ENSO. Indeed, the largest ENSO event on record significantly influenced the atmospheric angular momentum (Rosen et al., 1984).

Rosen et al. (1984) have shown for the 1982-83 ENSO that the tropical atmospheric angular momentum was at a minimum, while northern subtropics were at a maximum. During the strong ENSO winters of 1982-83 and 1991-92, as defined by the Southern Oscillation Index of the NCEP Climate Prediction Center, the eastern Pacific quasi-stationary cross-equatorial transport at 150 hPa is weaker than usual and shifted about 15° eastward (Figure A.31). This cross-equatorial transport is strongest during the La Niña winter of 1988-89 and is shifted 30° west. Furthermore, there is a weak center of southward momentum transport by the quasi-stationary eddies near the dateline in the 1982–83, 1986–87, and 1991–92 ENSO events.

The 1982-83 maximum in atmospheric angular momentum observed by Rosen et al. (1984) in the northern subtropics is not similarly observed in the quasi-stationary eddy northward transport of momentum (Figure A.32). The strong momentum transports in the winter of 1988–89 occur during a La Niña episode, but no definite conclusion can be reached. This result suggests transient and

mean fluxes are responsible for the subtropical atmospheric angular momentum maximum.

The dominant interannual variation of the equatorial quasi-stationary momentum flux is a weakening and eastward shift of the central Pacific cross-equatorial transports during ENSO and a strengthening and westward shift during La Niña. ENSO is associated with anomalously high surface pressure in the western Pacific, and anomalously low surface pressure in the eastern Pacific. The shift in atmospheric mass to the west Pacific during ENSO corresponds to a weakening of the upper tropospheric eastern Pacific cyclone typically present during northern winter. The weak upper-level winds in the eastern Pacific thus generate substantially less momentum transport. During La Niña the converse is true.

3.3 Northward Transport of Latent Heat

The northward transport of latent heat by the quasi-stationary eddies is shown in Figure A.33. The latent heat transport by quasi-stationary eddies exceeds the sensible heat transport in summer and is roughly 25% of the sensible heat flux in winter (Figure A.1). Northern mid-latitudes transport significant amounts of latent heat only during northern winter, while southern mid- and high-latitudes are dormant year-round. Other features of the transport include a 2 PW latent heat flux during June and July in the northern subtropics, a minima in the transport from 5°–10°N with an annual cycle that follows the ITCZ, and a poleward latent heat transport near 30°S present in all months and much stronger than in Oort (1983). Moreover, the interannual variations of the latent heat transport are much weaker than in the sensible heat flux. Despite the differences with Oort (1983),

the total transport of water vapor[6] in the NCEP/NCAR Reanalysis is comparable with that produced by the NASA Data Assimilation Office in mid-latitudes (Mo and Higgins, 1996), lending credence to the results of Figure A.33.

Zonal cross-sections of the latent heat transport (Figure A.34) reveal a strong annual cycle in the low-level tropical transport not present in other studies (Oort, 1983). During northern winter the tropical transport is southward with a center at about 10°N, while in summer a strong northward transport is centered at 10°S. In the extratropical atmosphere, the moisture transport is poleward in all months, strongest at 30°N in June and July, and absent above 700 hPa. The southern hemisphere extratropical moisture transport is an extremum between 850 and 925 hPa, while in the northern hemisphere extratropics the extremum is at 925 hPa. The interannual variations of the moisture transport by quasi-stationary eddies are similar in all months with a minor tendency for January, February, and March to have strong 1000 hPa deviations (Figure A.35). The variability in the NCEP/NCAR Reanalyses for this field is greater than that computed by Oort (1977).

3.3.1 Extratropics

Latitude-longitude maps of the quasi-stationary eddy moisture transport in the northern hemisphere are shown in Figures A.36, A.37, and A.38. From November to February the northern hemisphere extratropical transport of moisture by the quasi-stationary eddies is co-located with much of the sensible heat transport (see Figures A.5–A.7). During spring and fall the extratropical moisture transport

[6]Here the total transport refers to the combination of eddy and mean transport.

is negligible, but summer shows very strong transports into the western Pacific associated with the Indian monsoon and into continental North America from a northward flux of moist air off the Gulf of Mexico. Oort (1983) found similarly large moisture fluxes in the western Pacific during summer and in the north Atlantic during winter. The east Pacific and Alaskan cells in the NCEP/NCAR data were not represented in his analyses, however.

The interannual variability of the moisture transport by quasi-stationary eddies (not shown) is about 5 m s^{-1} g kg^{-1} in the north Atlantic and Gulf of Alaska during northern winter. Additionally, the west Pacific and American interior show 5 m s^{-1} g kg^{-1} deviations during summer. As with the sensible heat transport, the wintertime moisture transport in east Asia is less variable than the other active mid-latitude regions.

For the sake of completeness, the quasi-stationary eddy moisture transport for the southern hemisphere is shown in Figures A.39, A.40, and A.41. Little moisture transport exists beyond 30°S other than in the far eastern Pacific and Atlantic oceans near the coasts of South America and Africa, respectively. Oort (1983) also found minor amounts of moisture transport in the extratropical southern hemisphere. These regions will be examined in more detail in the next section, as they seem more a part of tropical structures.

3.3.2 Tropics

The annual cycle in the tropical moisture transport is dominated by the Indian monsoon (Figures A.42–A.44). From May to September the low-level winds push northward from the warm Indian ocean into southeast Asia, bringing very moist

air to the region. Oort's (1983) maps show a different Indian monsoon, with a maximum transport over Arabia rather than southeast Asia. The reason for this difference is unknown. The African interior also shows a persistent northward transport of moisture by the quasi-stationary eddies. Oort (1983) found stronger transport over the northwest African coast, rather than in the interior, though the sparse radiosonde network in continental north Africa (Peixoto and Oort, 1992) suggests the model-dependence of Figures A.42–A.44 in this region. The twin African cells in the interior are weakest in April, but remarkably constant throughout the year. In this region the low-level wind is strongly southward, carrying very dry air from the Sahara desert. The presence of this intense southward flow may be an open question, as several climatic atlases note it's presence (Hastenrath, 1985; Newell et al., 1972) while Oort (1983) does not. The western coast of southern Africa also shows a tendency for southward transport of moisture by the quasi-stationary eddies.

The eastern Pacific shows a strong southward, quasi-stationary transport of moisture from October to April at 850 hPa. Also, near Brazil and Argentina a southward transport of moisture is evident in all months. A more detailed analysis of the hydrological cycle in the NCEP/NCAR data over the Amazon has shown two distinct processes at work (Y. Hu, personal communication). Weak equatorial easterlies flow into South America and rain out much of their moisture, then turn southward as they interact with the Venezuelan plateau and Andes mountains. The winds are then channeled south between the Andes mountains and the eastern Brazil orography. This type of topographically bound low-level jet, or "channel flow", has been documented in numerical models (Paegle, 1989). The poleward transport in the far eastern Pacific, however, results from mid-latitude westerlies

contacting the Andes mountains and turning northward. The tropical air has more moisture than the winds pushing in from mid-latitudes, hence a southward quasi-stationary transport.

The interannual standard deviations of the moisture transport at 850 hPa do not reveal a significant pattern of variation (Figures A.45–A.47). The response of the tropical quasi-stationary moisture transport to ENSO may yield interesting results, however, especially in light of the strong influence seen on the quasi-stationary westerly momentum transport.

Figure A.48 shows a time series of the northward transport of water vapor by quasi-stationary eddies averaged from the equator to 10°S. In the northern winters of 1982–83, 1986–87, and 1991–92, all of which were ENSO years, the westward extension of the quasi-stationary eddy moisture transport did not extend as far into the Pacific as in non-ENSO years. The correlation is not perfect, however, as the beginning of 1988 also shows a weak extension of the moisture flux even though at this time an ENSO was not in effect. No clear ENSO signal is evident in eastern South America, the Atlantic, or the central Pacific. During the 1988–89 La Niña the moisture transport near 90°W is at it's largest value during the 1982–94 period. Such a pattern to the equatorial flux conforms to our understanding of ENSO. The surface wind during ENSO is weak in the eastern Pacific, resulting in a lowering of the thermocline and anomalously warm waters. The weaker surface easterlies thus do not transport moisture as far into the Pacific as in non-ENSO years.

The flux of water vapor by quasi-stationary eddies from 10°S–30°S is shown in Figure A.49. Unlike Figure A.48, no clear ENSO signal is evident. Very strong moisture fluxes are evident near 60°W during the 1991–92 ENSO, but not in the

other ENSO years. The moisture transport in other latitude bands across the Pacific was also investigated, and showed no distinct ENSO signal. This seems to suggest that the ENSO effect on the quasi-stationary transport of moisture is very much a local one, with only the near equatorial transport altered.

Chapter 4

Zonal Scales of the Quasi-Stationary Transports

In the previous chapter numerous characteristics of the quasi-stationary eddy transports were outlined. For example, the quasi-stationary eddy zonal mean sensible heat transports are strong at 850 hPa, 200 hPa, and 10 hPa in the northern hemisphere during winter, the high latitude southern hemisphere contains strong southward fluxes of sensible heat by quasi-stationary eddies in the stratosphere during austral spring, and the northward transports of westerly momentum and latent heat show intense maxima at several different pressure levels. By performing a spectral analysis of the transport, the dynamical mechanisms producing the transport may be clarified. A spectral analysis also provides additional observational evidence with which to validate stationary wave theory or numerical models.

In this chapter I will analyze the dominant zonal scales associated with the transports of sensible heat, momentum, and latent heat by the quasi-stationary eddies. The procedure for examining the zonal spectral components of the transports is due to Hayashi (1982), and involves a Fourier decomposition of the quasi-

stationary field into wavenumber space. In this manner a spectrally decomposed zonal mean quasi-stationary eddy transport is given by

$$[\bar{v}^*\bar{a}^*] = 2\sum_{k=1}^{\infty} V_1(k)A_1(k) + V_2(k)A_2(k) \tag{4.1}$$

for k equal to a positive integer, v the meridional velocity, and $a = T$,u, or q. The coefficients V_1 and A_1 (V_2 and A_2) refer to the real (imaginary) parts of the Fourier analysis of v and a, respectively. Equation 4.1 shows that only the products of the spectral components of similar scale contribute to the zonal mean eddy transport.

4.1 Northward Transport of Sensible Heat

Figures B.1–B.4[1] show the contributions of various wavenumbers to the quasi-stationary eddy sensible heat transport at 850 hPa. The strong 850 hPa sensible heat transport in northern winter by the quasi-stationary eddies arises principally from wavenumbers 2 and 3, both of which transport roughly 6 °C m s^{-1} on average from December to February. Wavenumber 1 is also a contributor to the heat flux in northern winter, while wavenumbers 4 and higher are of minimal importance. The interannual standard deviations of wavenumbers 1–3 are large during northern winter and explain most of the variation in the zonal mean transport. Figure B.2 also suggests that wavenumber 2 transports heat equatorward in some winters.

During northern summer wavenumbers 1 and 2 transport heat equatorward from 15°N–30°N. The magnitude of this transport (about 2–4 °C m s^{-1}) is more than double that found in other studies (Kao and Sagendorf, 1968; Speth

[1]All figures for this chapter are presented in Appendix B.

and Osthaus, 1980). Contrary to wavenumbers 1 and 2, wavenumber 3 transports heat poleward during summertime. Magnitudes of this transport approach 2 °C m s^{-1} near 30°N.

All of these waves are weak in the southern hemisphere except at very high latitudes where the results are less reliable because of a dearth of radiosonde measurements. Also, many of the 850 hPa gridpoints south of 60°S lie below the surface and hence are eliminated from the calculation. Thus not only is the raw data less reliable in southern high latitudes, but the the Fourier analysis is biased by the presence of only a few gridpoints.

The distribution of wave amplitude at 200 hPa (Figures B.5–B.8) is different than that at 850 hPa. The northern hemisphere quasi-stationary sensible heat transport is active for wavenumbers 1–3 from November to March, is a maximum between 50°N and 60°N, and has largest magnitudes for wavenumber 1. Also of interest, wavenumber 2 transports heat equatorward at high latitudes from December to February, a result absent in some analyses of the lower atmosphere (Kao and Sagendorf, 1968; Speth and Osthaus, 1980) and barely resolved in a stratospheric analysis (Geller et al., 1983). The standard deviation of wavenumber 2 in this region is large, however, and the limited time frames of the earlier studies may account for this discrepancy.

The southern hemisphere at 200 hPa contains a large southward heat flux at 60°S from September to November for wavenumber 1. All other wavenumbers do not transport significant amounts of heat at this level in the southern hemisphere. The presence of strong heat transports in austral spring, rather than in winter like the northern hemisphere, are indicative of fundamental differences in the ways quasi-stationary waves are generated in each hemisphere. Furthermore, the

absence of wavenumbers 2 and 3 in the southern hemisphere transports points to a difference in the transmission characteristics of the polar atmospheres.

At 10 hPa the quasi-stationary sensible heat transport is mostly due to wavenumber 1 (Figures B.9–B.11), which achieves a maximum at 70°N from December to February. Wavenumber 1 is also primarily responsible for large heat transports at 70°N in March and November and at 60°S in September and October. Wavenumber 2 is roughly one-third the strength of wavenumber 1 in the northern hemisphere from December to February and even weaker in November and March. Moreover, wavenumber 2 is of minimal importance in the southern hemisphere. Wavenumber 3 does not transport heat significantly at 10 hPa.

The lack of summertime waves, particularly in the upper troposphere and stratosphere, was first explained by Charney and Drazin (1961). The stationary waves depend on weak westerly winds for propagation: the weaker the wind, the shorter the waves that can propagate. Thermal wind balance requires the summertime middle atmospheric winds to be easterly and hence all wave propagation is prohibited. In winter the winds are westerly, thus allowing propagation for sufficiently long waves. The lack of small scale waves at 200 hPa is thus not surprising, as the wind is fairly strong at this level. At great heights only the longest waves can propagate due to the strong winds, so that at 10 hPa wavenumber 1 is dominant.

Figure B.9 also shows an annual cycle for wavenumber 1 in the stratosphere in agreement with many previous studies (e.g., Quintanar and Mechoso, 1995; Geller et al., 1983). Namely, in the northern hemisphere the sensible heat transport is strong from November to March, and in the southern hemisphere from August to October. Wavenumber 2 is also active in the northern hemisphere from November

to March, albeit with much smaller amplitudes than wavenumber 1. The southern hemisphere, however, shows no wavenumber 2 activity in the wintertime sensible heat transport, perhaps because of westerlies so strong that wave transmission is inhibited (Plumb, 1989).

4.2 Northward Transport of Westerly Momentum

The scales of motion responsible for $[\bar{u}^*\bar{v}^*]$ at 200 hPa are presented in Figures B.12–B.15. The strong fluxes of momentum at 30°N during winter are seen to be a consequence of wavenumbers 1 and 3. Wavenumber 1 is sharply peaked at 30°N at this time and has a minimum at 5°N from December to March. Wavenumber 3, on the other hand, transports large amounts of momentum from 20°N to 50°N from November to February. A look at Figures A.22–A.24 shows that the longitudinal pattern of the flux at 30°N–40°N resembles wavenumber 3, suggesting that this wavenumber should be significant. The large wavenumber 1 response is not immediately obvious from inspection, however. Wavenumber 2 reaches a maximum transport at 30°N in October which declines in magnitude throughout the winter. Of particular interest, however, are the high latitude transports, which show a tendency for wavenumber 2 to transport momentum equatorward from October to March. Both the heat and momentum transports by wavenumber 2 are equatorward at this level in these months. Wavenumbers 4–72 generally transport a small fraction of the zonal mean flux toward the pole.

In the southern hemisphere wavenumber 1 produces a considerable equatorward momentum transport at 10°S during winter. The tremendous zonal scale of

the Indian monsoonal circulation, from the east coast of Africa well into the western Pacific, causes this large wavenumber 1 transport. The other waves contribute little to the momentum flux at any southern latitude.

At 10 hPa (Figures B.16–B.18) wavenumber 1 dominates the momentum transport just as it does the heat transport. From November to February wavenumber 1 consistently transports 40 $m^2\ s^{-2}$ of momentum at 60°N. Wavenumber 2 carries about one-quarter the momentum flux of wavenumber 1 during these months, while wavenumber 3 is extremely weak. At 60°S in September and October wavenumber 1 transports larger amounts of momentum than at 60°N during northern winter. Wavenumber 1 is active in the southern hemisphere from May to November, though a minimum in the transport is evident in July. An examination of the zonal mean zonal wind does not reveal stronger July winds than in June or August for the southern hemisphere. The weak wavenumber 1 transport in July is thus not explained by the Charney–Drazin criterion outlined previously.

4.3 Northward Transport of Latent Heat

The dominant zonal scales of the latent heat transport show a distinctive annual cycle at 925 hPa in both hemispheres (Figures B.19–B.22) with the largest transports of moisture occuring during northern summer near 30°N. This strong flux of moisture is due to the Indian summer monsoon, as discussed previously, which elicits a response in wavenumbers 1 and 2 approaching 4 $m\ s^{-1}\ g\ kg^{-1}$ in June and July. Wavenumber 3 transports are fairly weak at this time, though generally poleward. The smaller scale waves also make a significant contribution to

the moisture flux in northern low-latitudes, as well as a large (2–3 m s^{-1} g kg^{-1}) equatorward transport at 10°S. This large transport in the southern hemisphere does result in a cross-equatorial flux that can feed the monsoon. Also of interest, the interannual standard deviations in the northern hemisphere during summer are quite small relative to other months, suggesting a very similar monsoonal circulation each year.

During northern winter the quasi-stationary eddies transport moisture poleward in both hemispheres. In the northern hemisphere wavenumber 1 produces a 1–2 m s^{-1} g kg^{-1} transport from 10°N to 40°N while wavenumber 3 contributes about 1 m s^{-1} g kg^{-1} at 40°N. The other waves generate even less of the flux. In the southern hemisphere wavenumber 3 transports 1.5 m s^{-1} g kg^{-1} southward at 25°S and wavenumbers 4 and higher transport 1 m s^{-1} g kg^{-1} southward at 30°S. The smaller wavenumbers (3 and higher) are the dominant contributors to the flux in the southern hemisphere—wavenumbers 1 and 2 are virtually non-existent in the moisture transport there.

The zonal waves contributing to the latent heat transport run to all scales, unlike the sensible heat transport which saw large scales producing much of the flux. Water vapor in the atmosphere is more strongly linked to small scale (and micro-scale) processes than is the temperature, and hence the 925 hPa transport has a marked contribution from wavenumbers 4–72. Also, the rapid decrease of water vapor with height keeps the largest moisture transports near the earth's surface where friction helps inhibit large scale transports.

Chapter 5

Eliassen-Palm Diagrams

The quasi-stationary eddy zonal mean transports outlined in the previous chapters also make up portions of the Eliassen-Palm (EP) flux vector, **F**, which is a useful diagnostic for studying the behavior of quasi-stationary waves in the atmosphere (Edmon et al., 1980). In this chapter I will present cross-sections of **F** and it's divergence for the northern and southern hemispheres. These cross-sections provide yet another diagnostic with which to validate numerical models and/or theoretical calculations, and also concisely detail the propagation of quasi-stationary eddies in the latitude-pressure plane.

5.1 Introduction

The EP flux vector is defined under the quasi-geostrophic approximation as

$$\mathbf{F} = \{F_{(\phi)}, F_{(p)}\} = \{-a\cos\phi[\bar{u}^*\bar{v}^*], fa\cos\phi[\bar{v}^*\bar{\theta}^*]/[\bar{\theta}]_p\} \tag{5.1}$$

where a is the Earth's radius, ϕ is latitude, θ is potential temperature, and $f = 2\Omega\sin\phi$ with Ω the Earth's angular velocity. The subscript p refers to a partial derivative with respect to pressure.

A plot of $\mathbf{F}$ in a latitude-pressure plane reveals the direction and magnitude of quasi-stationary eddy propagation since $\nabla \cdot \mathbf{F}$ appears in a conservation equation for linear conservative waves (Edmon et al., 1980), namely

$$\frac{\partial A}{\partial t} + \nabla \cdot \mathbf{F} = 0 \; . \tag{5.2}$$

In Equation 5.2 A is the wave activity defined under the quasi-geostrophic approximation as

$$A = \frac{a \, [\bar{q}^{*2}]}{2 \, [\bar{q}]_{\phi}} \; . \tag{5.3}$$

In this equation q is the quasi-geostrophic potential vorticity given by

$$q = \frac{1}{f_o} \nabla^2 \Phi + f + \frac{\partial}{\partial p} \left(\frac{f_o}{\sigma} \frac{\partial \Phi}{\partial p} \right) \tag{5.4}$$

where f_o is taken at some reference latitude ϕ_o, Φ is geopotential, and

$$\sigma = \frac{-RT_o}{p} \frac{d \ln \theta_o}{dp} \; . \tag{5.5}$$

In the definition of σ, T_o and θ_o refer to the basic state temperature and potential temperature, respectively, and R is the gas constant.

The divergence of $\mathbf{F}$ is given by

$$\nabla \cdot \mathbf{F} = \frac{1}{a \cos \phi} \frac{\partial}{\partial \phi} F_{(\phi)} \cos \phi + \frac{\partial}{\partial p} F_{(p)} \tag{5.6}$$

and can be shown (e.g., Edmon et al., 1980) to represent the sole eddy forcing of the zonal mean state of u and T. When the divergence of $\mathbf{F}$ is zero, as happens for steady, linear, conservative waves, the effect of the eddies on the zonal mean state is completely cancelled by the effects of meridional motions induced by the eddies. Contouring $\nabla \cdot \mathbf{F}$ in the latitude-pressure plane thus reveals where the eddies are forcing the zonally averaged u and T.

Furthermore, when WKBJ theory is appropriate

$$\mathbf{F} = \mathbf{c}A \tag{5.7}$$

where $\mathbf{c}$ is the meridional projection of the group velocity. Equation 5.7 thus suggests that the vector $\mathbf{F}$ fundamentally represents the direction in which quasi-stationary waves are propagating when WKBJ theory is valid. WKBJ theory also posits that the magnitude and direction of $\mathbf{F}$ is dependent on the value of the refractive index, Q_k[1], given by

$$Q_k = \frac{a[\bar{q}]_\phi}{[\bar{u}]} - \frac{k^2}{\cos^2\phi} - \frac{a^2 f^2}{4N^2H^2} \tag{5.8}$$

where k is the zonal wavenumber, N is the buoyancy frequency, and H is a representative scale height. The dependence of $\mathbf{F}$ on the refractive index is but an extension of the Charney-Drazin criterion to the real atmosphere where vertical and horizontal shears of the zonal wind influence wave propagation. Moreover, the trajectories of $\mathbf{F}$ are curved up the gradient of $\tilde{Q}_k$ defined by (Butchart et al., 1982)

$$\tilde{Q}_k \equiv Q_k / \sin^2\phi \, . \tag{5.9}$$

Ray tracing techniques (Karoly and Hoskins, 1982) and model studies (Matsuno, 1970) have also shown that the waves not only travel up the gradient of $\tilde{Q}_k$, but prefer to travel along ridges in the refractive index.

The plotting conventions used herein are identical to those used by Edmon et al. (1980). To wit, the quantity $\triangle$ represented by

$$\triangle = \frac{\partial}{\partial\phi}\left(2\pi a g^{-1}\cos\phi F_{(\phi)}\right) + \frac{\partial}{\partial p}\left(2\pi a^2 g^{-1}\cos\phi F_{(p)}\right) \tag{5.10}$$

---

[1]More precisely, Q_k is the square of the refractive index. Throughout this thesis, however, it will be referred to as the refractive index.

will be plotted in the latitude-pressure plane. The usefulness of $\triangle$ for plotting purposes arises from the relation

$$\int \nabla \cdot \mathbf{F} dm = \int \triangle \, d\phi \, dp \tag{5.11}$$

which states that $\triangle d\phi \, dp$ is the divergence of $\mathbf{F}$ weighted by the mass element dm of an annular ring $d\phi \, dp$. The corresponding vectors

$$\{\hat{F}_{(\phi)}, \hat{F}_{(p)}\} \equiv 2\pi a^2 g^{-1} \cos\phi \{a^{-1} F_{(\phi)}, F_{(p)}\} \tag{5.12}$$

appearing in Equation 5.10 are thus the proper form of $\mathbf{F}$ in the latitude-pressure plane. The different latitudinal and pressure scales, however, necessitate that these vectors are rescaled by

$$\hat{\mathbf{F}} \rightarrow \{b\hat{F}_{(\phi)}, \hat{F}_{(p)}\} \tag{5.13}$$

where b is a constant value equal to the coordinate units representing 1 radian of latitude divided by the coordinate units representing 1 Pascal of pressure. The vector directions are thus determined uniquely by b, while the vector lengths are determined up to a constant of proportionality. Throughout the thesis reference is made to $\mathbf{F}$ and $\nabla \cdot \mathbf{F}$, rather than to $\hat{\mathbf{F}}$ and $\triangle$, in accordance with common usage in the literature.

Plots of the refractive index are complicated by the presence of a singular point in Q_k when $[\bar{u}] = 0$. In practice then, Q_k will be modified to

$$Q_k = \frac{a[\bar{q}]_\phi}{\left([\bar{u}] - \frac{i\alpha}{ka}\right)} - \frac{k^2}{\cos^2\phi} - \frac{a^2 f^2}{4N^2 H^2} \tag{5.14}$$

where α is a small positive quantity dependent on height in the manner outlined by Holton (1976). Physically, α may be thought of as a coefficient of Newtonian

cooling or Rayleigh friction (Matsuno, 1970). Though simply a mathematical artifice, the use of α removes the singularity and hence makes plots of Q_k easier to read.

5.2 Eddy Propagation in the Northern Hemisphere

The average January and July EP cross-sections from 1982–1994 are presented in Figure C.1.[2] The January picture is very similar to other studies (e.g., Edmon et al. (1980)), with strong upward propagation of quasi-stationary waves near the surface in mid-latitudes, a center of convergence at 400 hPa and 60°N, and equatorward turning of the waves at upper levels. The low-level convergence of the EP flux in the NCEP/NCAR Reanalyses is much stronger than found by Edmon et al. (1980). Caution is warranted, however, in assessing the significance of this difference since the atmospheric boundary layer contains a host of sub-grid scale processes which can only be parameterized by the NCEP/NCAR Reanalysis model, whereas Edmon et al. (1980) used radiosonde data. The sensitivity of the EP fluxes to these parameterizations is unknown. In July the flux is generally weak and upward throughout the mid-latitude troposphere, with downward fluxes occuring below 850 hPa. In contrast, Edmon et al. (1980) found the EP flux to be downward at all mid-latitude levels in July, as well as considerably stronger in magnitude. A region of flux divergence is present in mid-latitudes during July not found in the Edmon et al. (1980) study, though again the EP fluxes may be

[2]All figures for this chapter are presented in Appendix C

very sensitive to the boundary layer physics in the Reanalysis.

The July pattern of the EP flux in Figure C.1 may be due to the effects of condensational heating, particularly by the Indian monsoon. Holopainen (1970) studied the energy budget of the quasi-stationary disturbances and found that diabatic heating was the primary generation mechanism in summer. Since the monsoonal circulation represents the largest source of diabaticity in the northern summer we expect the EP cross-section to capture this feature. Indeed, the equatorward EP fluxes at 30°N, 200 hPa are due to the strong momentum fluxes brought about by the Indian monsoon[3] and the divergent center in the subtropics near 700 hPa could be due to the latent heat release in air rising over the Indian subcontinent. A climatology of the summer season (Newell et al., 1974) shows that a significant amount of latent heat release occurs in the location of the divergent center. An analysis of the condensational heating in the NCEP/NCAR Reanalysis could clarify this point further.

In general, then, the EP fluxes in the NCEP/NCAR Reanalyses depicted in Figure C.1 are stronger than Edmon et al. (1980) for January and weaker for July. Also, the upper tropospheric source of downward propagating, summertime quasi-stationary waves found in that study was not apparent in the NCEP/NCAR data. Rather, the EP flux in summer seems to result primarily from the Indian monsoon. Further study of the EP fluxes can be undertaken by decomposing the flux into the contributions from various wavenumbers to gain some insight into how these individual waves propagate.

Figures C.2–C.4 present the annual cycle of the EP flux and it's divergence

---

[3]See the discussion of section 3.2.2 for futher details.

in the northern hemisphere from 1000 hPa to 50 hPa for wavenumber 1. The wintertime picture is one of generally upward propagation at low levels with maximum amplitude near 45°N. A bifurcation in the flux appears at 300 hPa with one branch propagating upward and poleward while the other branch propagates equatorward into the westerly jet. A flux convergence is concentrated near the surface and at 15°N, 200 hPa.

By April the EP flux is weak in the northern hemisphere mid-troposphere, a pattern that continues throughout the summer. The summertime quasi-stationary eddies generally show a downward propagation in mid-latitudes below 700 hPa from April to September. The divergence and convergence of **F** is heavily concentrated at the earth's surface during summer. The large contribution of wavenumber 1 to the divergent center at 25°N, 700 hPa reinforces the hypothesis that the monsoonal circulation is the root of this feature since the Indian monsoon has a tremendous scale during summer, extending from Africa to the dateline. Also, centers of divergence and convergence are evident in the tropical atmosphere. The quasi-geostrophic approximation fails at low latitudes, however, and hence **F** is not well defined there. As such, no detailed attempt will be made to explain features of the EP flux in the equatorial regions.

Wavenumber 2 has a different EP flux pattern than wavenumber 1 (Figures C.5–C.7). For wavenumber 2 the EP flux in northern winter is largest at 50°N in the lower troposphere and has little amplitude south of 40°N. At upper levels wavenumber 2 primarily turns poleward, in contrast to wavenumber 1. Near the surface an EP flux divergence is present at 60°N, while a center of convergence is located at 45°N. Wavenumbers 1 and 3 do not have these twin surface cells. A region of convergence by wavenumber 2 in winter exists at 25°N and 200 hPa, as

well as a broad region convergence from 40°N–60°N and 600 hPa–200 hPa. From April to September wavenumber 2 is weak in the mid- to upper-troposphere in the northern hemisphere. Low levels are characterized by downward EP fluxes. The divergence of the EP flux is weaker than in wavenumber 1 and the two-celled structure present in winter is absent.

The EP flux vectors for wavenumber 3 (Figures C.8–C.10) in winter are qualitatively similar to those for wavenumber 1: upward propagation at low levels followed by an equatorward turning of the flux near 300 hPa. However, the wavenumber 3 flux is much stronger than wavenumber 1, extends from 35°N–65°N at low levels, and has a much larger surface convergence. Some semblance of a flux convergence from 600 hPa–400 hPa in mid-latitudes is also evident in January and February. In contrast to wavenumbers 1 and 2, wavenumber 3 is weak at all levels during the summer months and exhibits some signs of upward propagation.

In Chapter 4 we saw that wavenumbers 1 and 2 gave the largest contributions to the quasi-stationary eddy sensible heat and momentum fluxes in the stratosphere. As such we expect these waves to give the largest contributions to the stratospheric quasi-stationary EP flux. Figure C.11 presents mean January and July EP cross-sections for wavenumbers 1 and 2 in the stratosphere. The complete dearth of EP flux in July was anticipated from the analysis of Chapter 4 and is presented simply as a verification of the absence of quasi-stationary eddy activity in the summer stratosphere. During the winter, however, quasi-stationary waves are active in the stratosphere, though again the NCEP/NCAR data is of questionable validity above 100 hPa.

The January cross-sections show a strong propagation of EP flux upward

from the troposphere near 50°N. In the stratosphere the flux has a poleward tilt below 30 hPa, and an equatorward tilt above 30 hPa. Both wavenumbers 1 and 2 exhibit this behavior. The January cross-sections also suggest a strong EP flux divergence in the upper atmosphere near 10 hPa. The validity of this feature can be questioned due to uncertainties in the NCEP/NCAR Reanalysis at this level, the numerical differentiation near the data boundaries, and the sensitivity to the gravity wave drag parameterization.

A plot of the refractive index (Figure C.12) helps to explain some features of the EP flux diagrams. A minimum in $\tilde{Q}_k$ exists near 70 hPa at 30°N , and perhaps is responsible for the bifurcation of the waves near the tropopause. Waves that propagate into the region of small $\tilde{Q}_k$ from mid-latitudes would be refracted downward or poleward. Also, the meridional gradient of $\tilde{Q}_k$ for wavenumber 2 appears greater than that for wavenumber 1 near 60°N, which might enhance wave propagation. Of course, $\tilde{Q}_k$ is not perfectly horizontal in the zonal direction and may have a particular longitudinal phase relationship with wavenumber 2 that contributes to the vertical propagation of wavenumber 2 into the stratosphere. Also, above 30 hPa the gradient of $\tilde{Q}_k$ is large and increasing toward the equator, hence the waves tilt southward. The absence of wavenumber 3 in the stratosphere can be explained by the lack of strong gradients in the lower stratospheric $\tilde{Q}_k$ and the evanescence of these waves at high latitudes. In summer the presence of easterlies in the stratosphere makes all waves evanescent there, and no significant ridges in $\tilde{Q}_k$ are available to encourage wave propagation.

5.3 Eddy Propagation in the Southern Hemisphere

The southern hemisphere's seasonal cycle in the EP flux is presented in this section. Wavenumbers 1 and 2 are most active in the southern hemisphere and hence will be the only waves discussed.

Figure C.13 shows the EP cross-sections for January, April, July, and October for wavenumber 1 in the southern hemisphere troposphere. Noticeable differences are evident with the northern hemisphere cross-sections just examined: little mid-latitude upward propagation of wavenumber 1, a strong surface EP flux convergence in polar regions, and an absence of strong waves in the upper troposphere. The surface flux convergence near the pole must be viewed cautiously, as poor data resolution in this region is a problem. In October, when strong sensible heat fluxes are present, the EP flux does show weak upward propagation from 50°S–60°S into the stratosphere.

The wavenumber 2 EP fluxes (Figure C.14) are much smaller than wavenumber 1, showing again how weak quasi-stationary eddies are in the southern hemisphere. A small surface convergence is evident at 65°S in April. Minor upward propagation by wavenumber 2 occurs from 60°S–70°S from austral fall to spring.

The largest southern hemisphere sensible heat fluxes for the quasi-stationary eddies occur during austral spring when the polar vortex is dispersing. Figure C.15 shows that the stratospheric EP fluxes in September (and all of austral spring) indicate upward and equatorward propagation of wavenumber 1 at 60°S. Above 50 hPa the waves acquire a much stronger meridional tilt than at lower levels, especially for quasi-stationary waves equatorward of 60°S. Wavenumber 2, as at

lower levels, is not a significant source of EP flux.

Figure C.16 shows that the observed southern hemisphere EP fluxes correspond well with WKBJ theory. In January and April the lower atmosphere has almost no vertical gradient in $\tilde{Q}_k$ so that any eddies which are generated should propagate into the equatorial zero wind line or converge on the pole. The presence of easterlies in the stratosphere at these times also serves to inhibit the wave propagation. In July, on the other hand, westerlies prevail in the southern stratosphere and hence wave propagation is possible. Interestingly, however, the gradient in $\tilde{Q}_k$ at high latitudes is very weak, so that wave propagation is unlikely. The October picture shows a small tongue of $\tilde{Q}_k$ extending from the troposphere into the high latitude stratosphere, thus serving to channel waves there. Also, the meridional gradients in the refractive index above 100 hPa are stronger near 50°S in October than in July, which further encourages wave propagation.

Plumb (1989) has suggested that the wave-mean flow interaction in this region may be non-linear, with the waves interacting with the mean flow in a manner which encourages further wave propagation. The EP fluxes in the NCEP/NCAR Reanalysis, however, are consistent with a WKBJ interpretation of waves propagating along ridges in $\tilde{Q}_k$, which accordingly suggests that the waves are approximately linear on monthly time scales. In light of the uncertainty in the NCEP/NCAR stratospheric transports, the linearity of these waves should be regarded as tentative until further evidence is documented.

Chapter 6

Conclusion

In this thesis I have examined the quasi-stationary eddy transports in the NCEP/NCAR Reanalysis data. This chapter will summarize the major findings of this thesis and suggest future work.

Chapter 3 presented an overview of the eddy variability in the transports of sensible heat, momentum, and latent heat for the northern and southern hemispheres. The transports were examined in zonal mean and latitude-longitude plots. The sensible heat flux was stronger than in previous observational studies, had maxima at 850, 200, and 10 hPa, and was markedly invariable at 850 hPa near east Asia where the transport is large. The northward transport of momentum near the equator was found to result from the three-dimensional structure of the Walker circulation and had a sensitivity to ENSO. The latent heat transport was found to be significant in both the southern and northern hemispheres, and a degree of correlation with ENSO was evident in southern climes.

Chapter 4 outlined the various scales of motion inherent to the large-scale transports. Wavenumbers 2 and 3 were the largest contributors to the northern hemisphere sensible heat transport in the lower troposphere, while wavenumbers

1 and 2 were largest in the upper troposphere and stratosphere. The southern hemisphere heat transport was dominated by wavenumber 1 during austral spring. The northward transport of momentum by quasi-stationary eddies was achieved primarily by wavenumbers 1 and 3 (2) in the northern (southern) hemisphere. The latent heat transport showed no particular preference to large-scale waves.

In Chapter 5 the influences on quasi-stationary eddy propagation were described. The northern and southern hemisphere eddy propagation was examined through plots of the EP flux and it's divergence for various wavenumbers The northern hemisphere EP sections in July were different than in Edmon et al. (1980) and indicated that condensational heating is a significant generator of quasi-stationary eddies in this month. Also, both the northern and southern hemispheres showed approximately linear waves on monthly time scales.

The findings of this thesis present insights into the quasi-stationary eddy structure and variability. Further work can be performed, however, by undertaking a model study to determine which forcing and basic state mechanisms are contributing to the eddy variability. Also, a comparison of the results of Chapter 4 with output from general circulation models would help to clarify how well those models simulate the quasi-stationary eddies. The transports of heat are very important to the climate, and hence an understanding of the models strenghths and weaknesses in this regard is warranted. An examination of the three-dimensional propagation of the eddies could be performed with the NCEP/NCAR Reanalysis. Finally, the procedures undertaken in this thesis could be extended over the full 40 year Reanalysis period to assess the inter-decadal variability of the transports, as well as to corroborate the conclusions reached from only 13 years of data.

Appendix A

Transport Climatology and Variability: Figures

The following appendix presents the figures discussed in detail in Chapter 3. For all contour plots the zero contour has been omitted. The latitude-longitude maps use the 2.5° by 2.5° resolution land-sea mask as a description of the topography.

Figure A.1: Total northward transport of sensible heat by quasi-stationary eddies in Petawatts. Heavy solid line is the 13 year average. Thin solid lines are the interannual standard deviation.

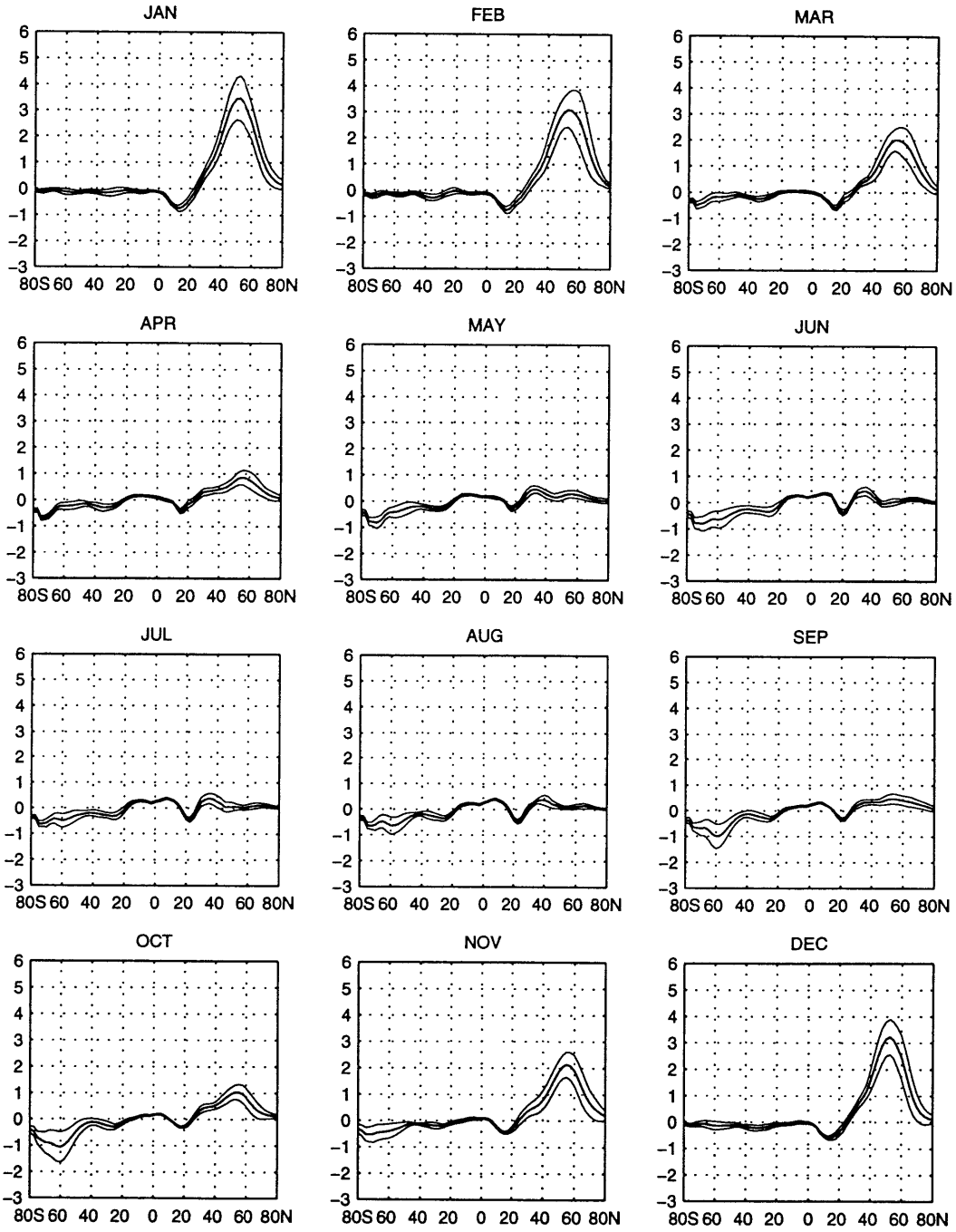

Figure A.2: Zonal mean cross-section of the 13 year average northward transport of sensible heat by quasi-stationary eddies, $[\bar{v}^*\bar{T}^*]$. Contour interval is 5°C m s^{-1}, vertical axis in hPa. Dotted lines indicate negative values.

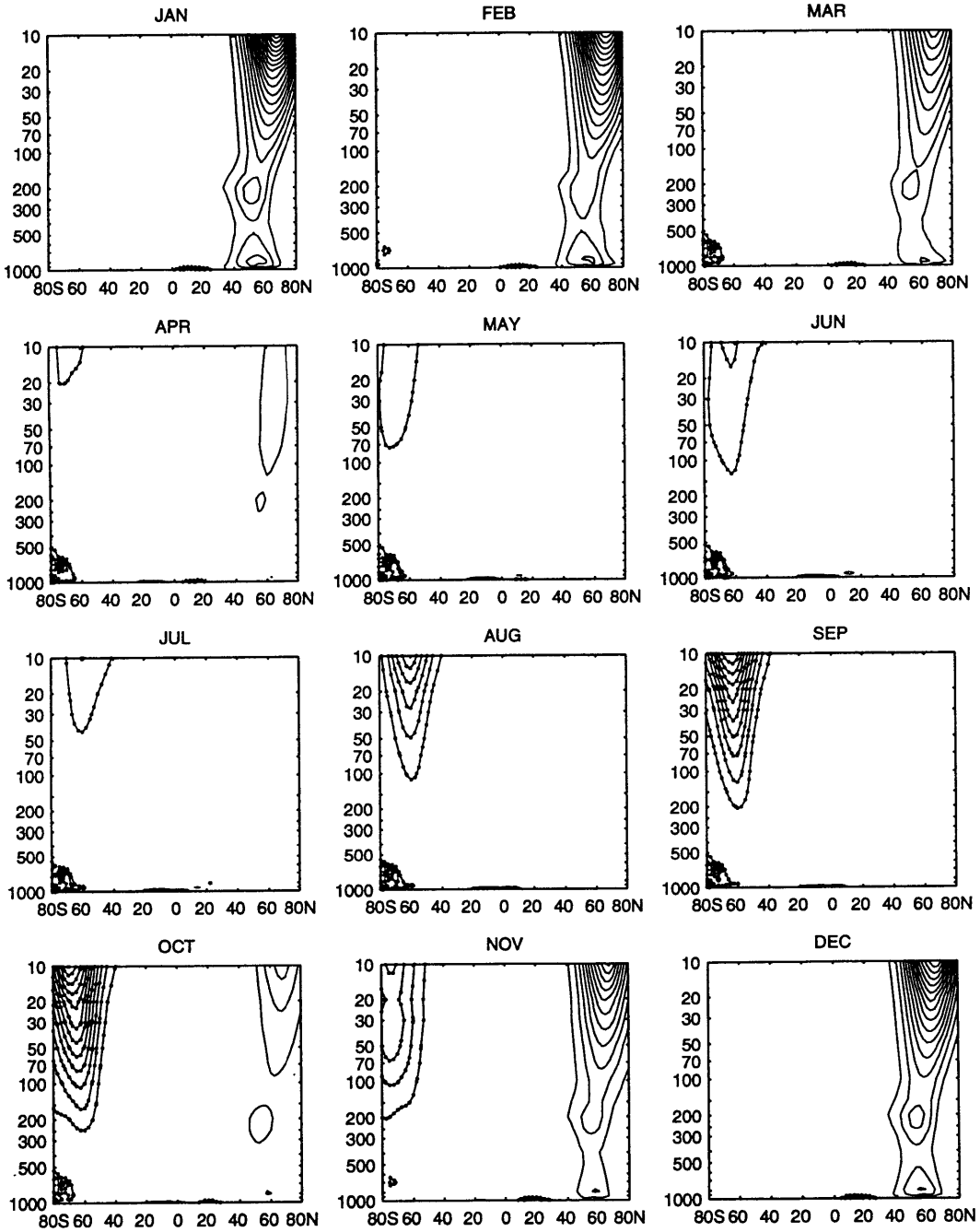

Figure A.3: Zonal mean cross-section of the interannual standard deviation of the northward transport of sensible heat by quasi-stationary eddies for the troposphere. Contour interval is 2°C m s^{-1}, vertical axis in hPa.

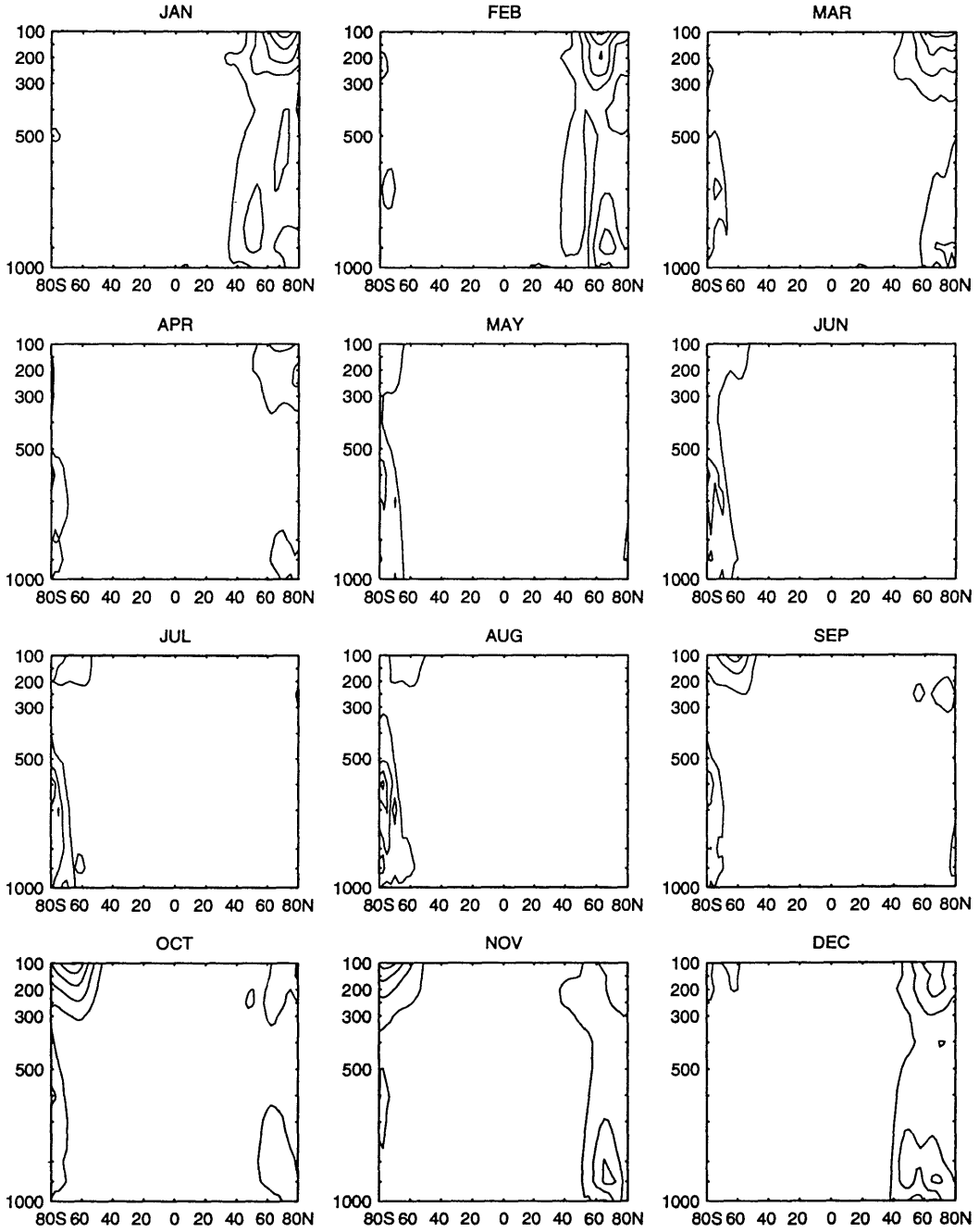

Figure A.4: Zonal mean cross-section of the interannual standard deviation of the northward transport of sensible heat by quasi-stationary eddies for the stratosphere. Contour interval is 5°C m s^{-1}, vertical axis in hPa.

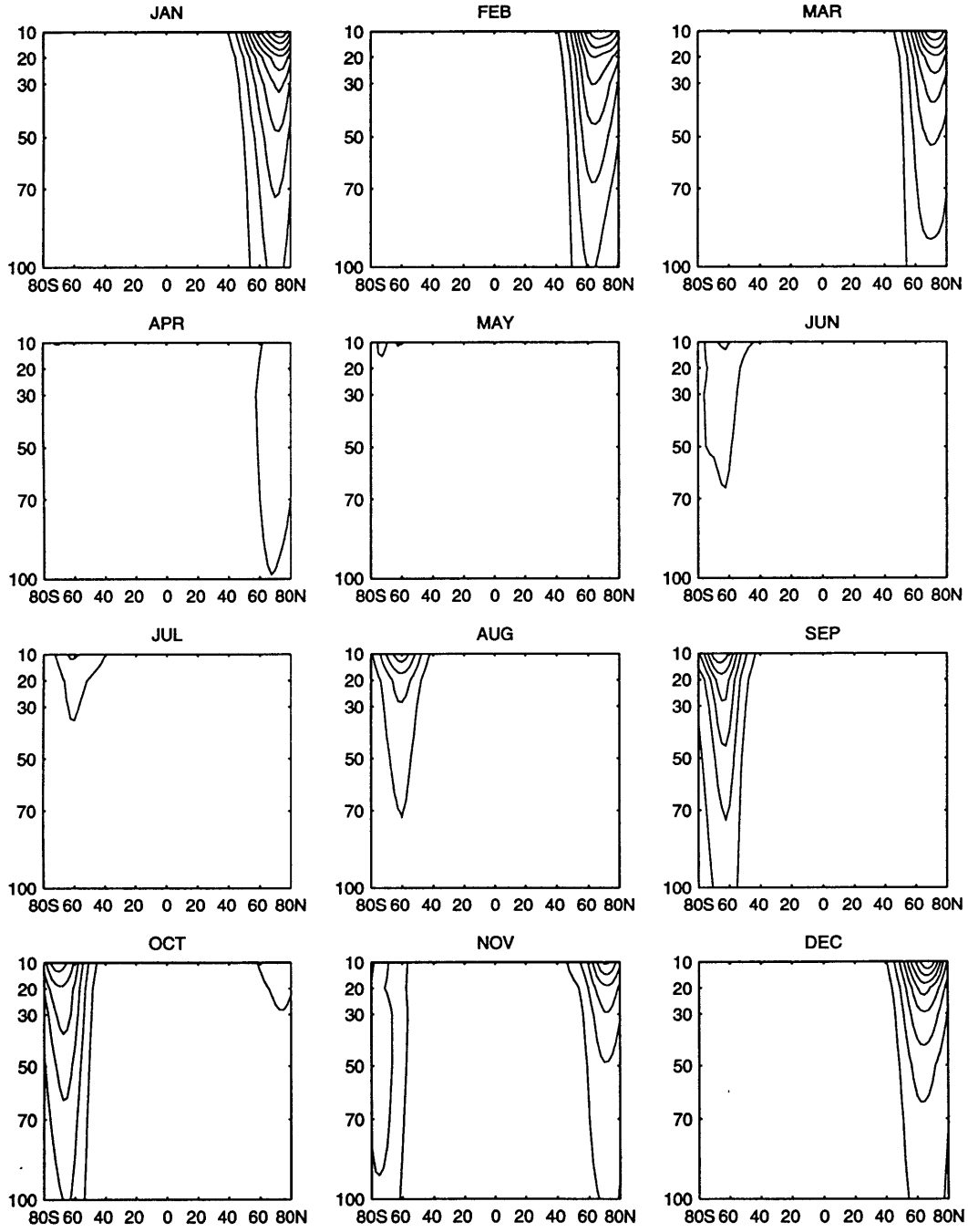

Figure A.5: Northward transport of sensible heat by quasi-stationary eddies at 850 hPa in the northern hemisphere from January to April. Contour interval is 10°C m s^{-1}. Dotted contours indicate negative values.

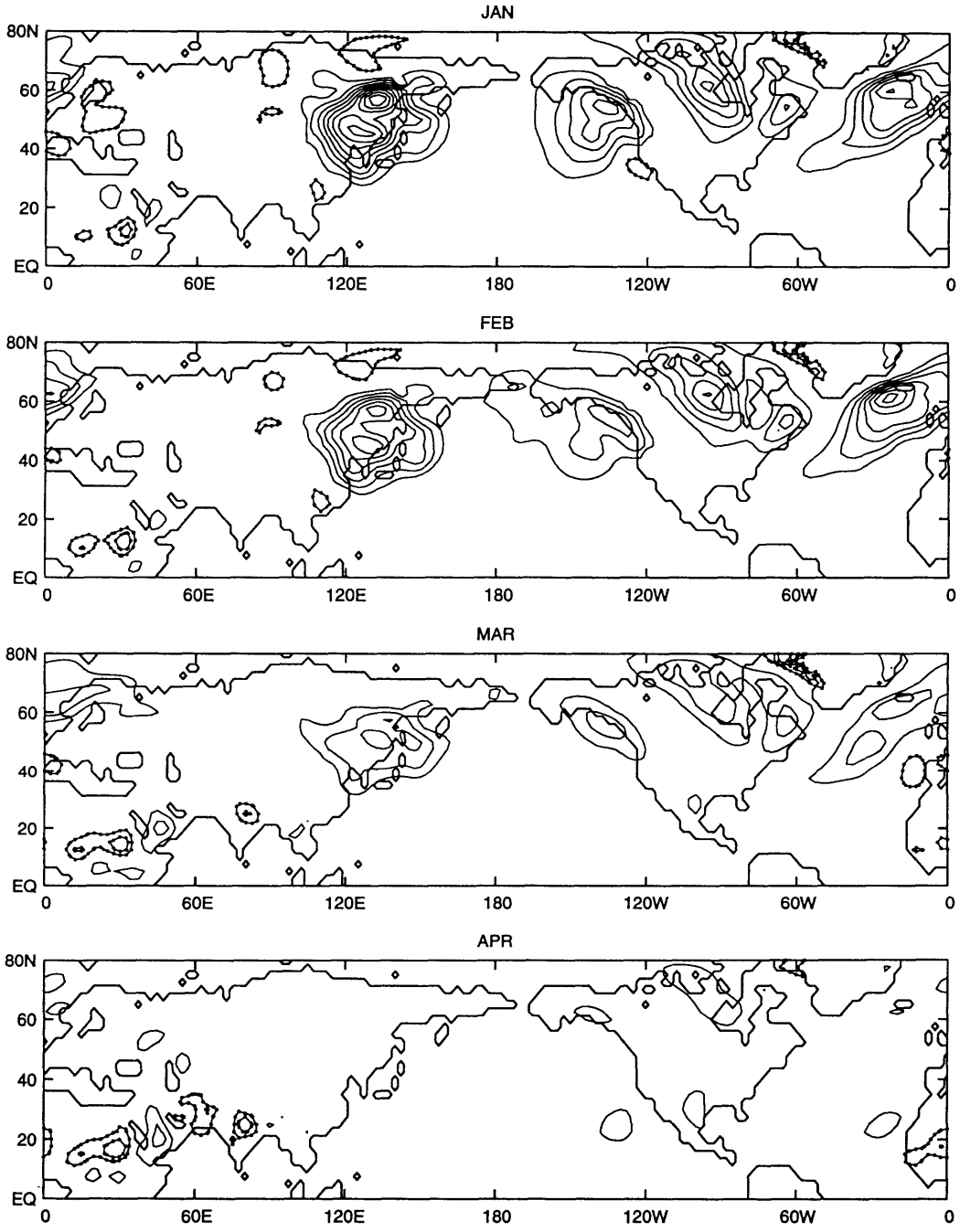

Figure A.6: As in Figure A.5 but for May to August.

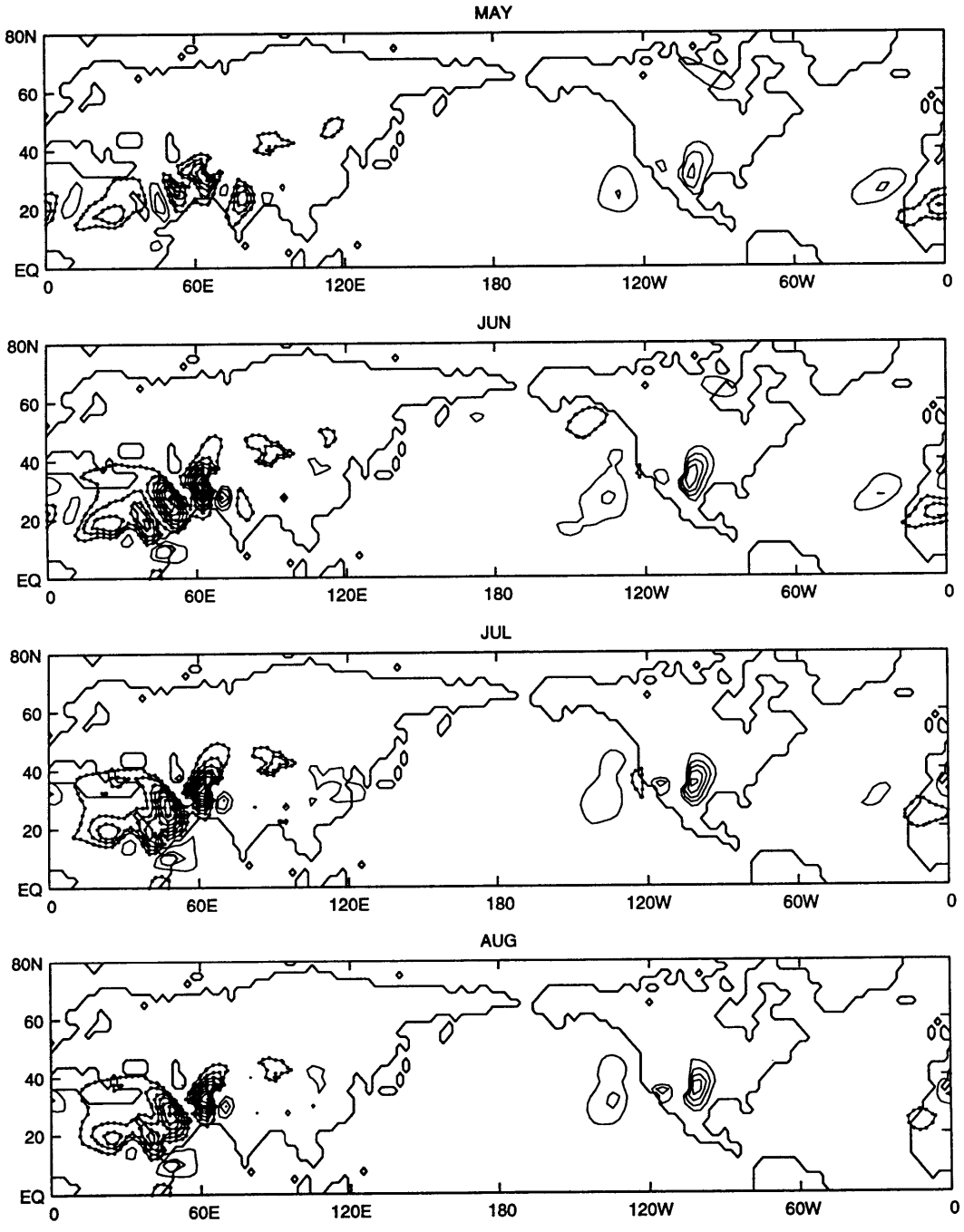

Figure A.7: As in Figure A.5 but for September to December.

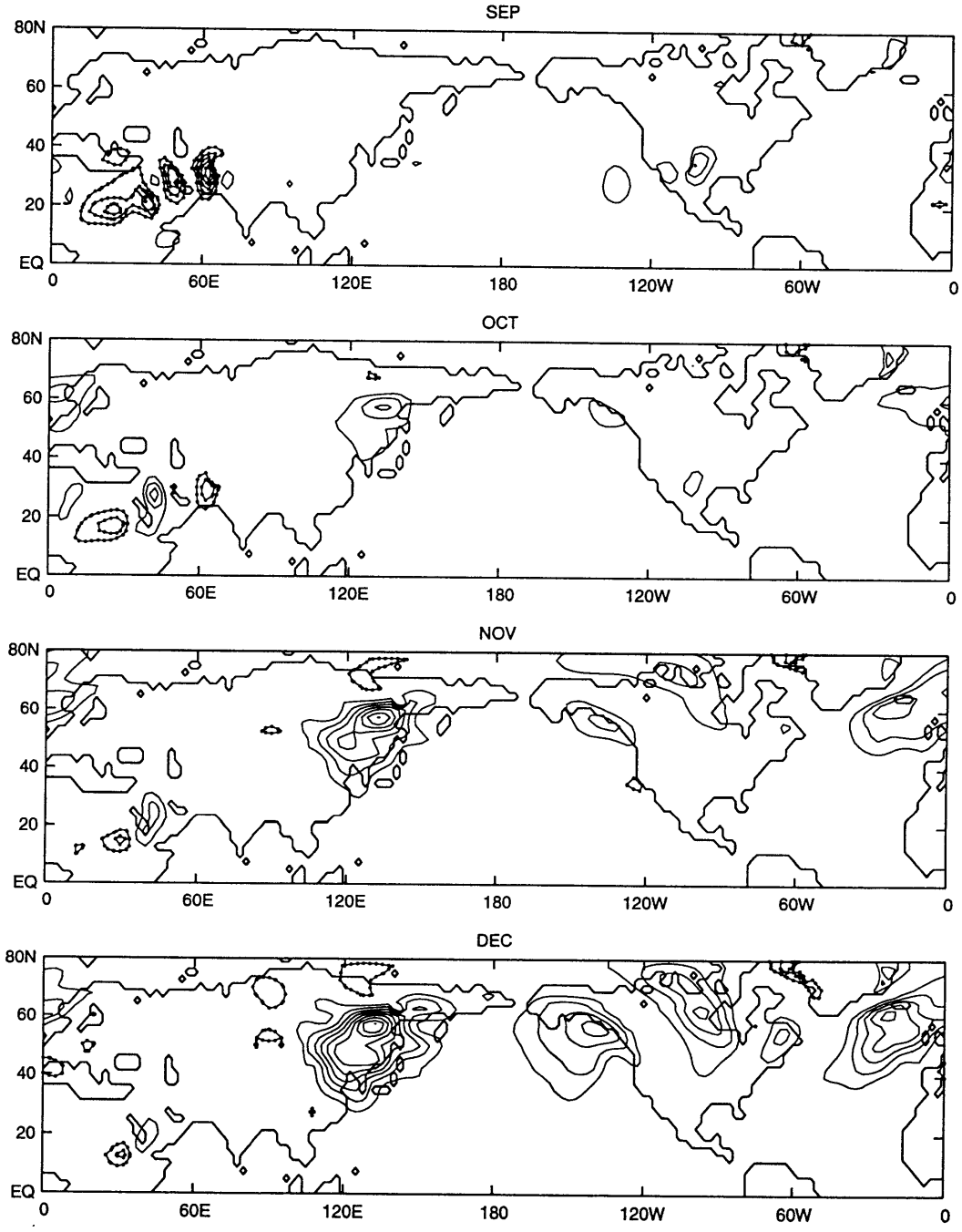

Figure A.8: The interannual standard deviation of the 850 hPa quasi-stationary northward transport of sensible heat for January to April. Contour interval is 10°C m s^{-1}.

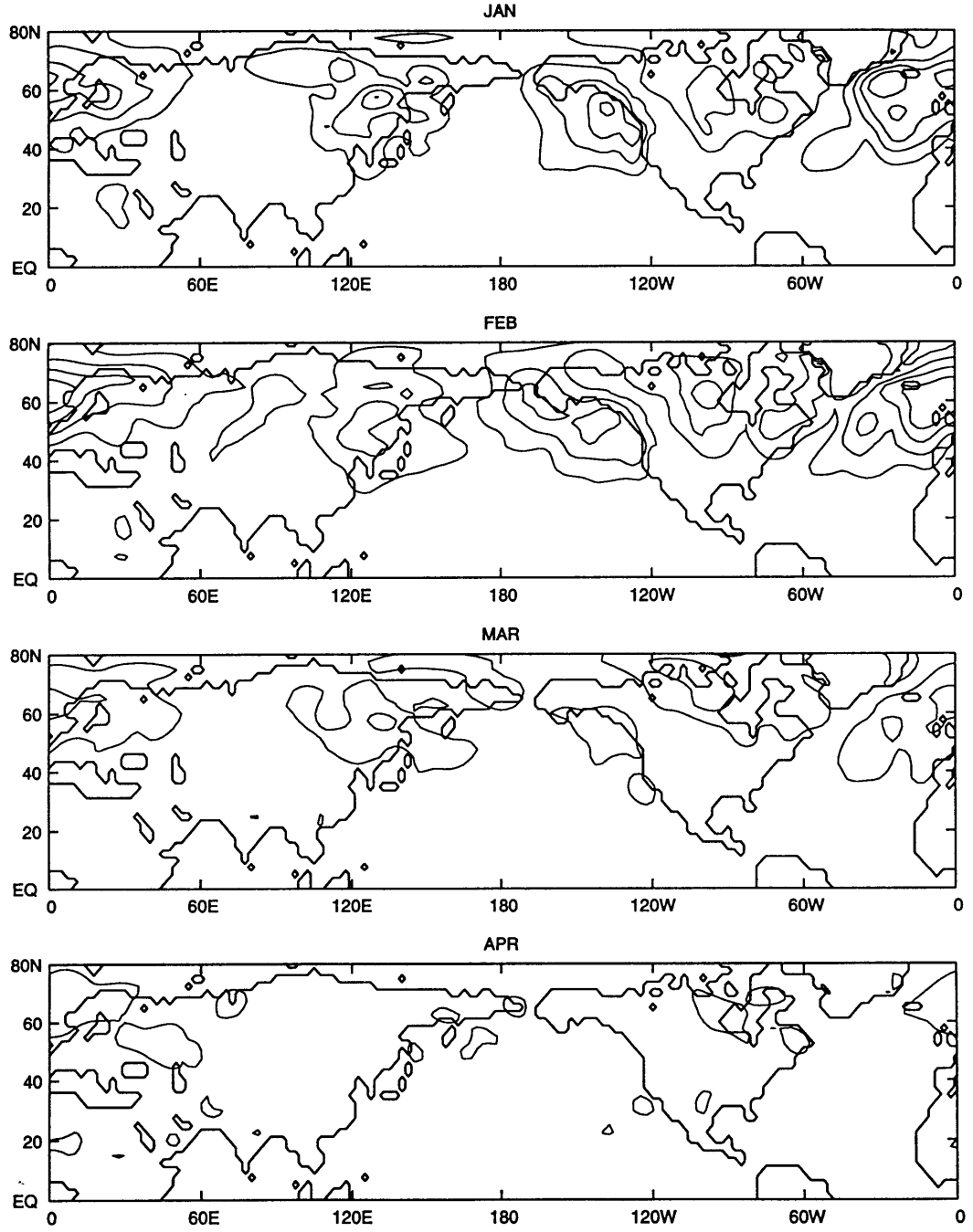

Figure A.9: As in Figure A.8 but for May to August.

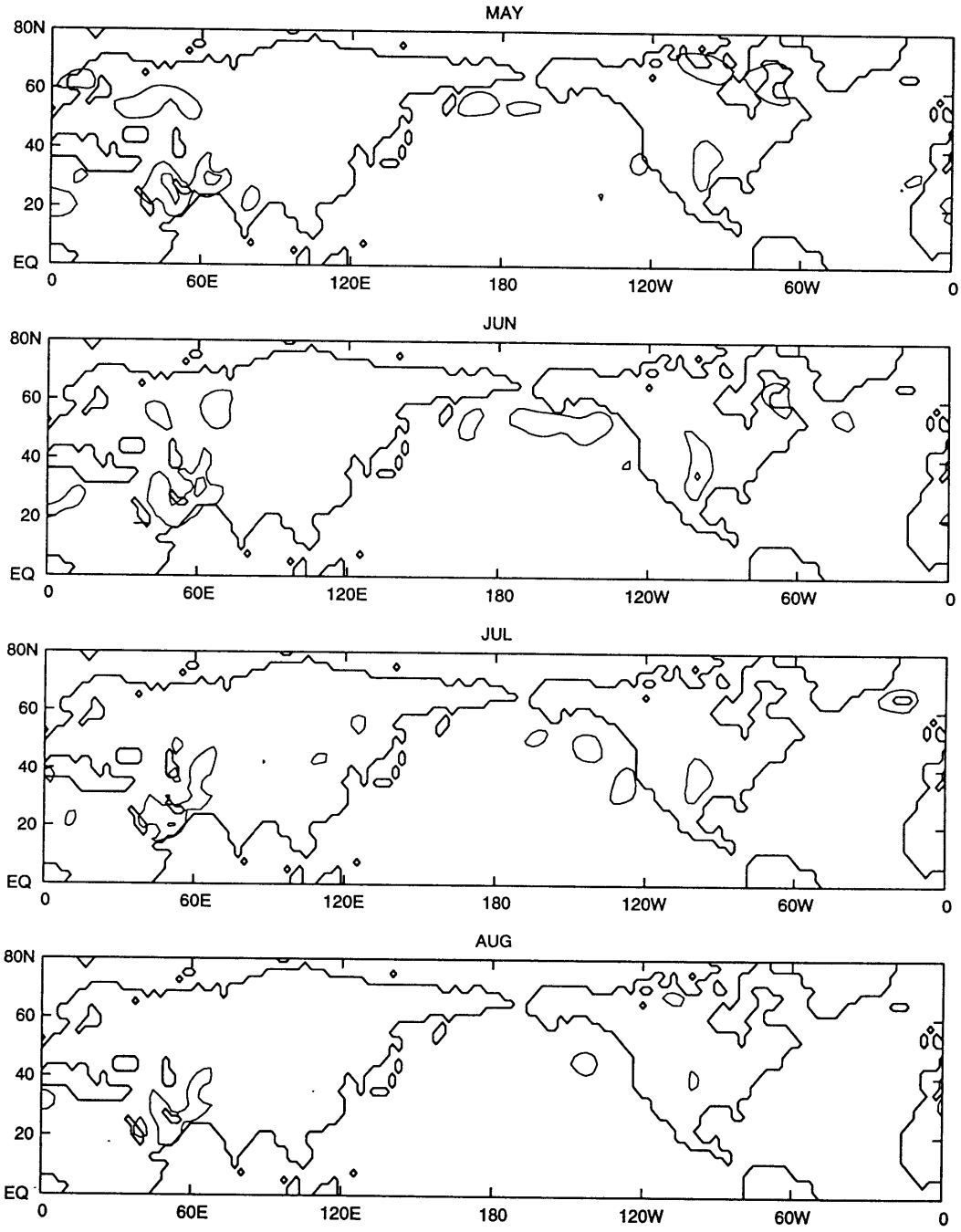

Figure A.10: As in Figure A.8 but for September to December.

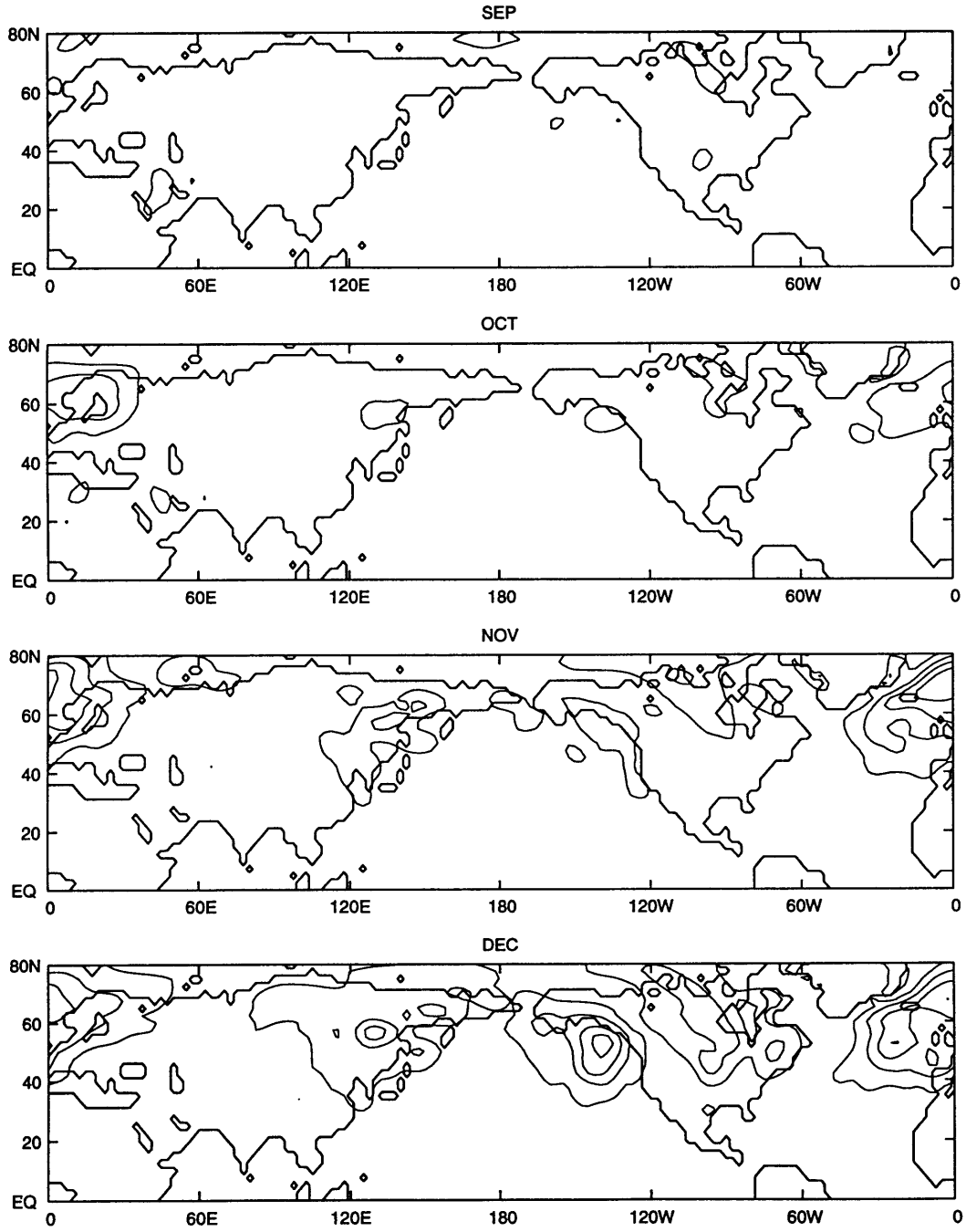

Figure A.11: Northward transport of sensible heat by quasi-stationary eddies at 200 hPa in the northern hemisphere from January to April. Contour interval is 10°C m s^{-1}. Dotted contours indicate negative values.

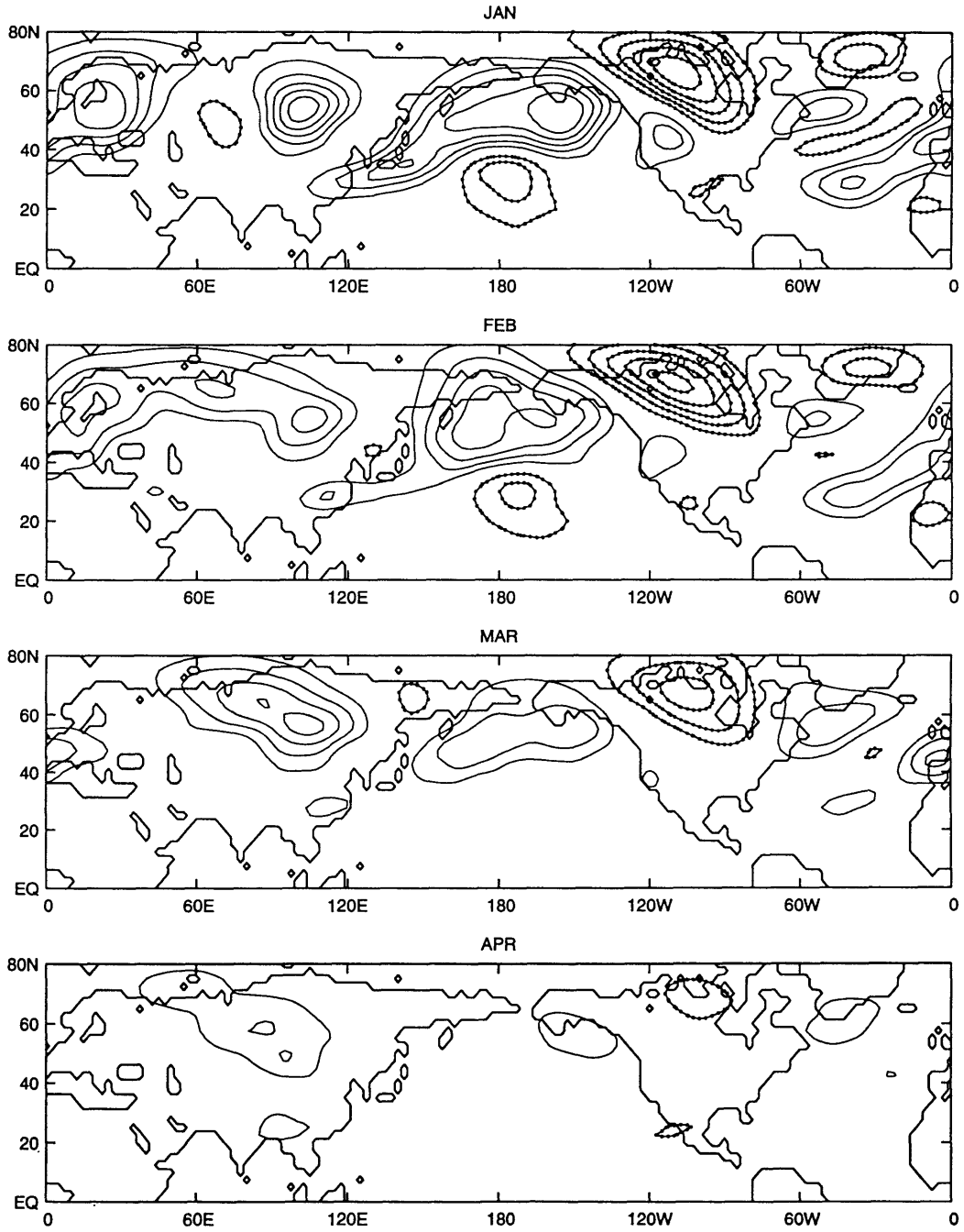

Figure A.12: As in Figure A.11 but for May to August.

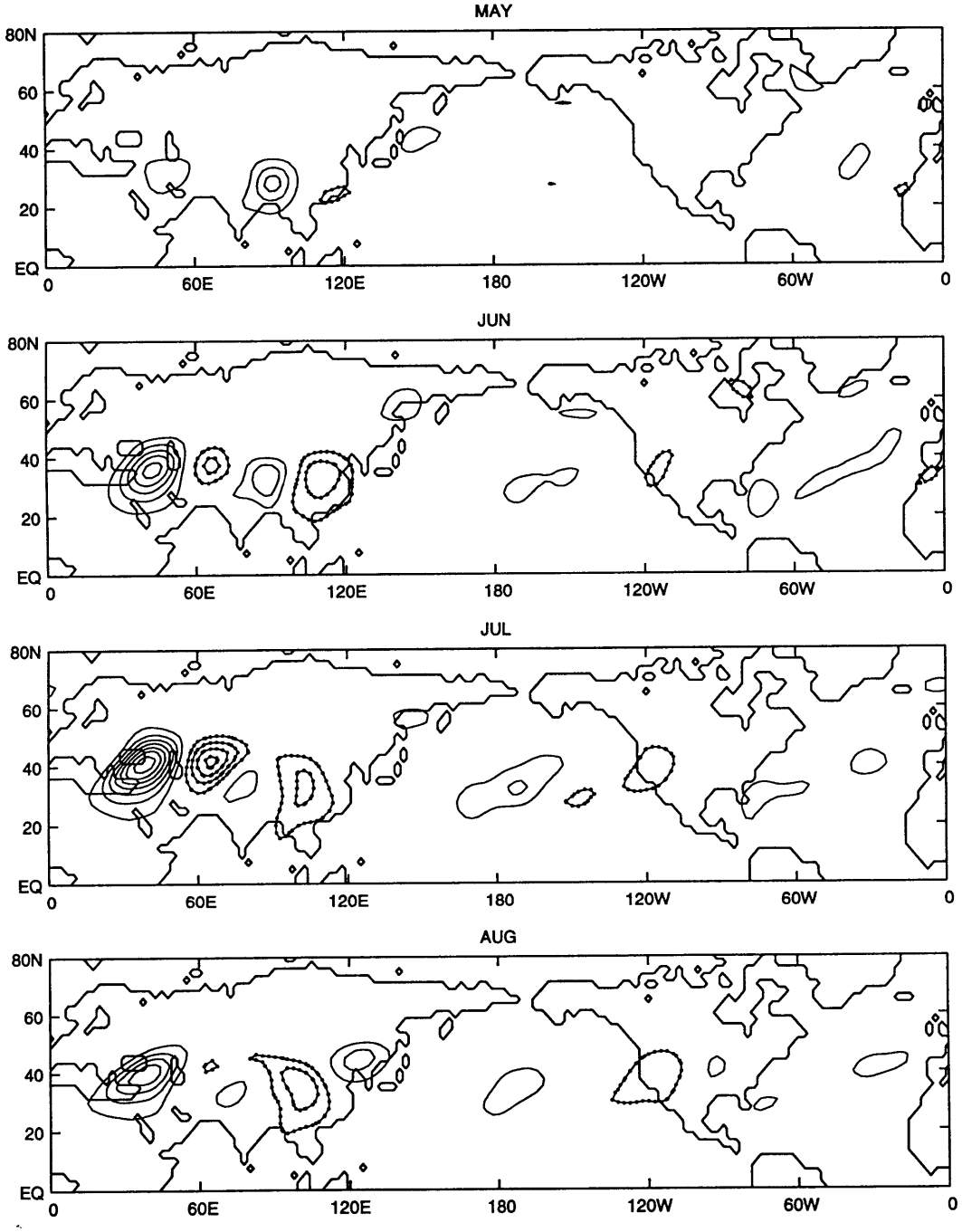

Figure A.13: As in Figure A.11 but for September to December.

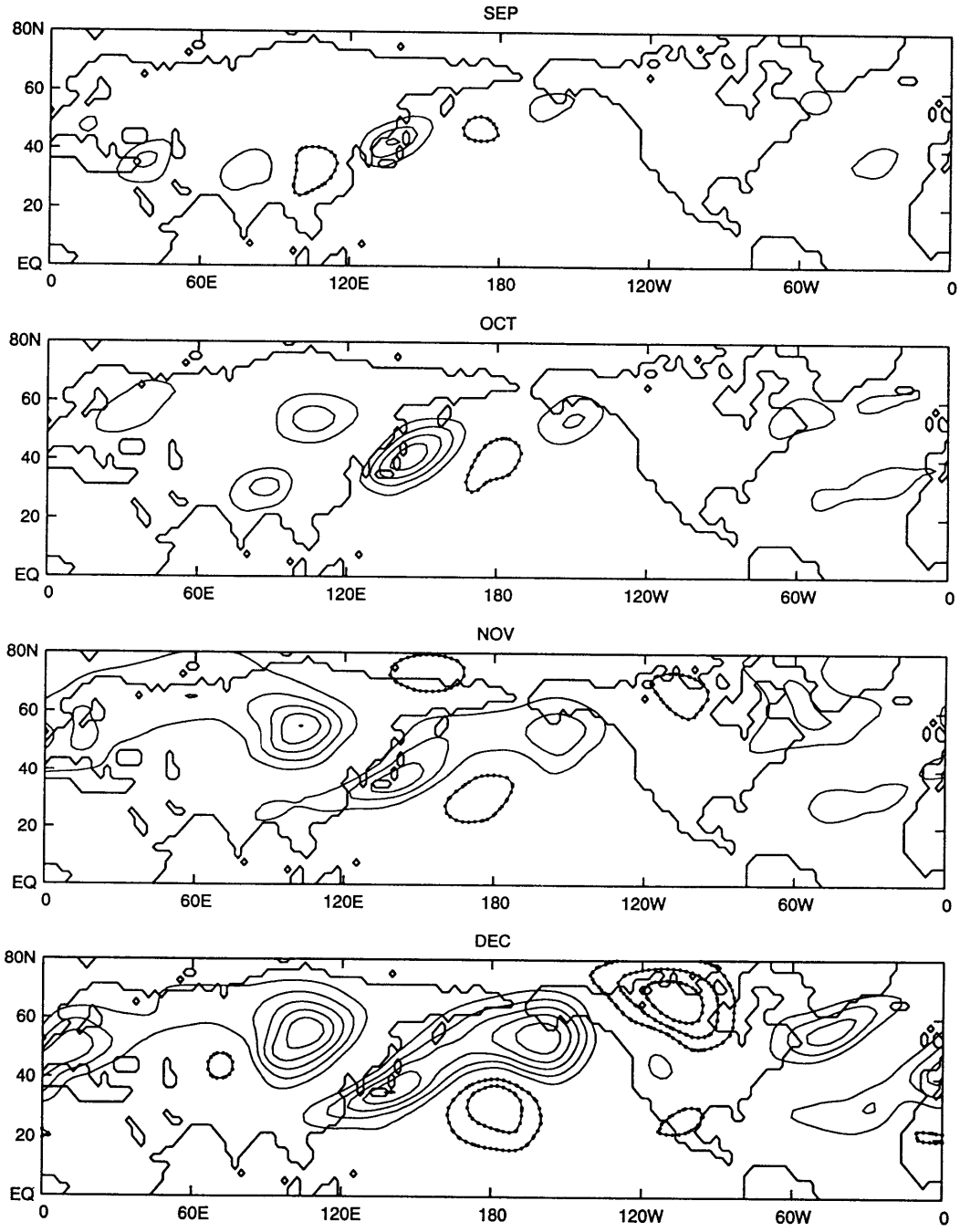

Figure A.14: The interannual standard deviation of the 200 hPa quasi-stationary northward transport of sensible heat for January to April. Contour interval is 10°C m s^{-1}.

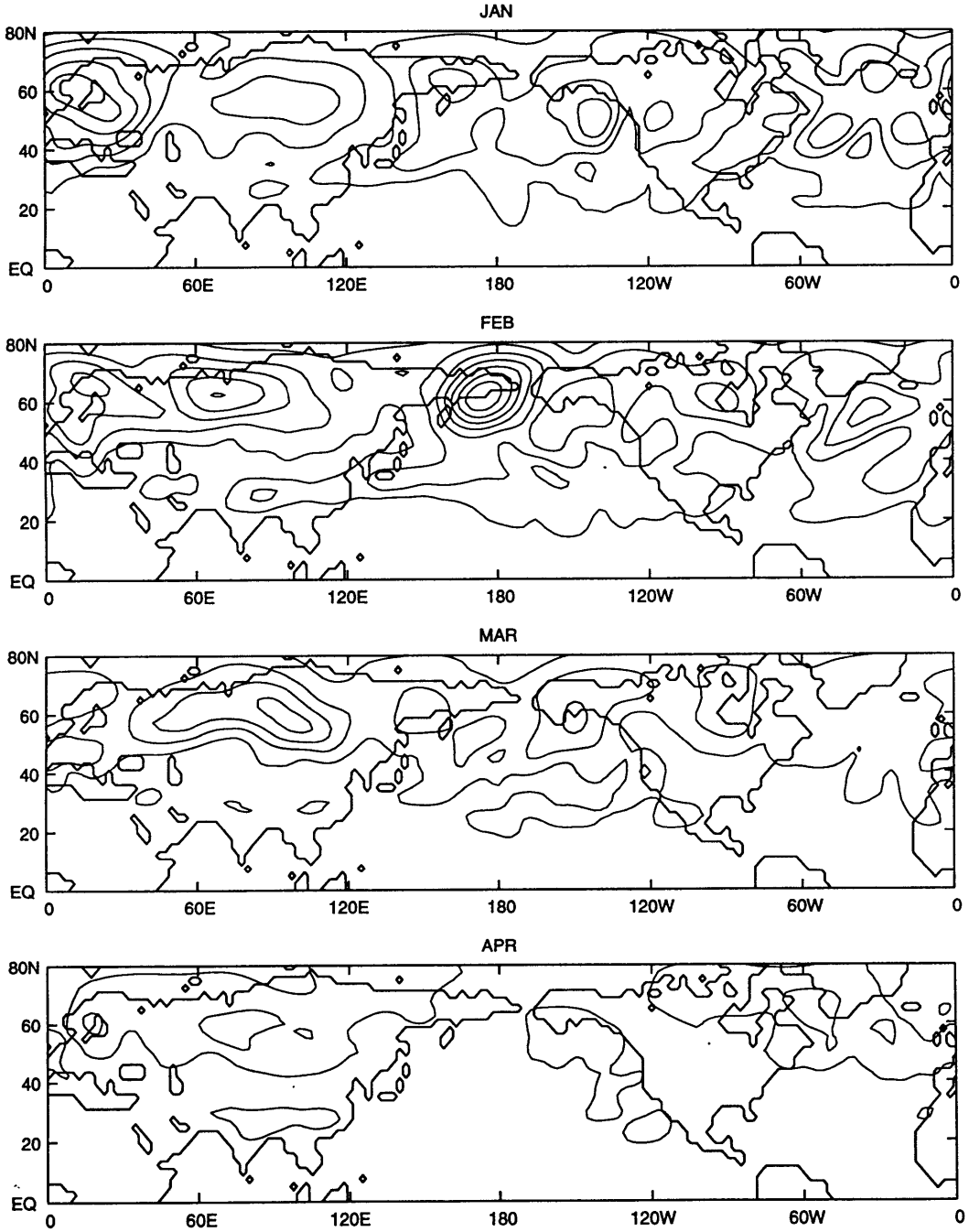

Figure A.15: As in Figure A.14 but for May to August.

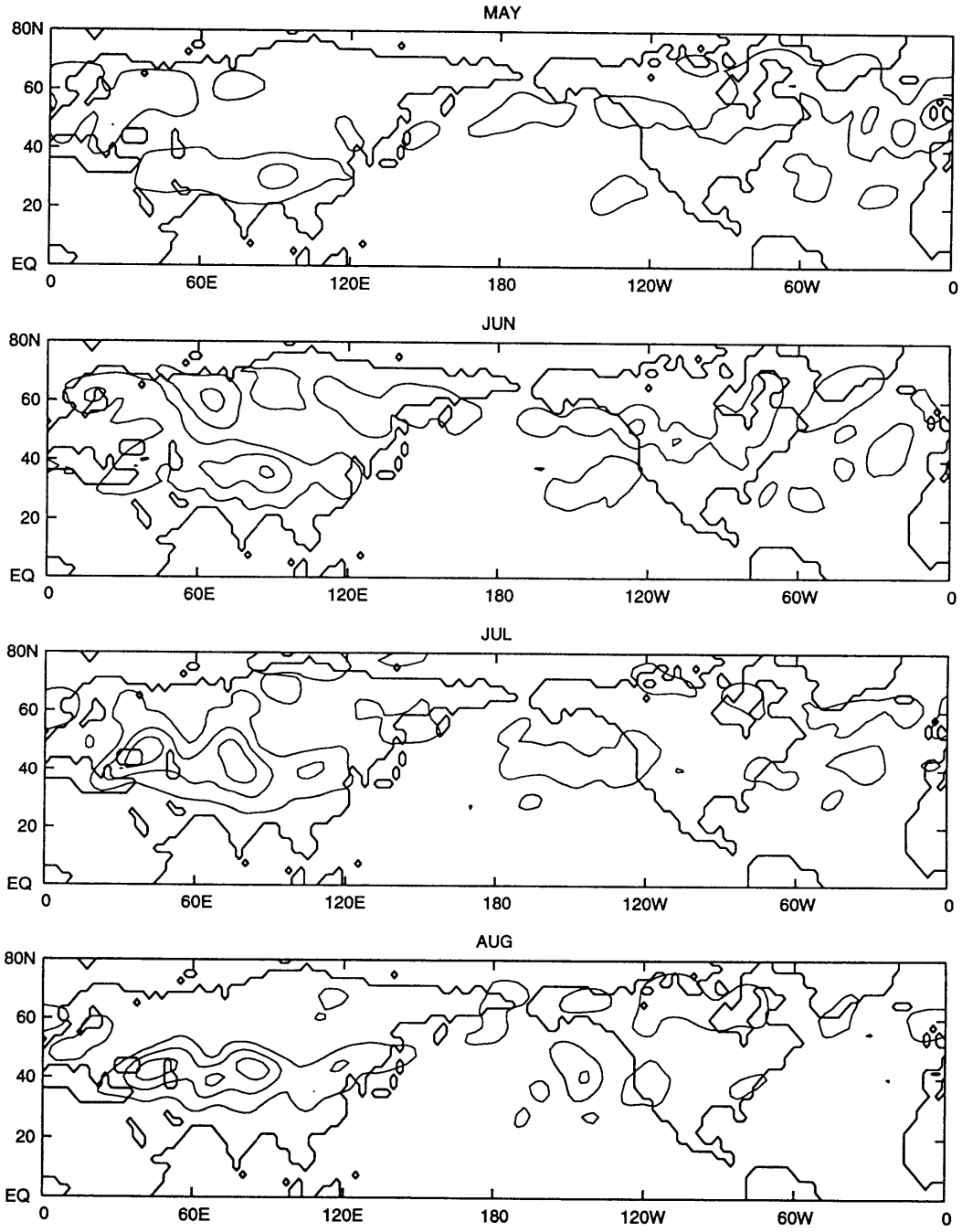

Figure A.16: As in Figure A.14 but for September to December.

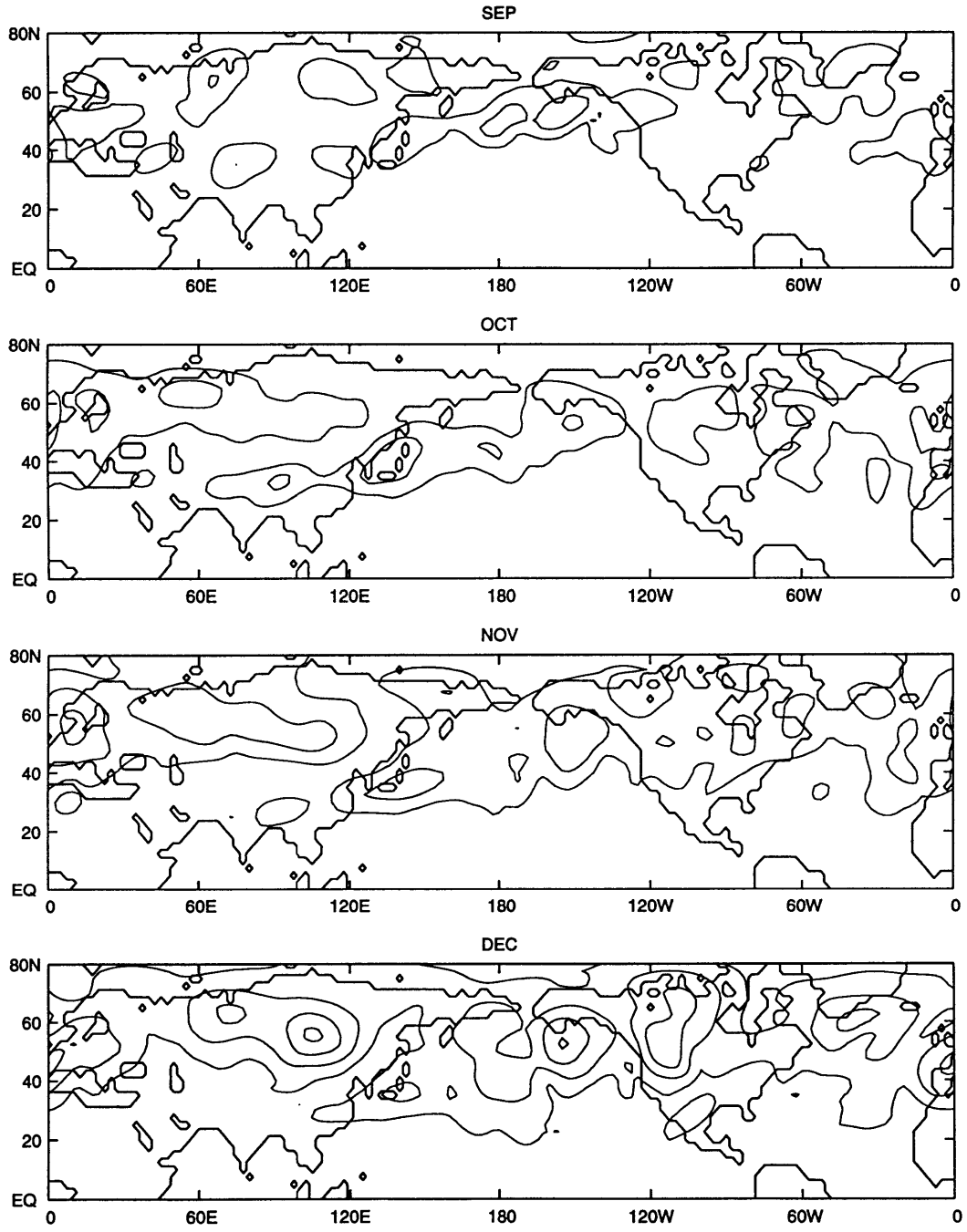

Figure A.17: Northward transport of heat by quasi-stationary eddies in the southern hemisphere at 70 hPa. Contour interval is 10 °C m s^{-1}. Dotted contours indicate negative values.

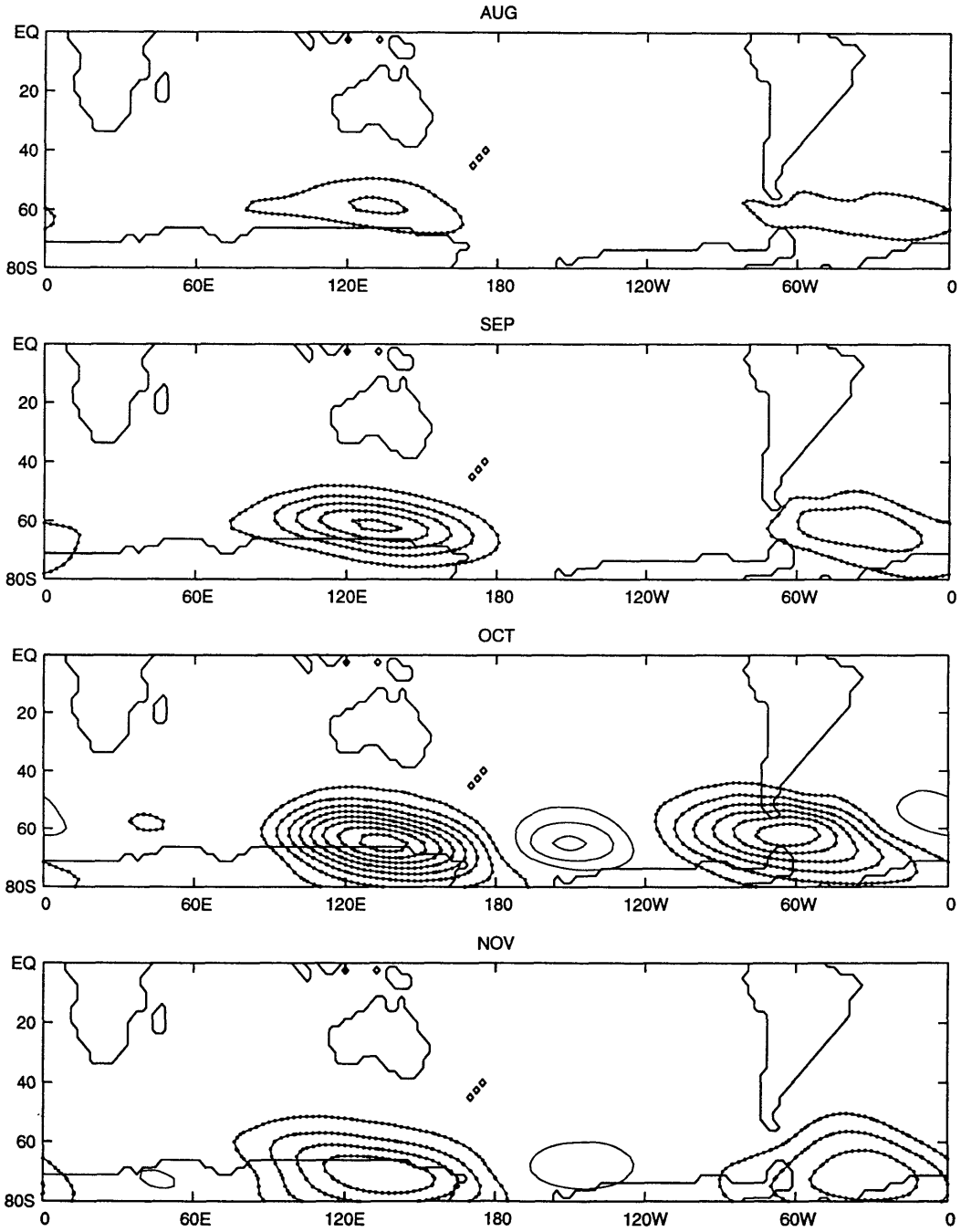

Figure A.18: Interannual standard deviation of the northward transport of heat by quasi-stationary eddies in the southern hemisphere at 70 hPa. Contour interval is 10 °C m s^{-1}.

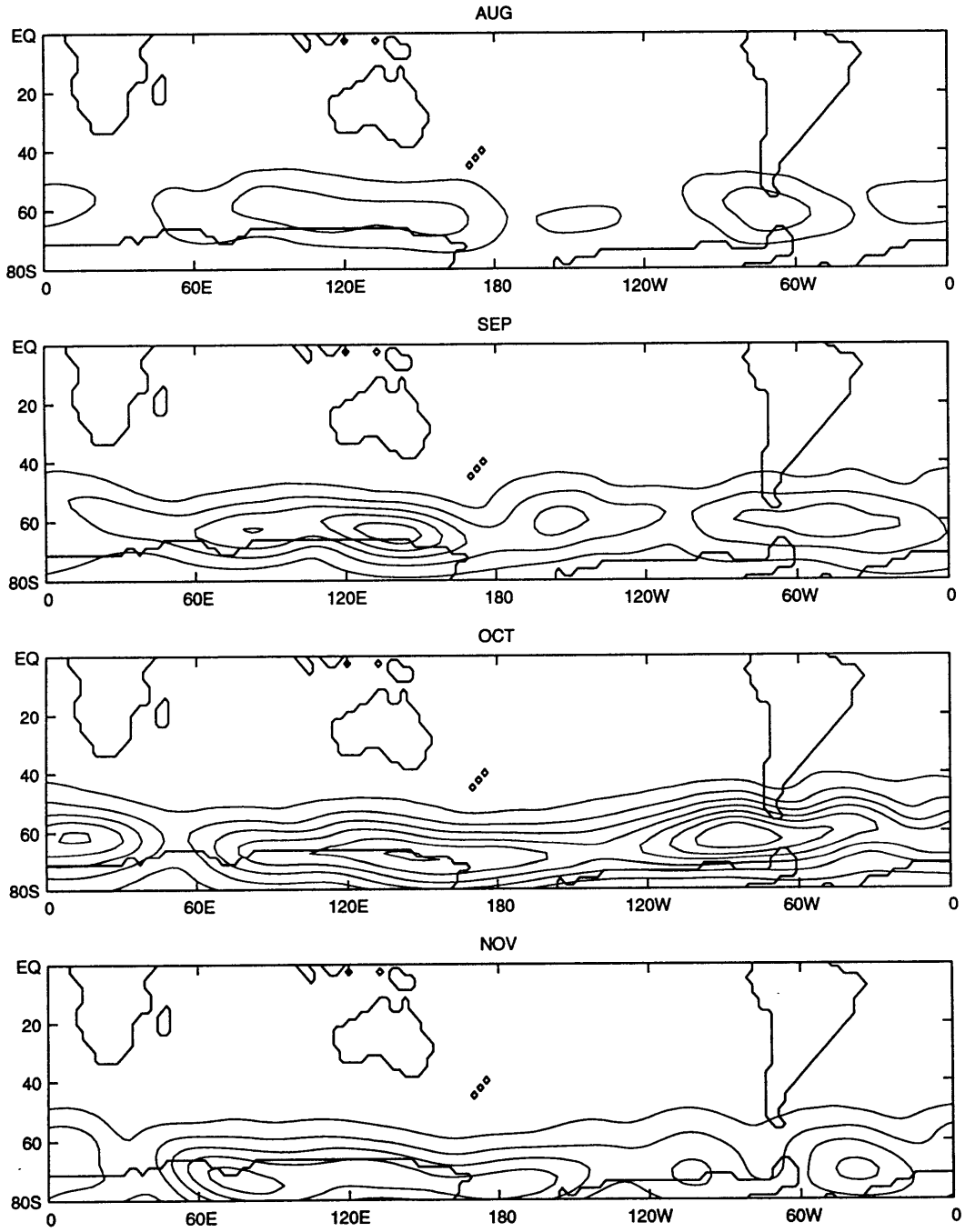

Figure A.19: Zonal and vertical mean northward transport of westerly momentum by quasi-stationary eddies in $m^2\ s^{-2}$. Heavy solid line is the 13 year average. Thin solid lines are the interannual standard deviation.

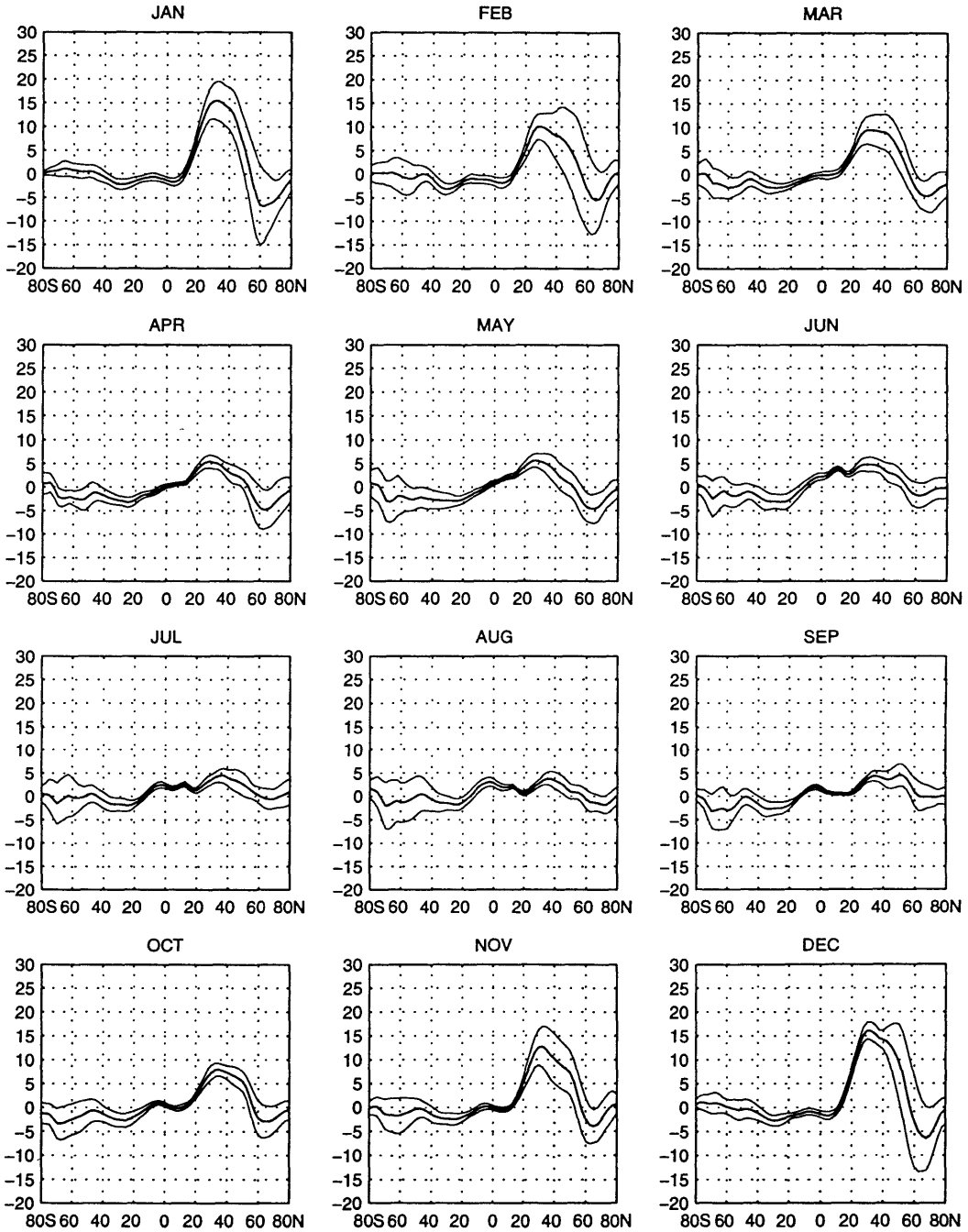

Figure A.20: Zonal mean cross-section of the 13 year average northward transport of westerly momentum by quasi-stationary eddies, $[\bar{u}^*\bar{v}^*]$. Contour interval 5 m^2 s^{-2}, vertical axis in hPa. Dotted lines indicate negative values.

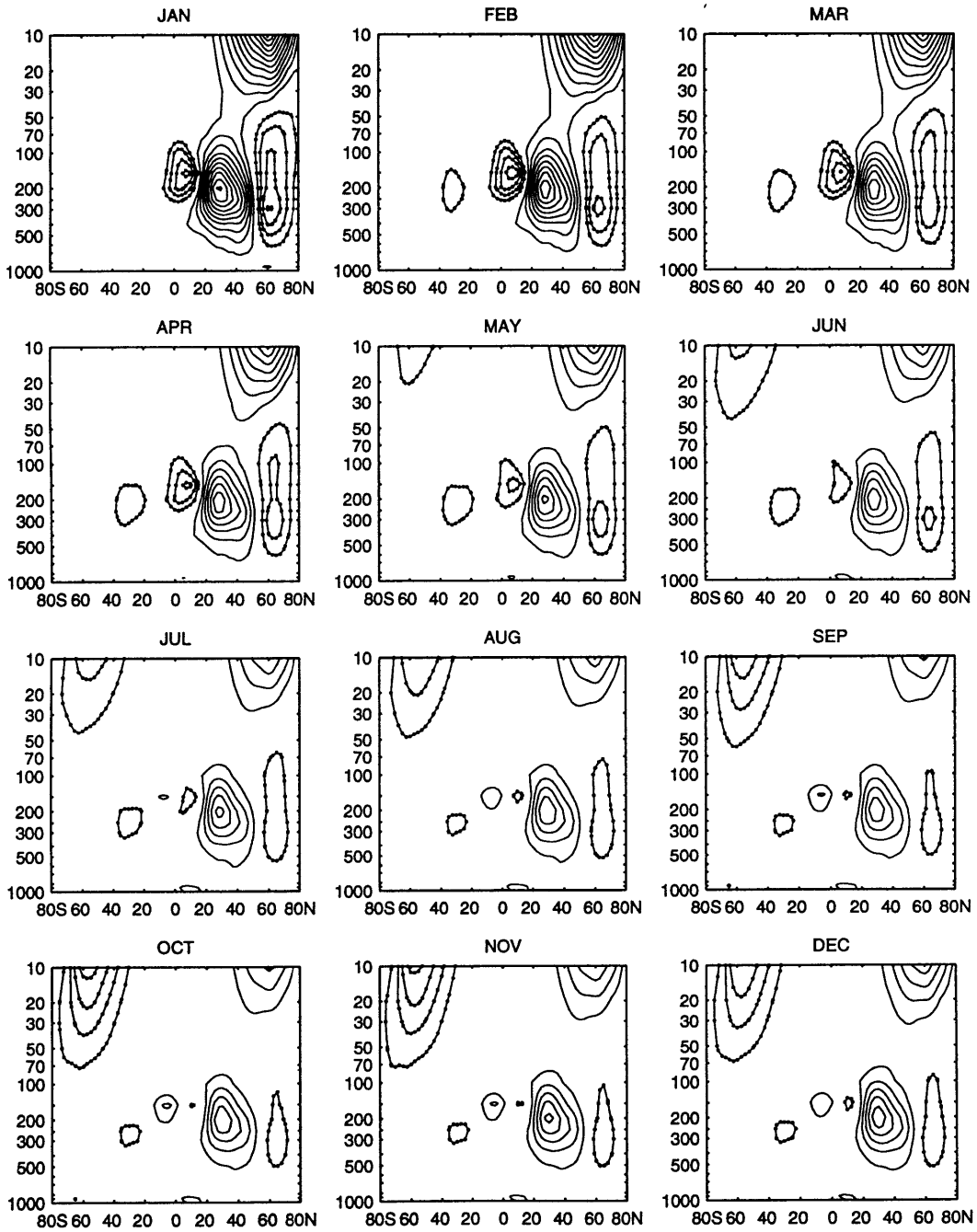

Figure A.21: Zonal mean cross-section of the interannual standard deviation of the northward transport of westerly momentum by quasi-stationary eddies. Contour interval is 5 $m^2\ s^{-2}$, vertical axis in hPa.

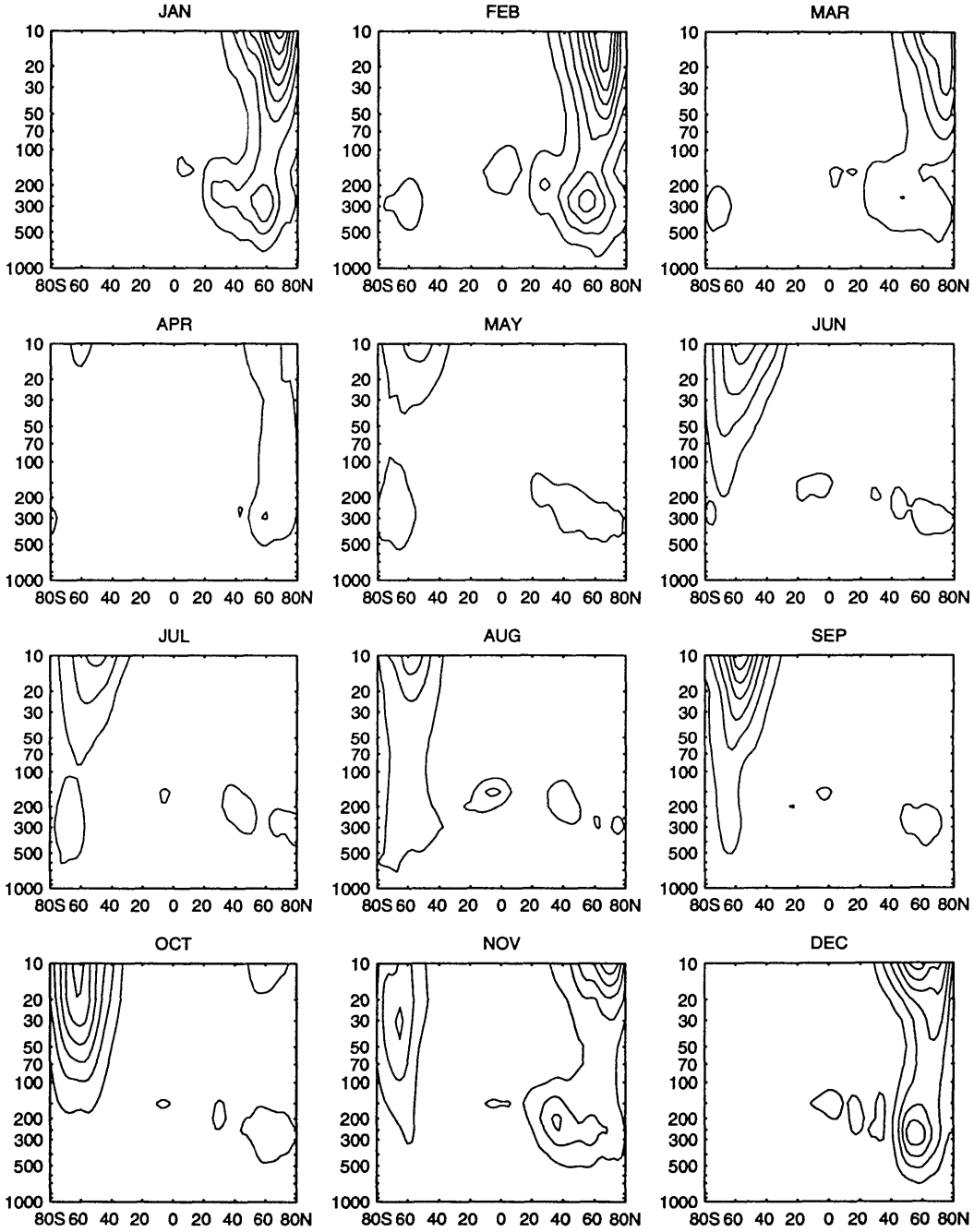

Figure A.22: Northward transport of westerly momentum by quasi-stationary eddies at 200 hPa in the northern hemisphere from January to April. Contour interval is 40 m^2 s^{-2}. Dotted contours indicate negative values.

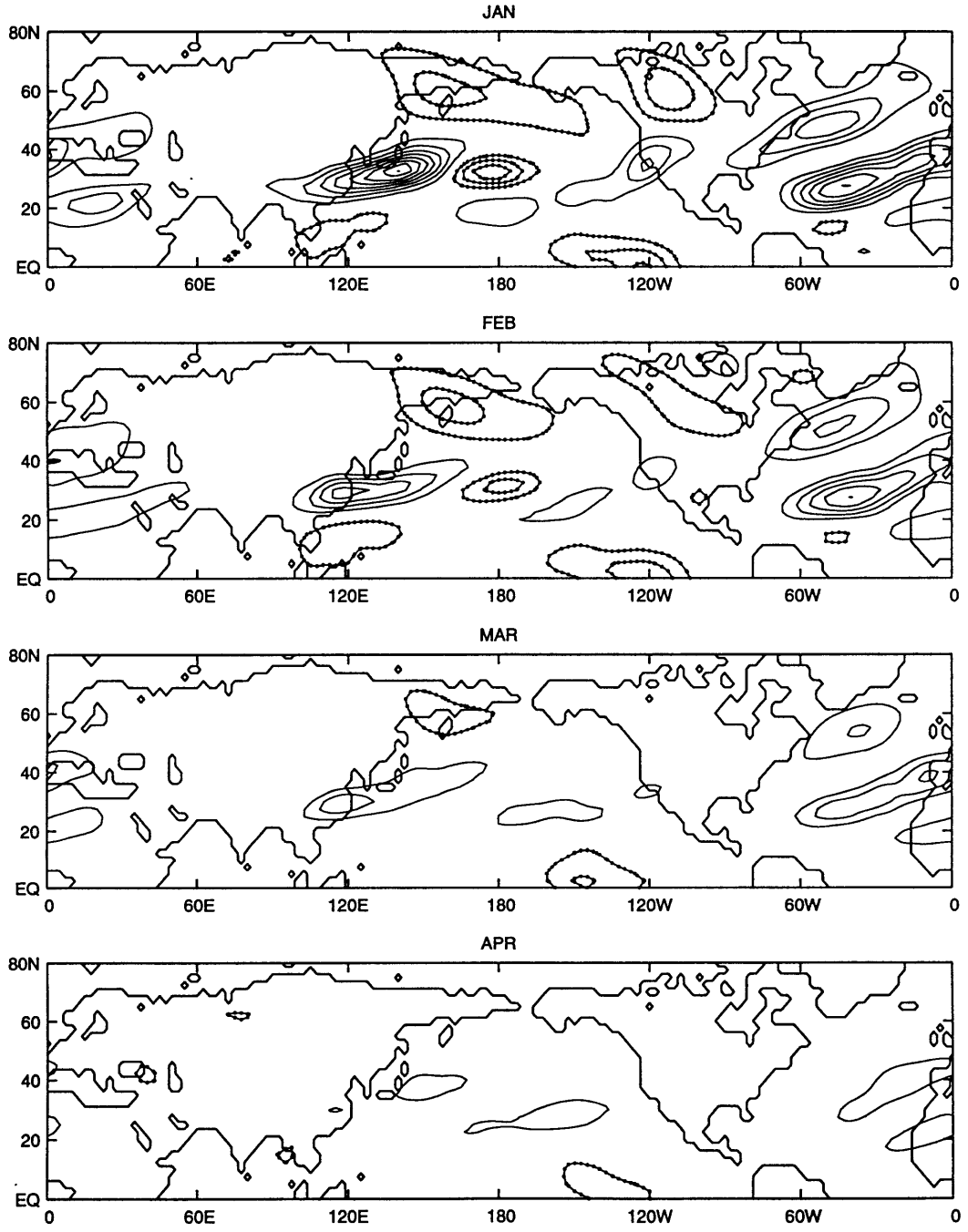

Figure A.23: As in Figure A.22 but for May to August.

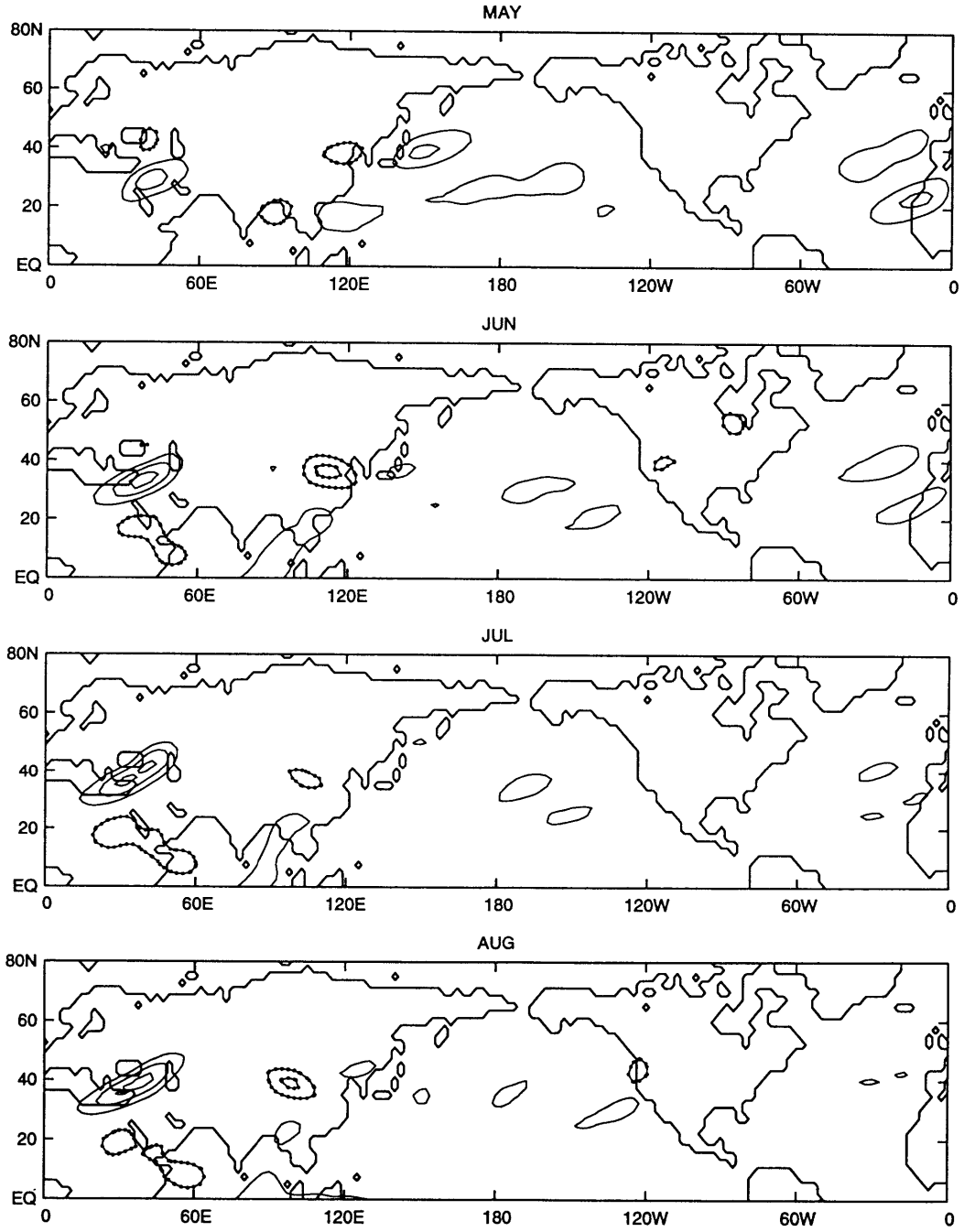

Figure A.24: As in Figure A.22 but for September to December.

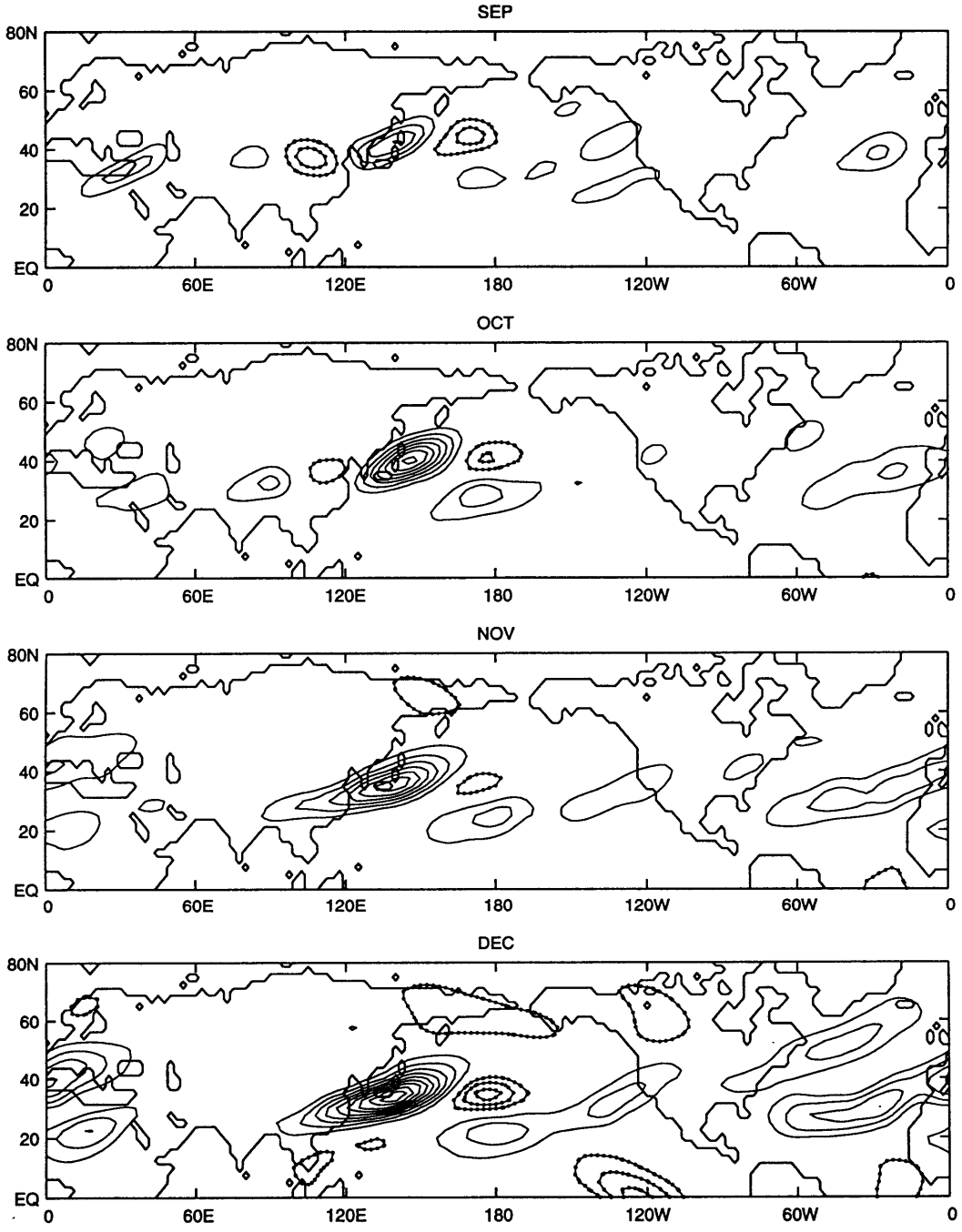

Figure A.25: Interannual standard deviation of the northward transport of westerly momentum at 200 hPa by quasi-stationary eddies for January to April. Contour interval is 20 $m^2\ s^{-2}$.

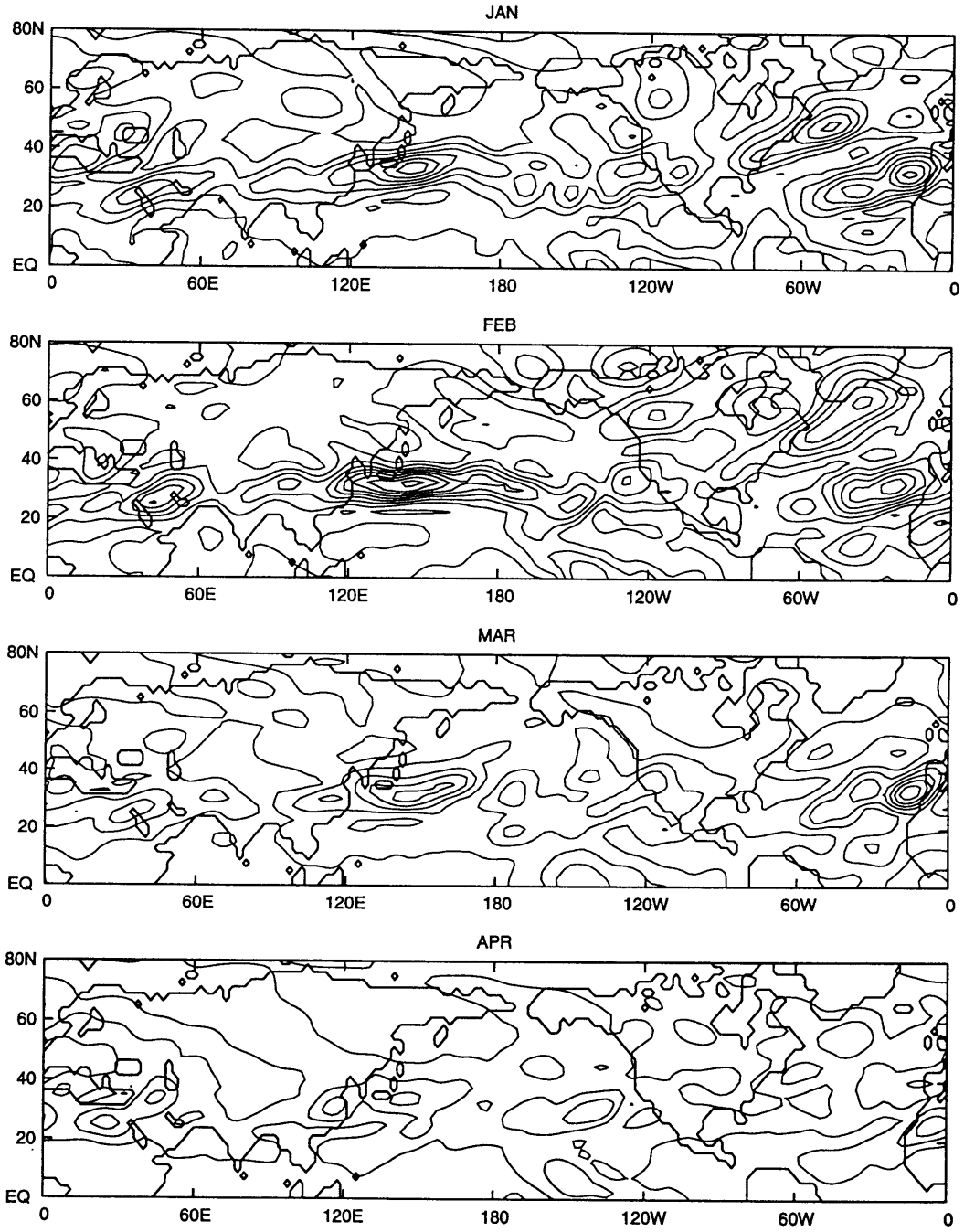

Figure A.26: As in Figure A.25 but for May to August.

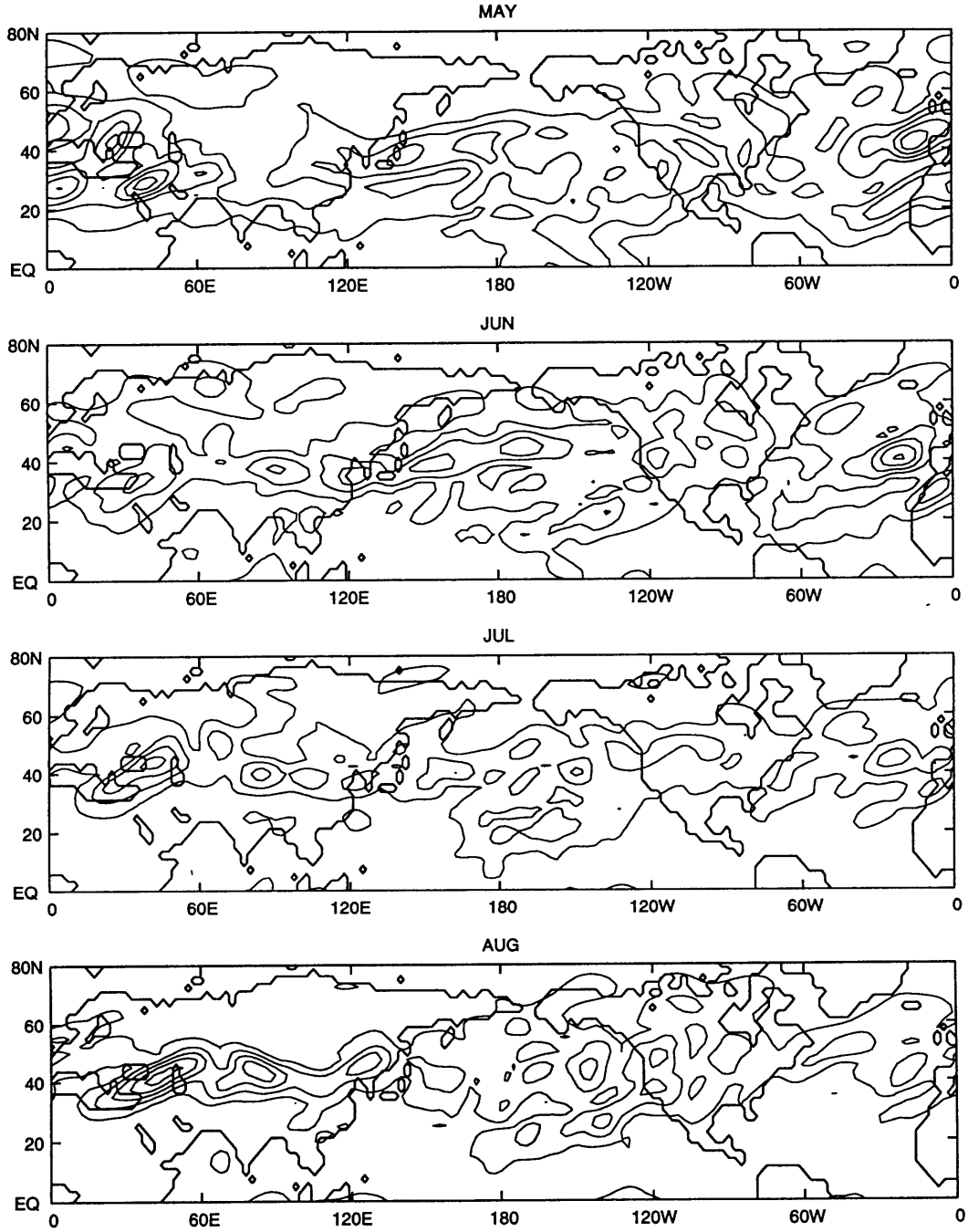

Figure A.27: As in Figure A.25 but for September to December.

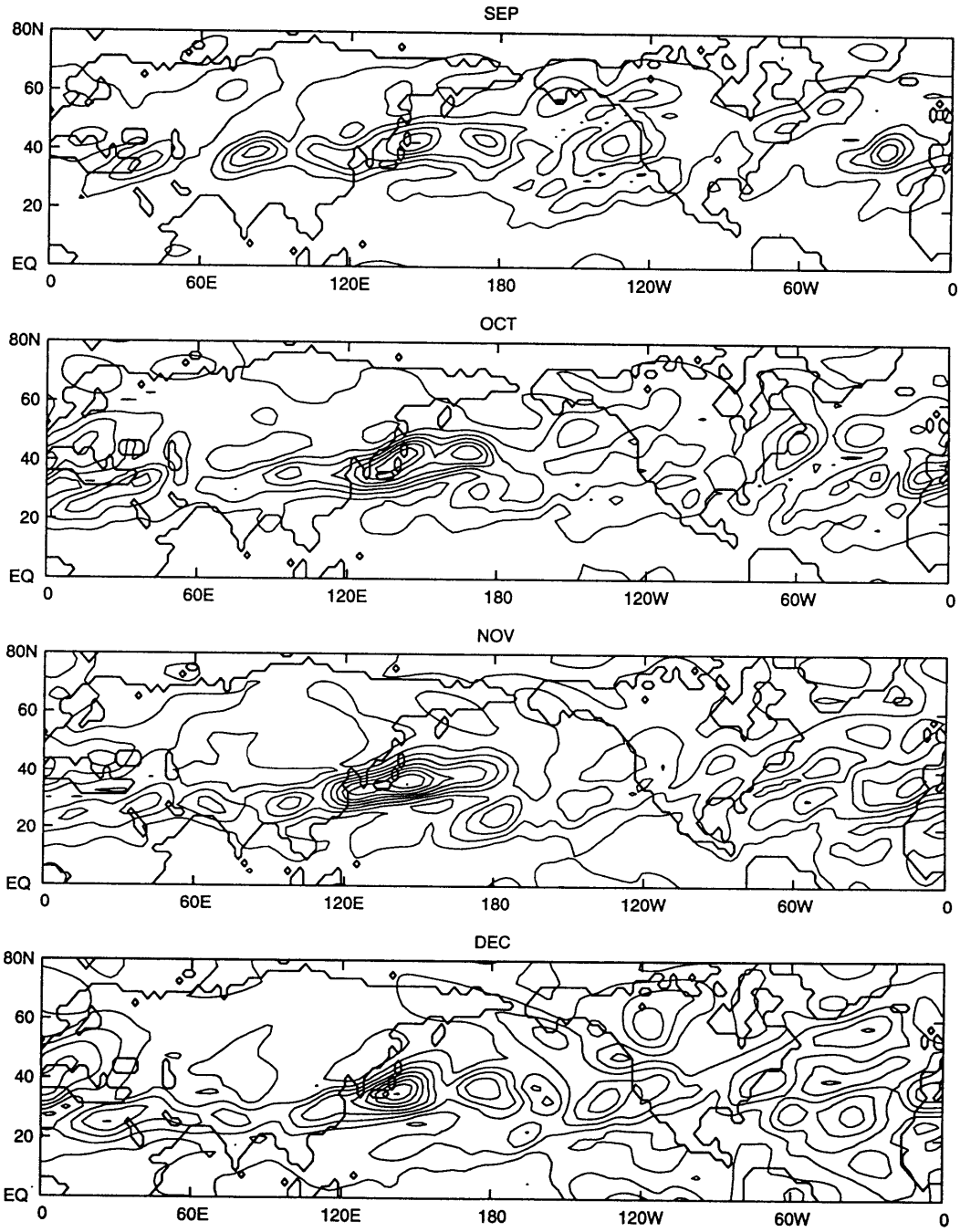

Figure A.28: Northward transport of westerly momentum by quasi-stationary eddies at 150 hPa from January to April. Contour interval is 20 $m^2\ s^{-2}$. Dotted contours indicate negative values.

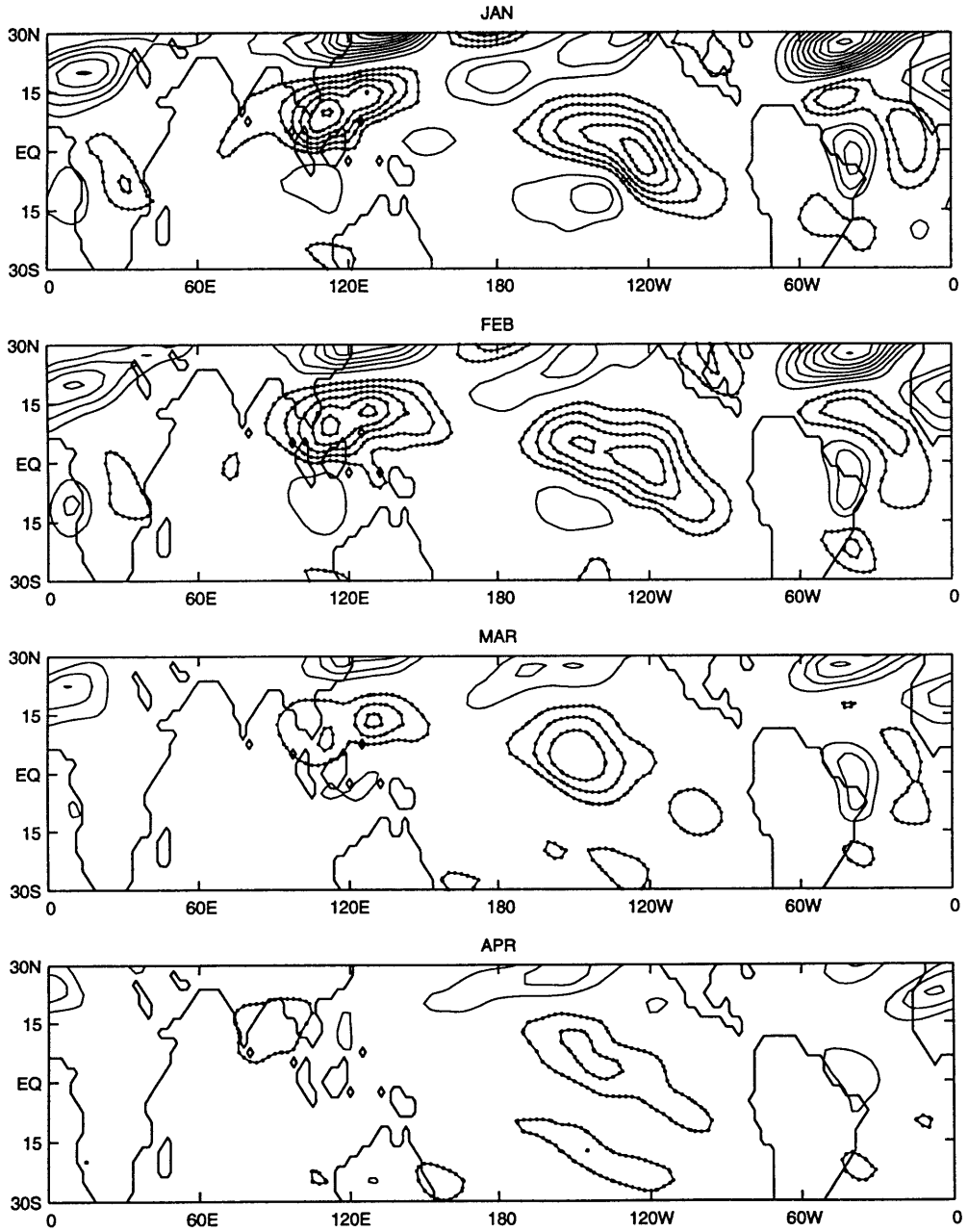

Figure A.29: As in Figure A.28 but for May to August.

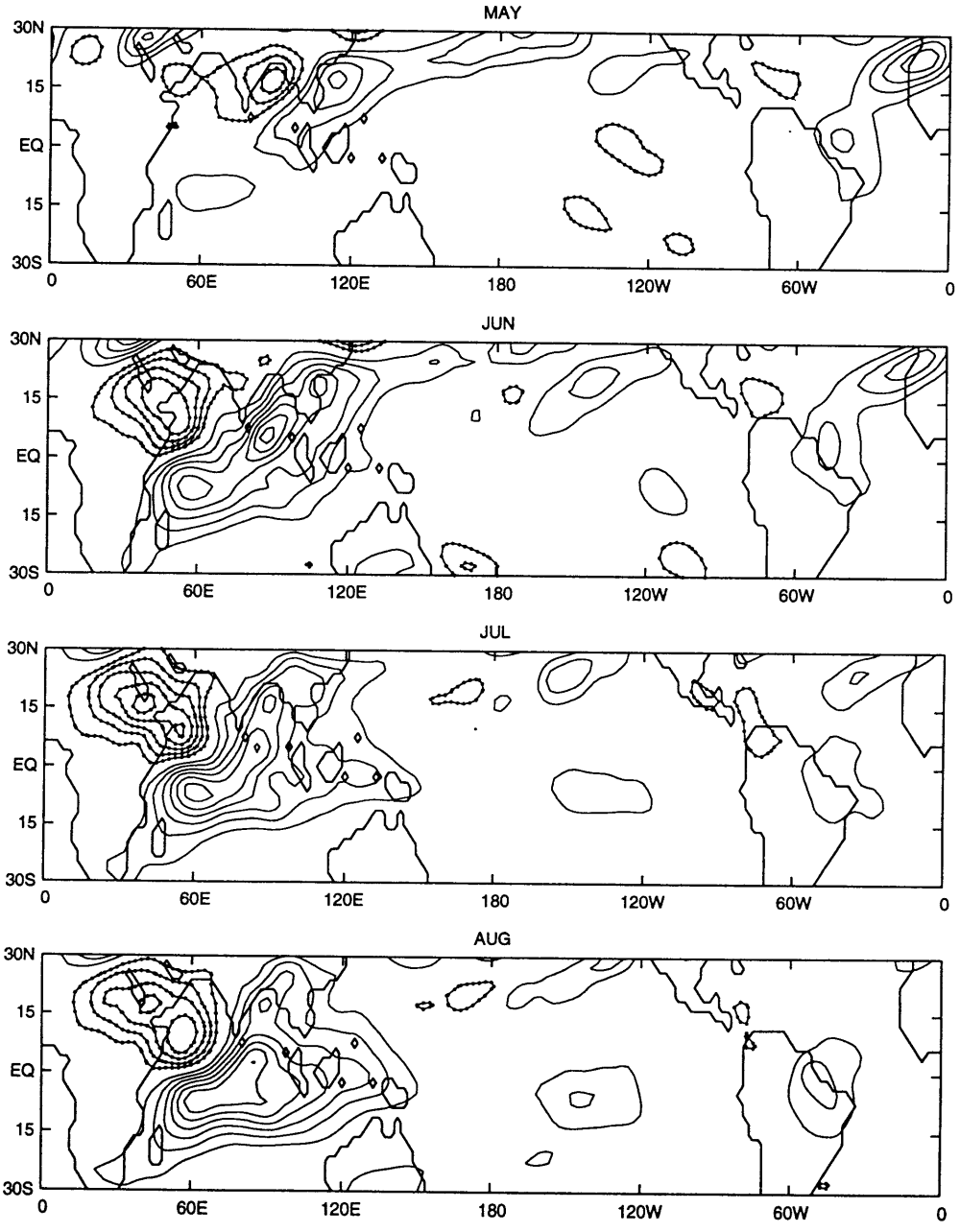

Figure A.30: As in Figure A.28 but for September to December.

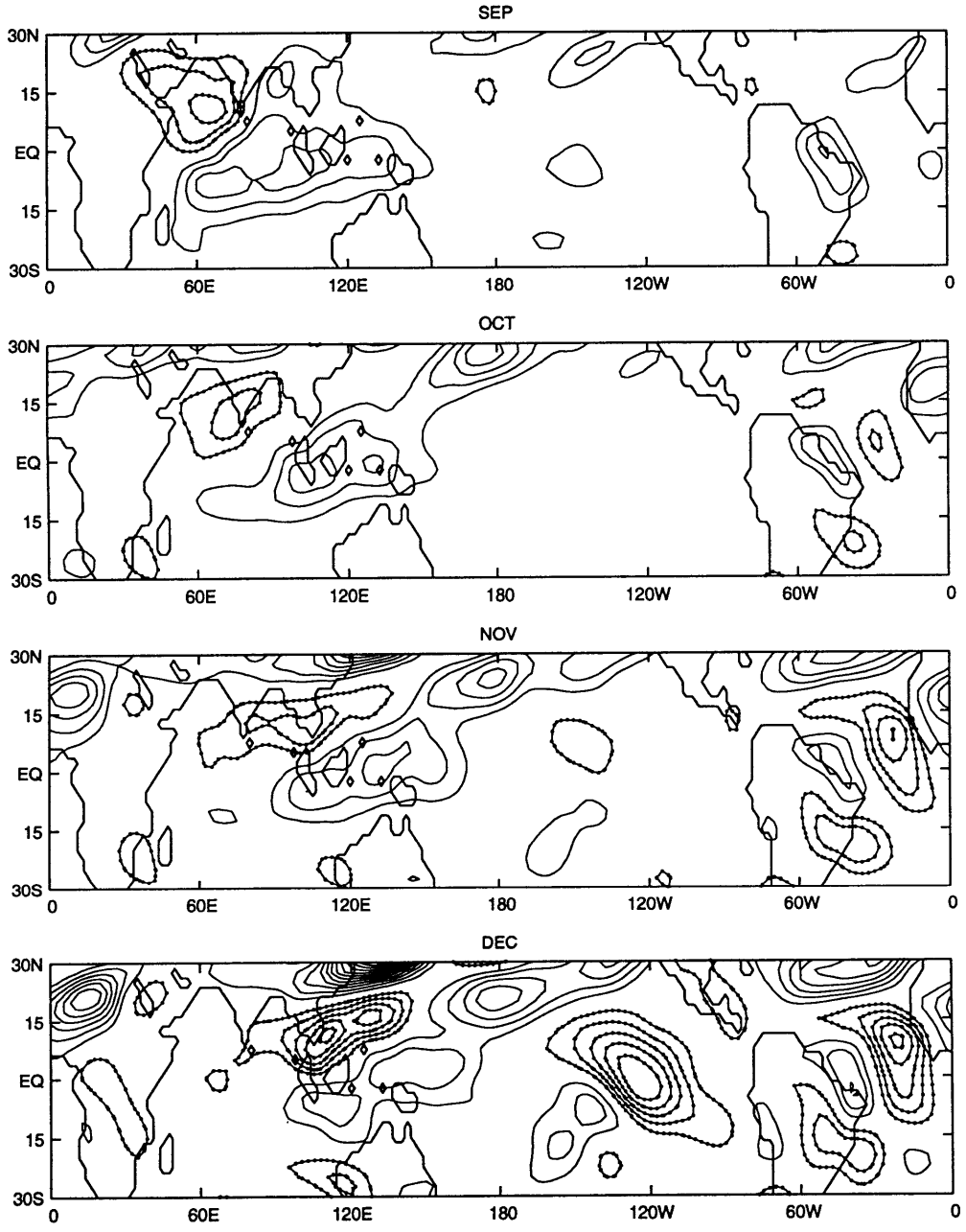

Figure A.31: Time series of mean $\bar{u}^*\bar{v}^*$ from 5°N–10°S for January 1982 to December 1994. Contour interval 40 $m^2\ s^{-2}$.

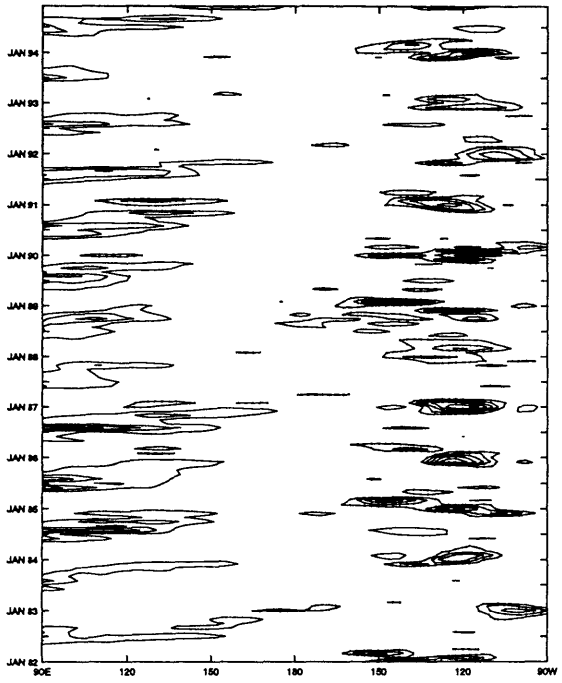

Figure A.32: Time series of $\bar{u}^*\bar{v}^*$ averaged over the latitude band 20°N–30°N. Contour interval 50 $m^2\ s^{-2}$.

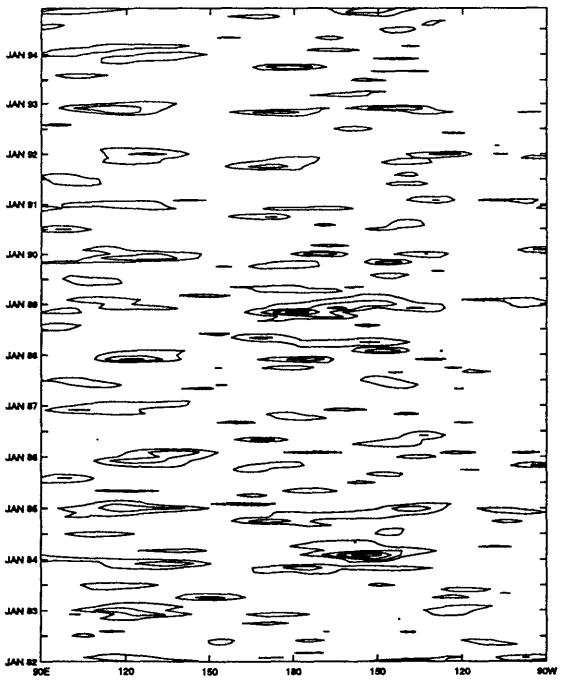

Figure A.33: Total northward transport of latent heat by quasi-stationary eddies in Petawatts. Heavy solid line is the 13 year average. Thin solid lines are the interannual standard deviation.

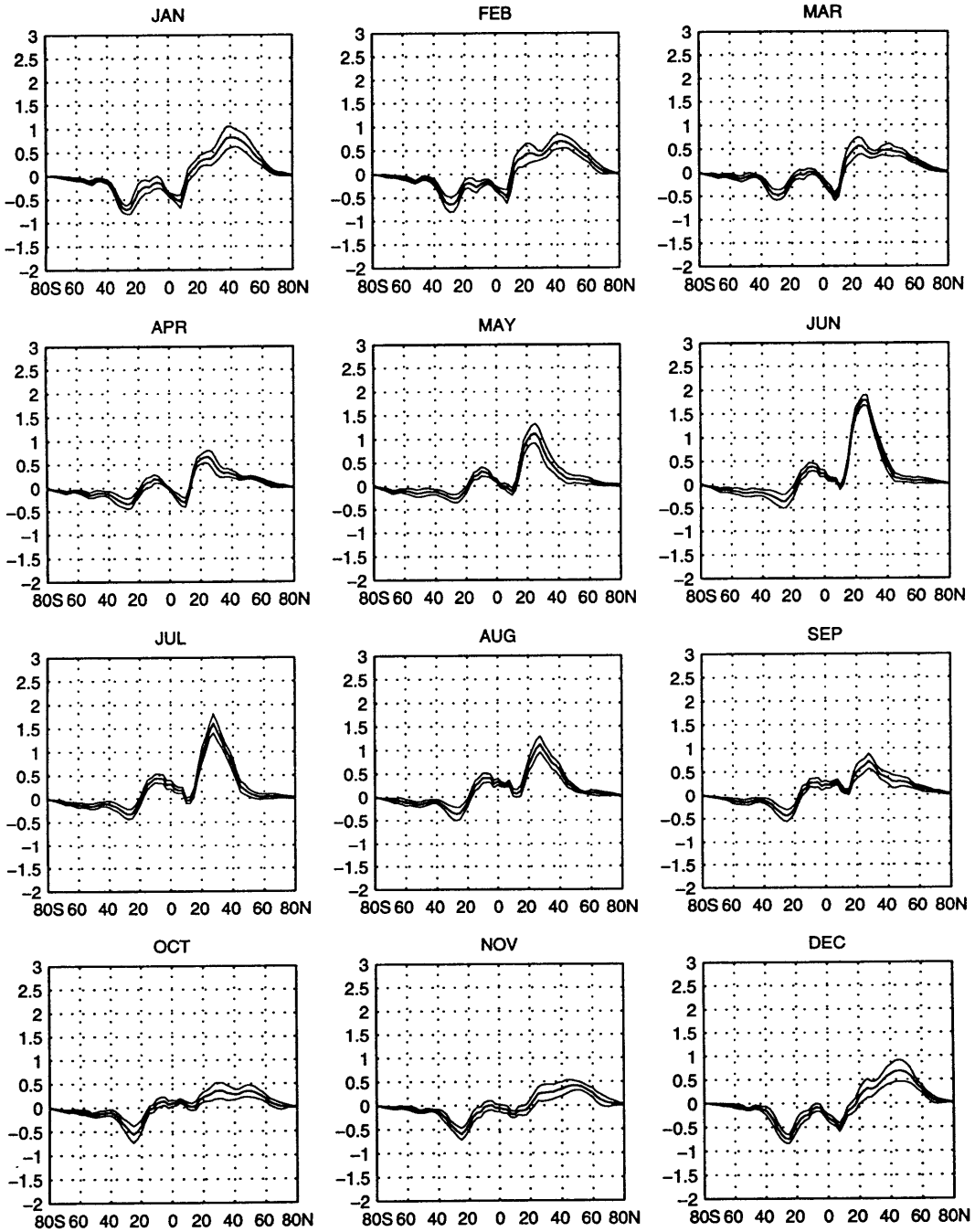

Figure A.34: Zonal mean cross-sections of the northward transport of moisture by the quasi-stationary eddies for all months. Contour interval is 1 m s^{-1} g kg^{-1}, vertical axis in hPa. Dotted lines indicate negative values.

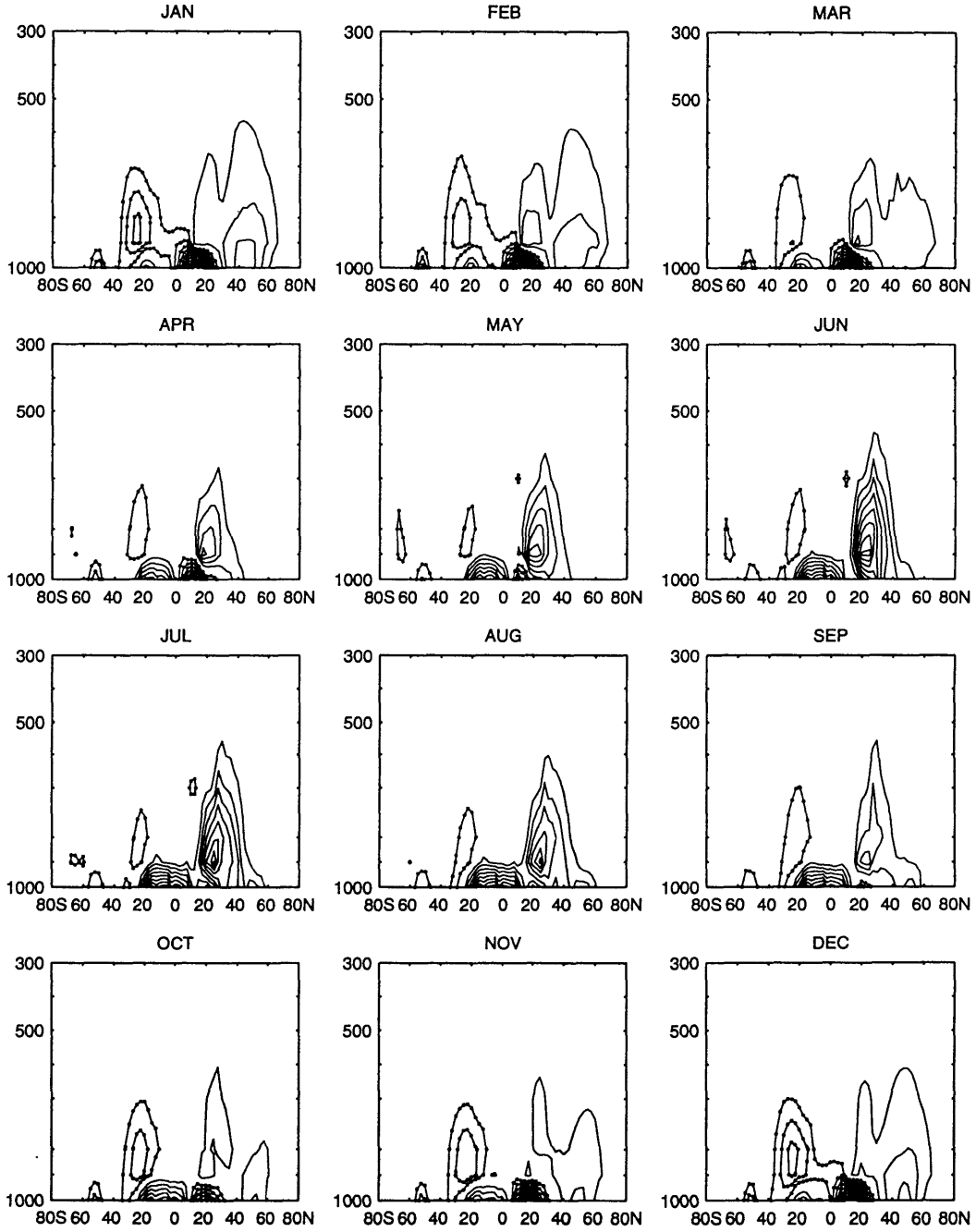

Figure A.35: Zonal mean cross-sections of the interannual standard deviation of the northward transport of moisture by quasi-stationary eddies. Contour interval is 0.2 m s^{-1} g kg^{-1}.

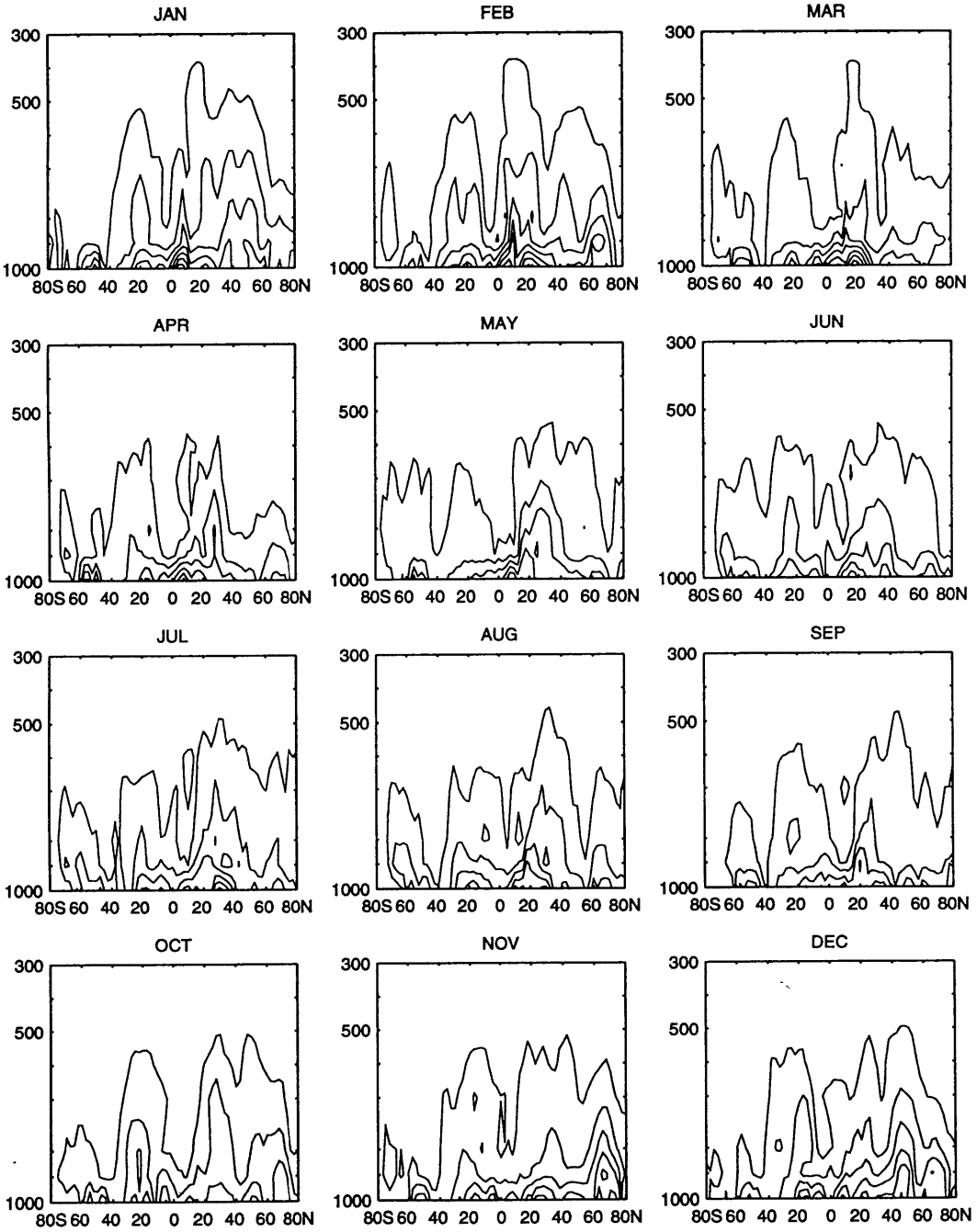

Figure A.36: Northward transport of moisture by quasi-stationary eddies at 850 hPa from January to April. Contour interval is 5 m s^{-1} g kg^{-1}. Dotted lines indicate negative values.

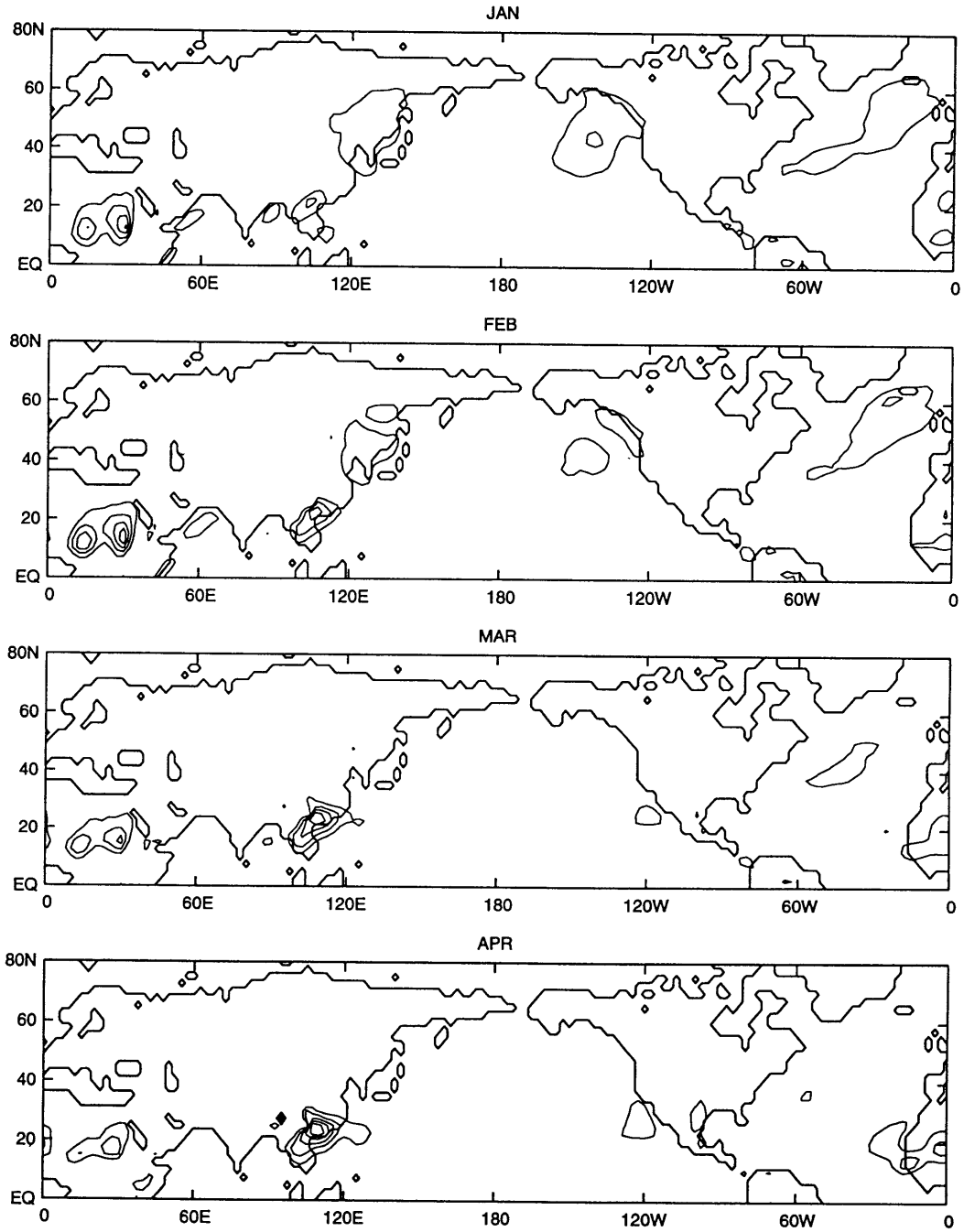

Figure A.37: As in Figure A.36 but from May to August.

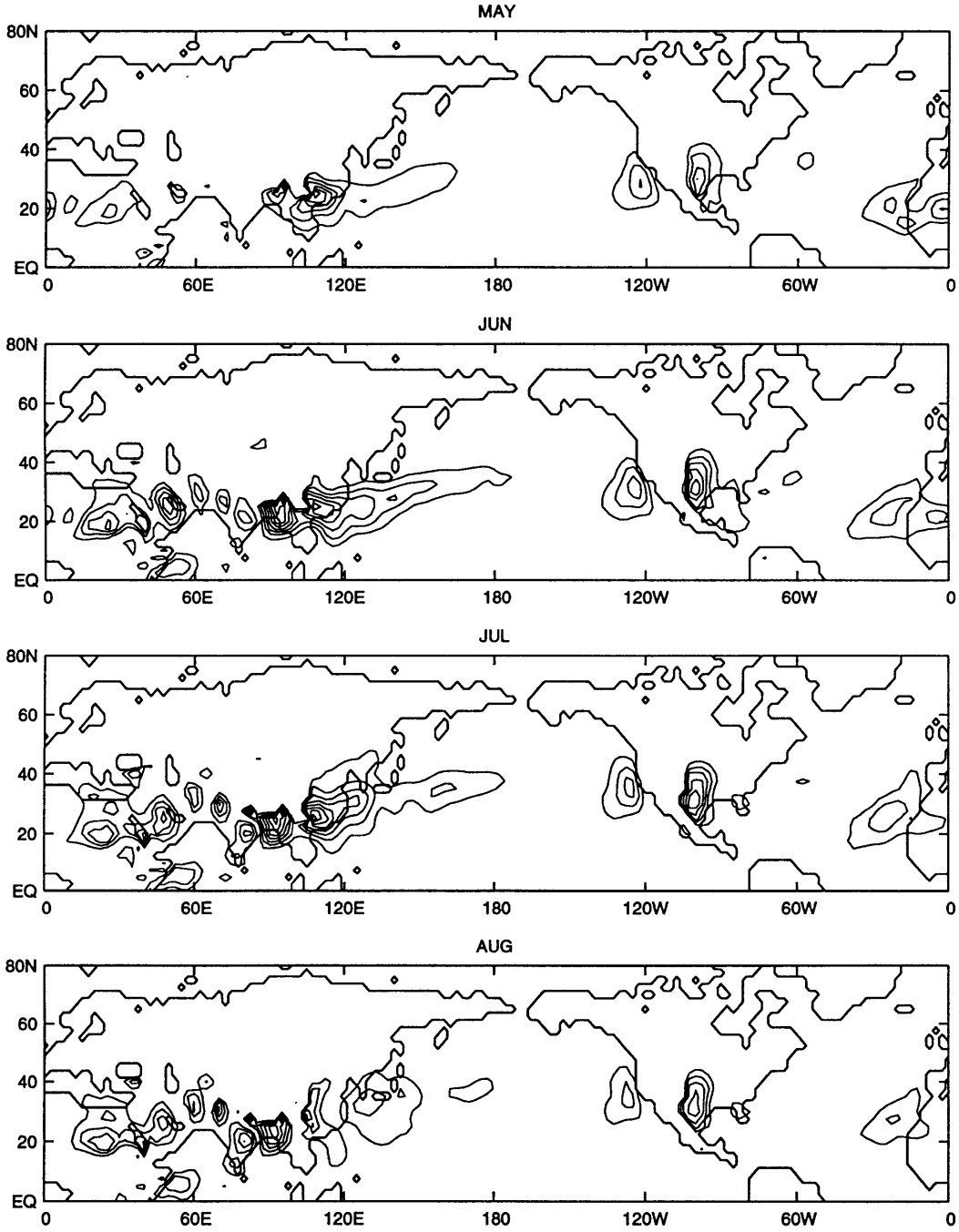

Figure A.38: As in Figure A.36 but from September to December.

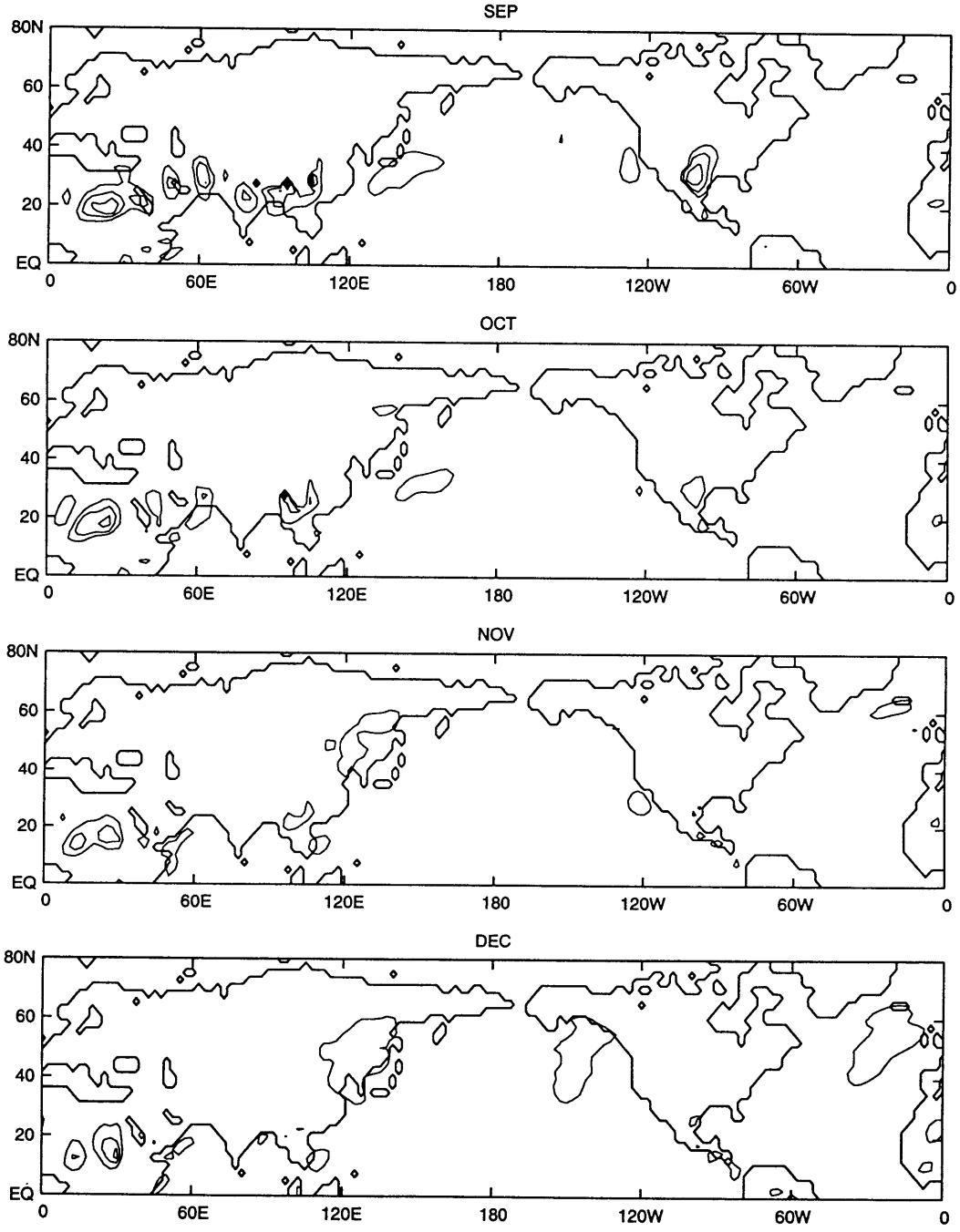

Figure A.39: Northward transport of moisture by quasi-stationary eddies at 850 hPa from January to April. Contour interval is 5 m s^{-1} g kg^{-1}. Dotted lines indicate negative values.

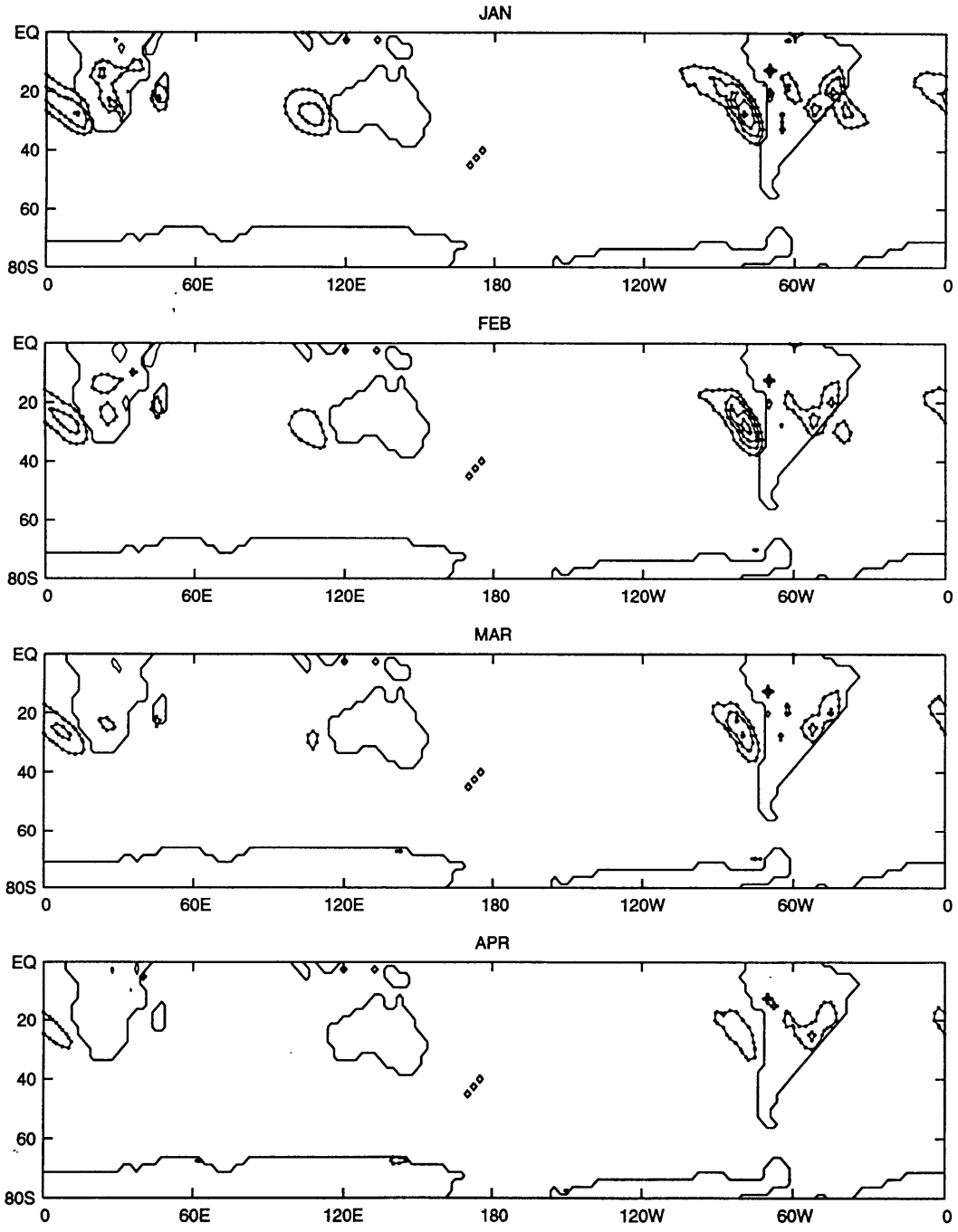

Figure A.40: As in Figure A.39 but for May to August.

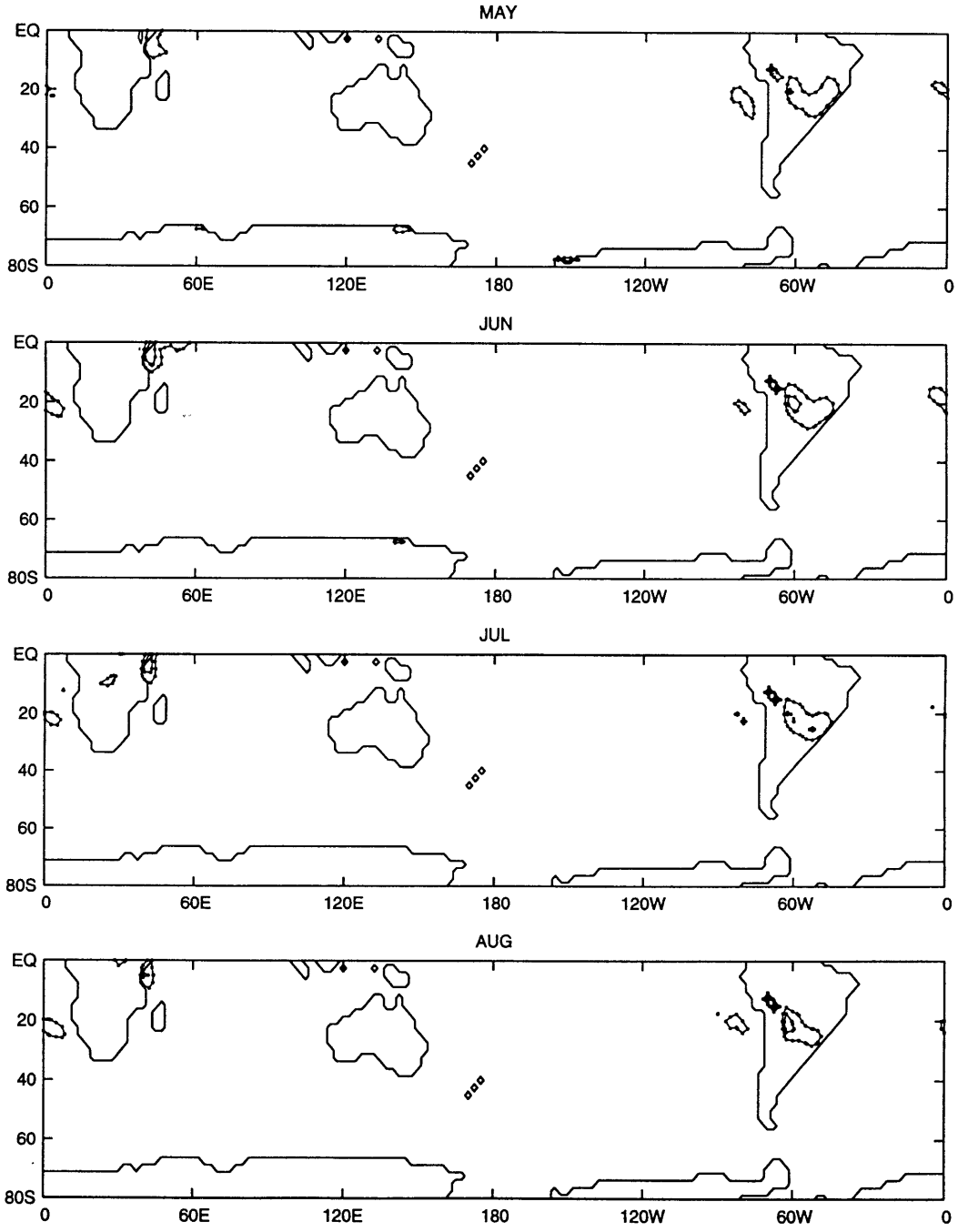

Figure A.41: As in Figure A.39 but for September to December.

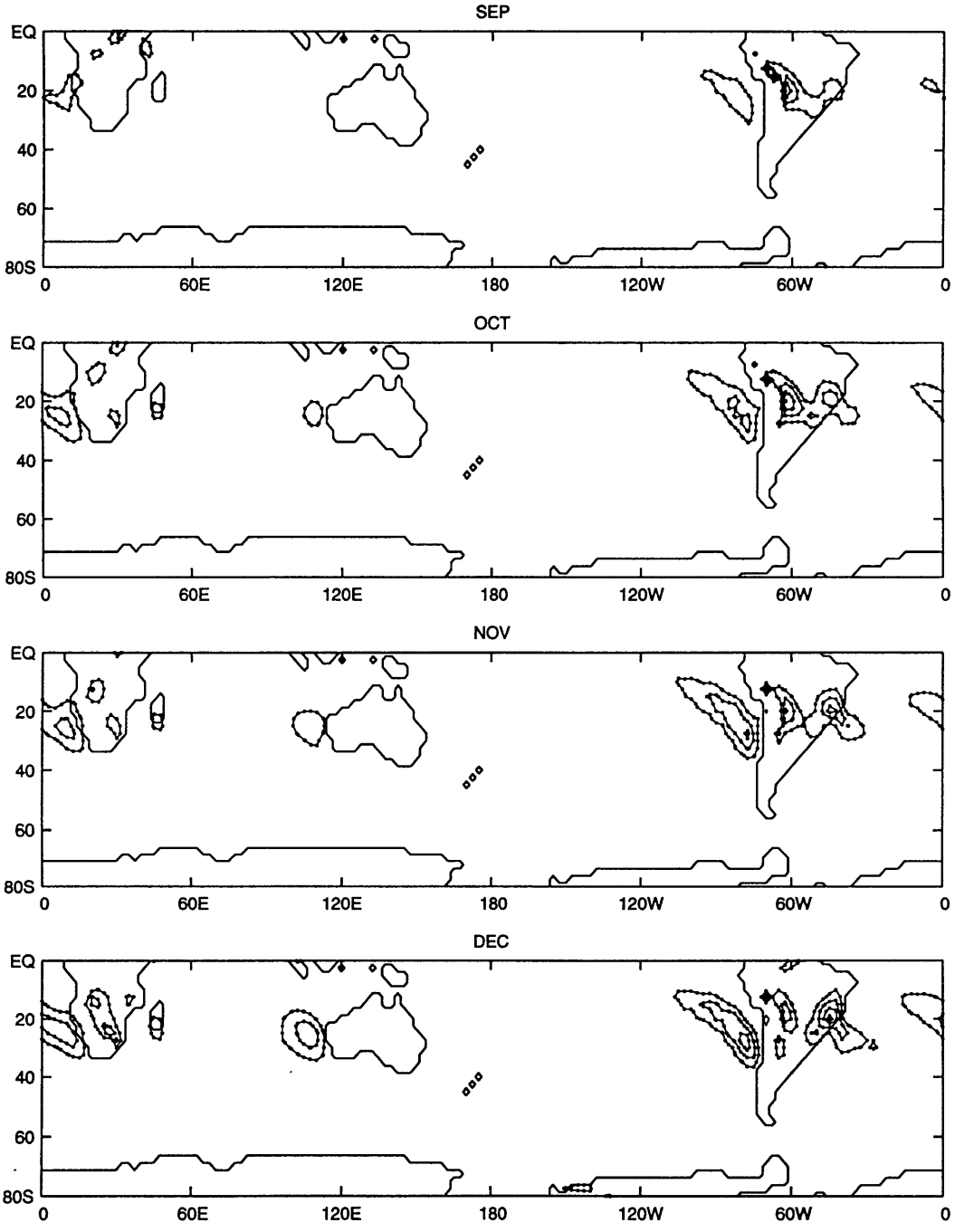

Figure A.42: Northward transport of moisture by quasi-stationary eddies at 850 hPa from January to April. Contour interval is 5 m s^{-1} g kg^{-1}. Dotted lines indicate negative values.

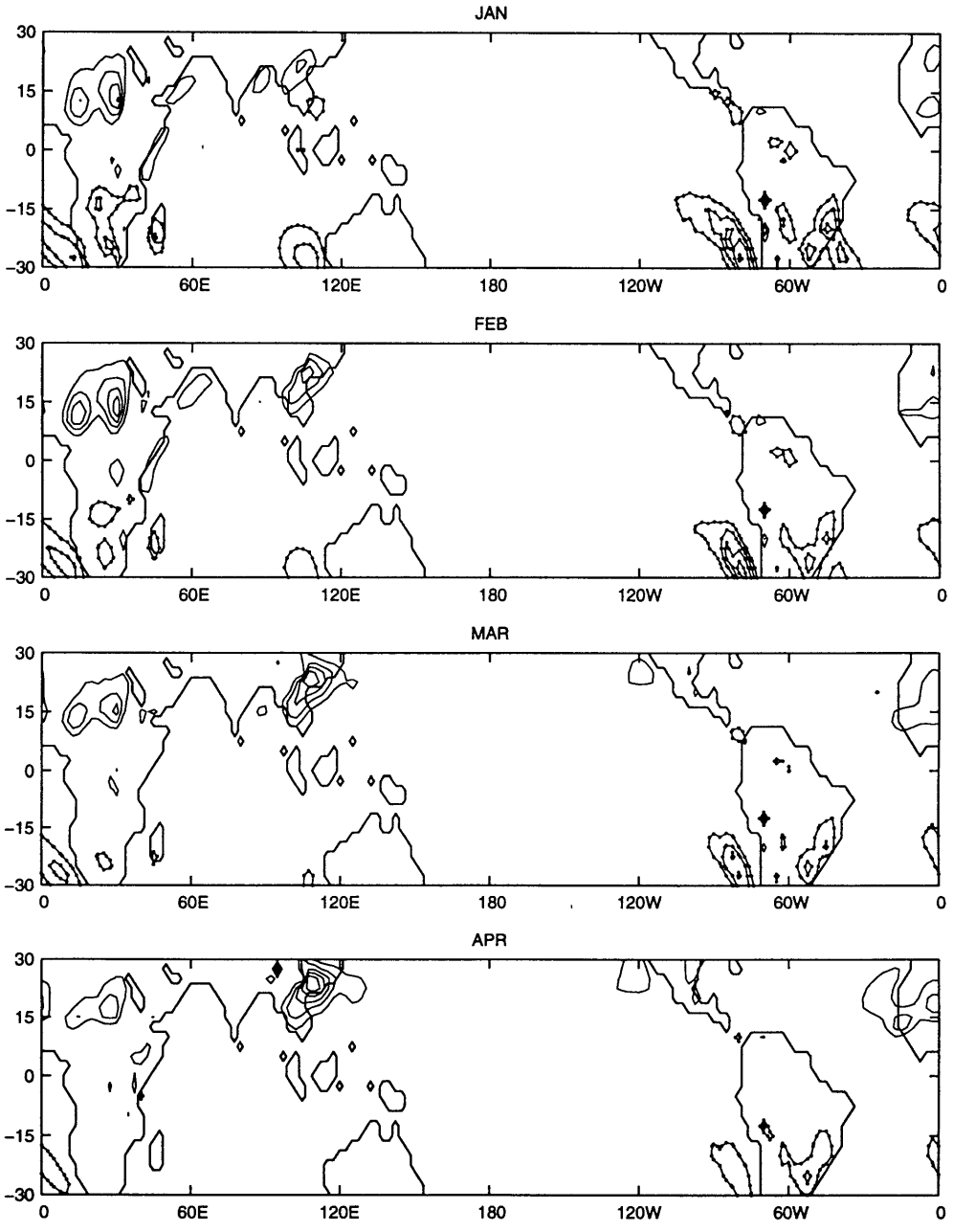

Figure A.43: As in Figure A.42 but for May to August.

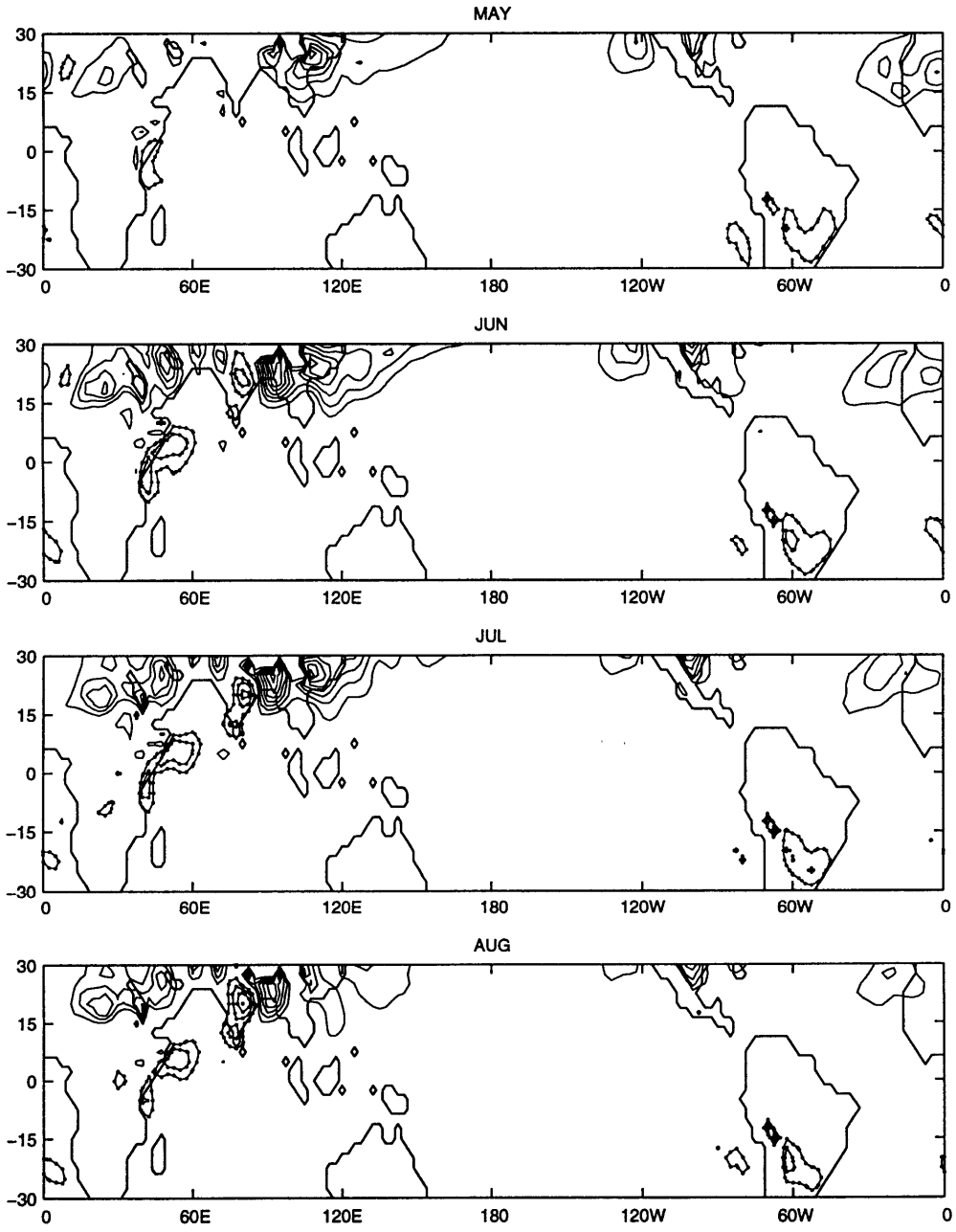

Figure A.44: As in Figure A.42 but from September to December.

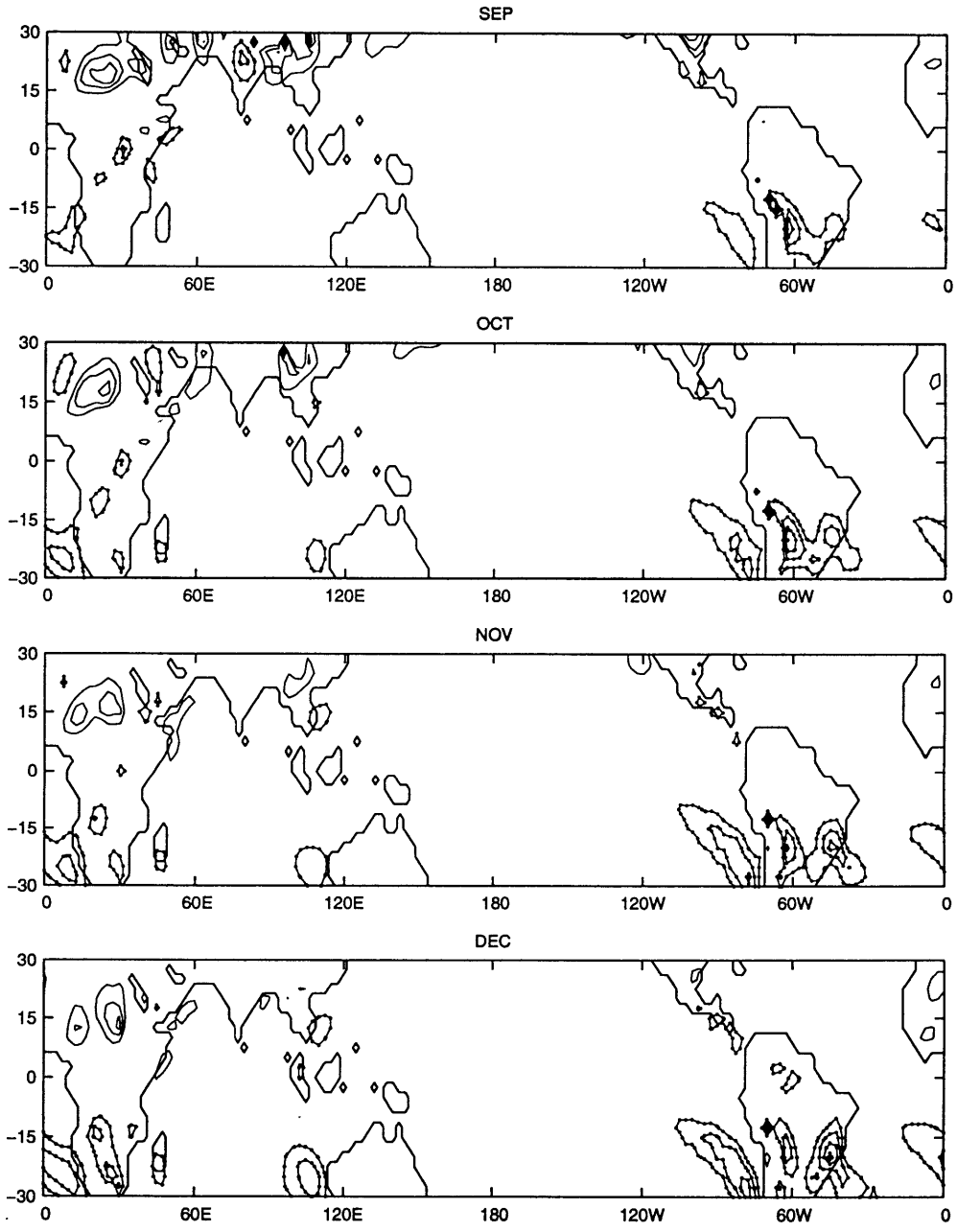

Figure A.45: Interannual standard deviation of the northward transport of moisture by quasi-stationary eddies at 850 hPa from January to April. Contour interval is 5 m s^{-1} g kg^{-1}.

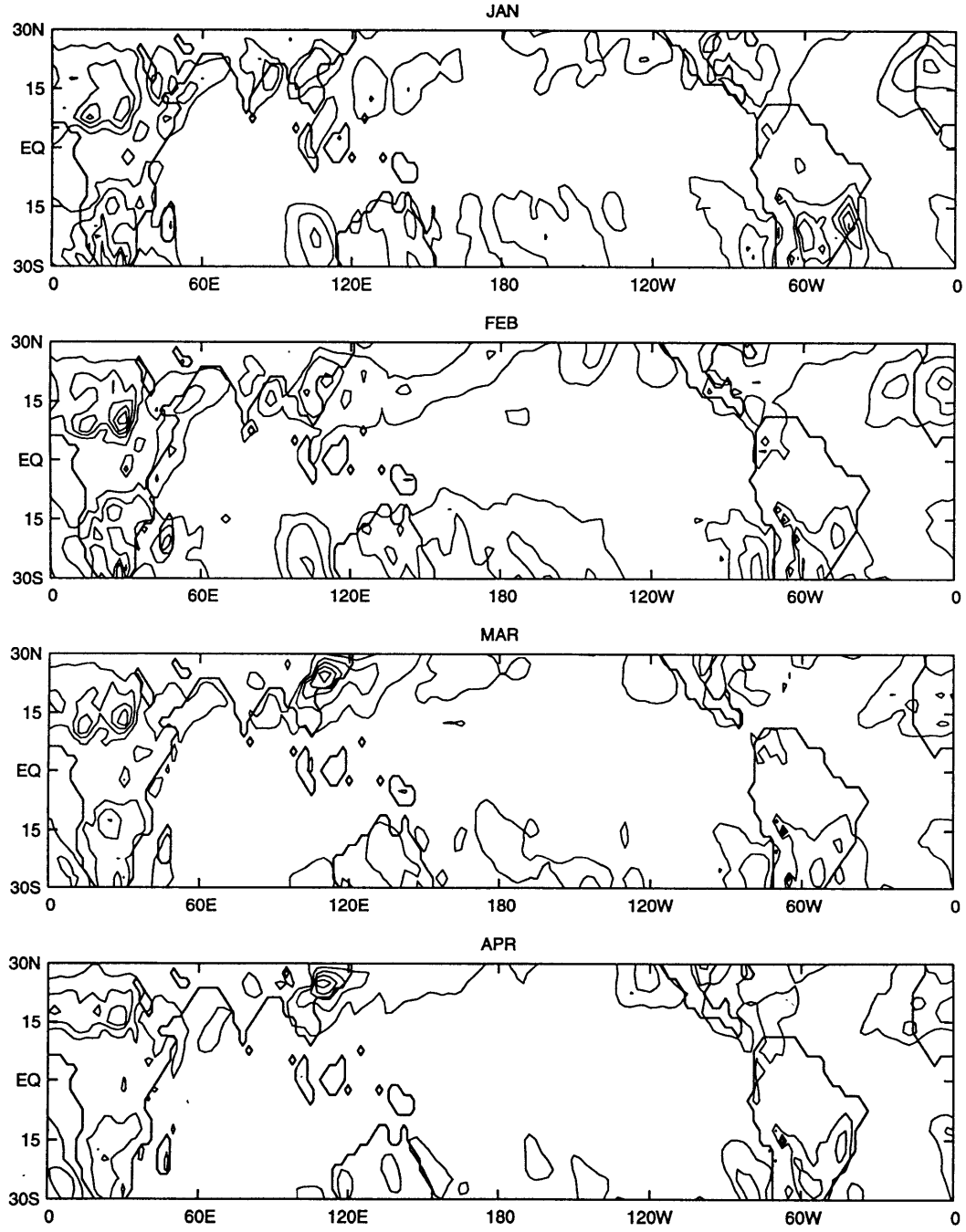

Figure A.46: Interannual standard deviation of the northward transport of moisture by quasi-stationary eddies at 850 hPa from May to August. Contour interval is 5 m s^{-1} g kg^{-1}.

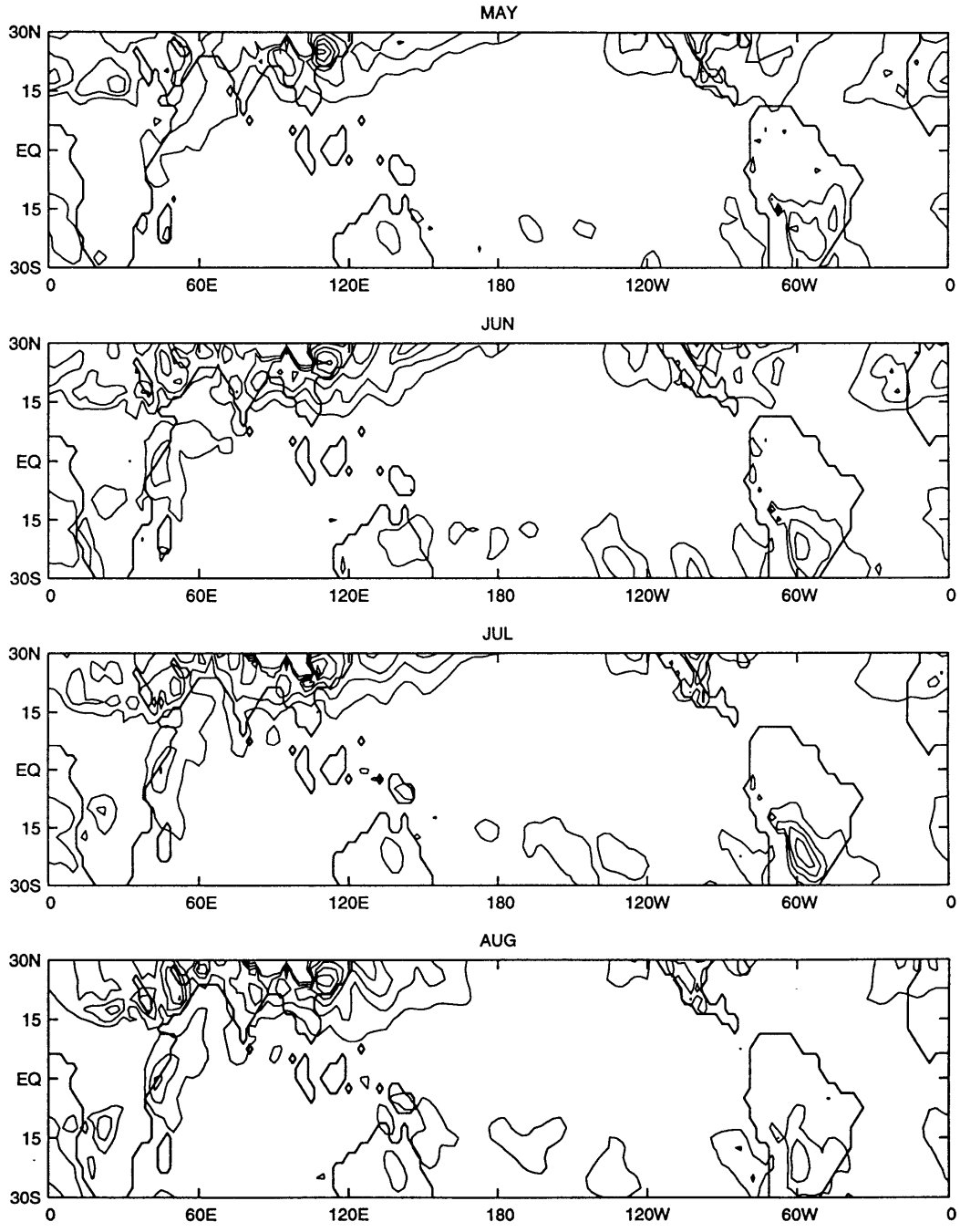

Figure A.47: Interannual standard deviation of the northward transport of moisture by quasi-stationary eddies at 850 hPa from September to December. Contour interval is 5 m s^{-1} g kg^{-1}.

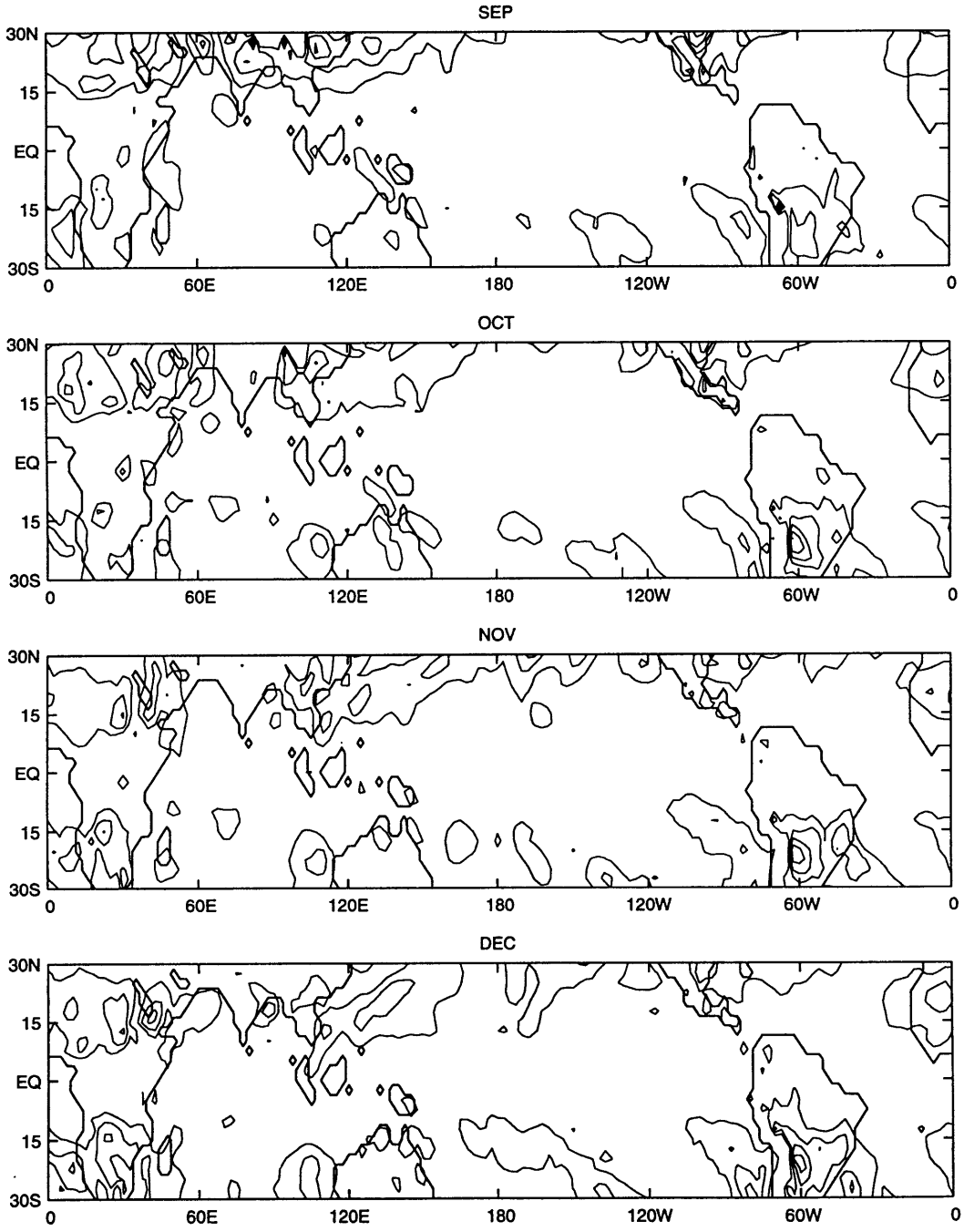

Figure A.48: Time series of $[\bar{v}^*\bar{q}^*]$ at 925 hPa averaged from 0°–10°S. Contour interval is 3m s^{-1} g kg^{-1}. Dotted lines indicate negative values.

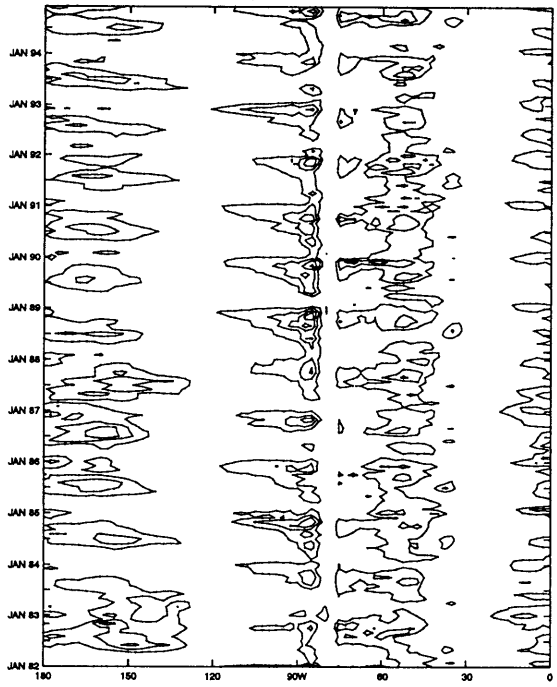

Figure A.49: As in Figure A.48 but averaged from 10°S–30°S.

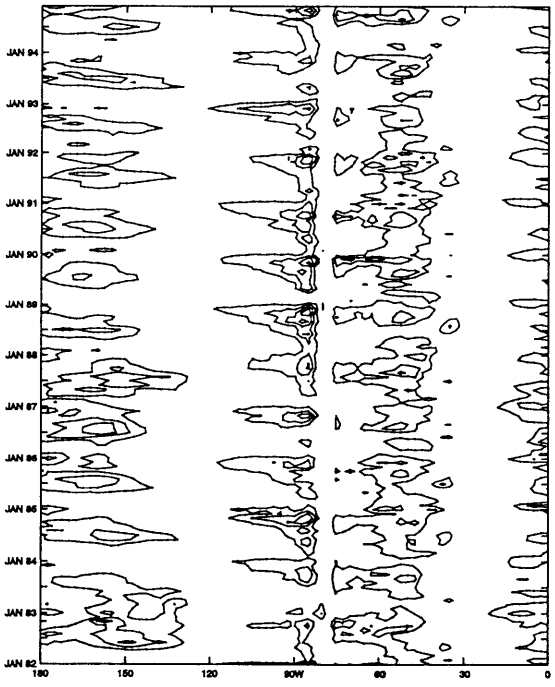

Appendix B

Zonal Scales of the Transports: Figures

The following appendix presents the figures discussed in Chapter 4.

Figure B.1: The quasi-stationary northward transport of sensible heat for wavenumber 1 at 850 hPa in °C m s^{-1}. Heavy solid line is the 13 year average. Thin solid lines represent the interannual standard deviation.

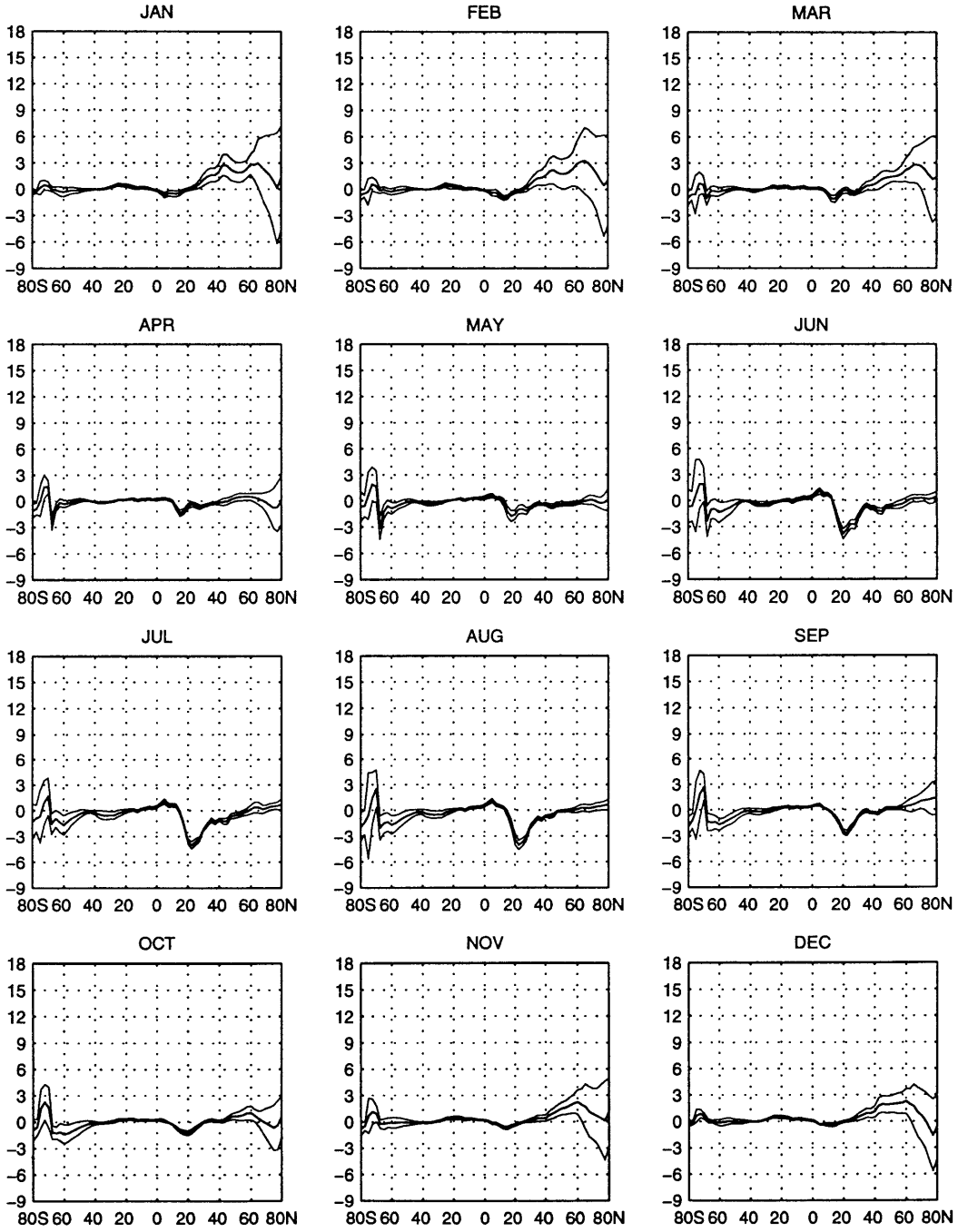

Figure B.2: As in Figure B.1 but for wavenumber 2.

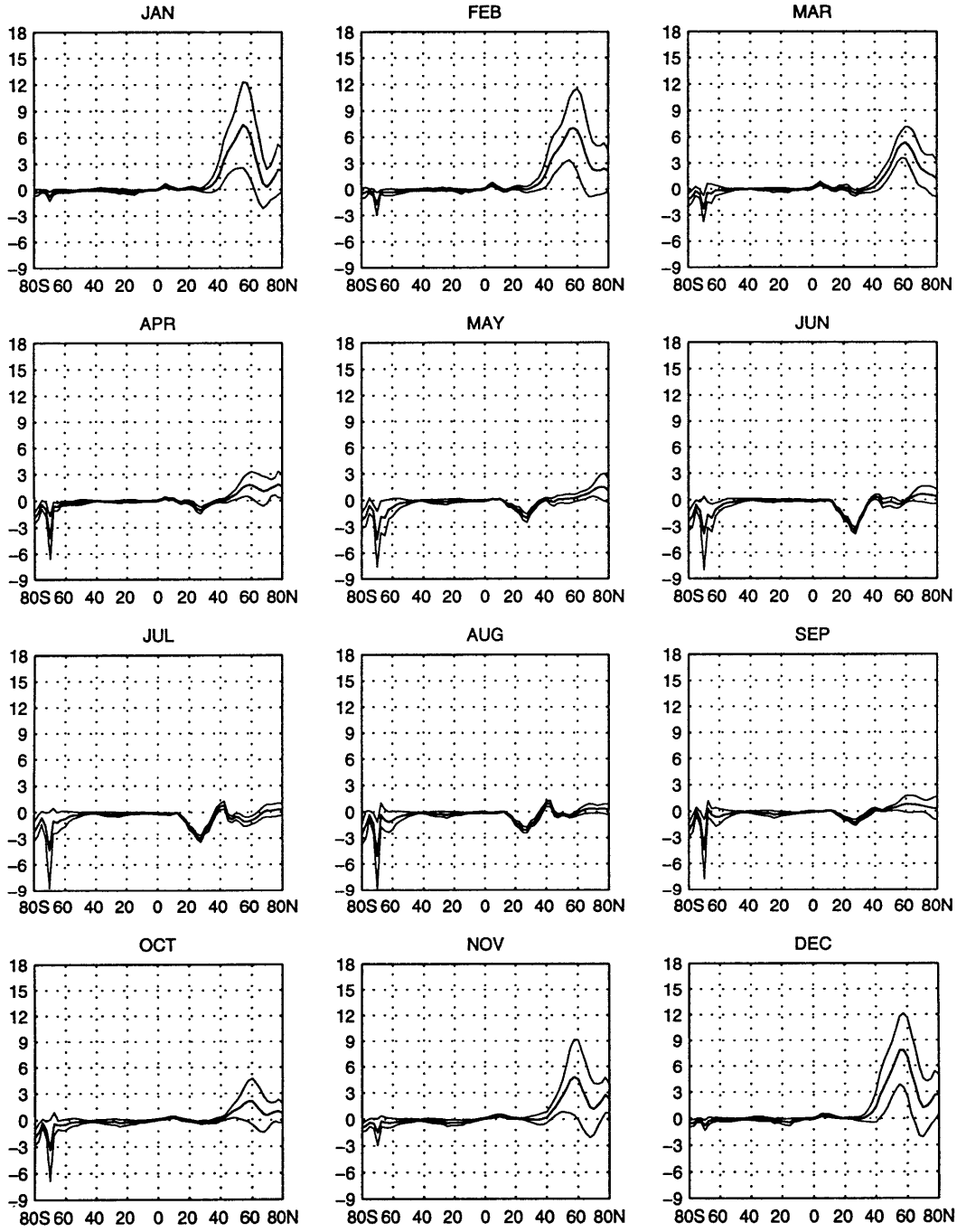

Figure B.3: As in Figure B.1 but for wavenumber 3.

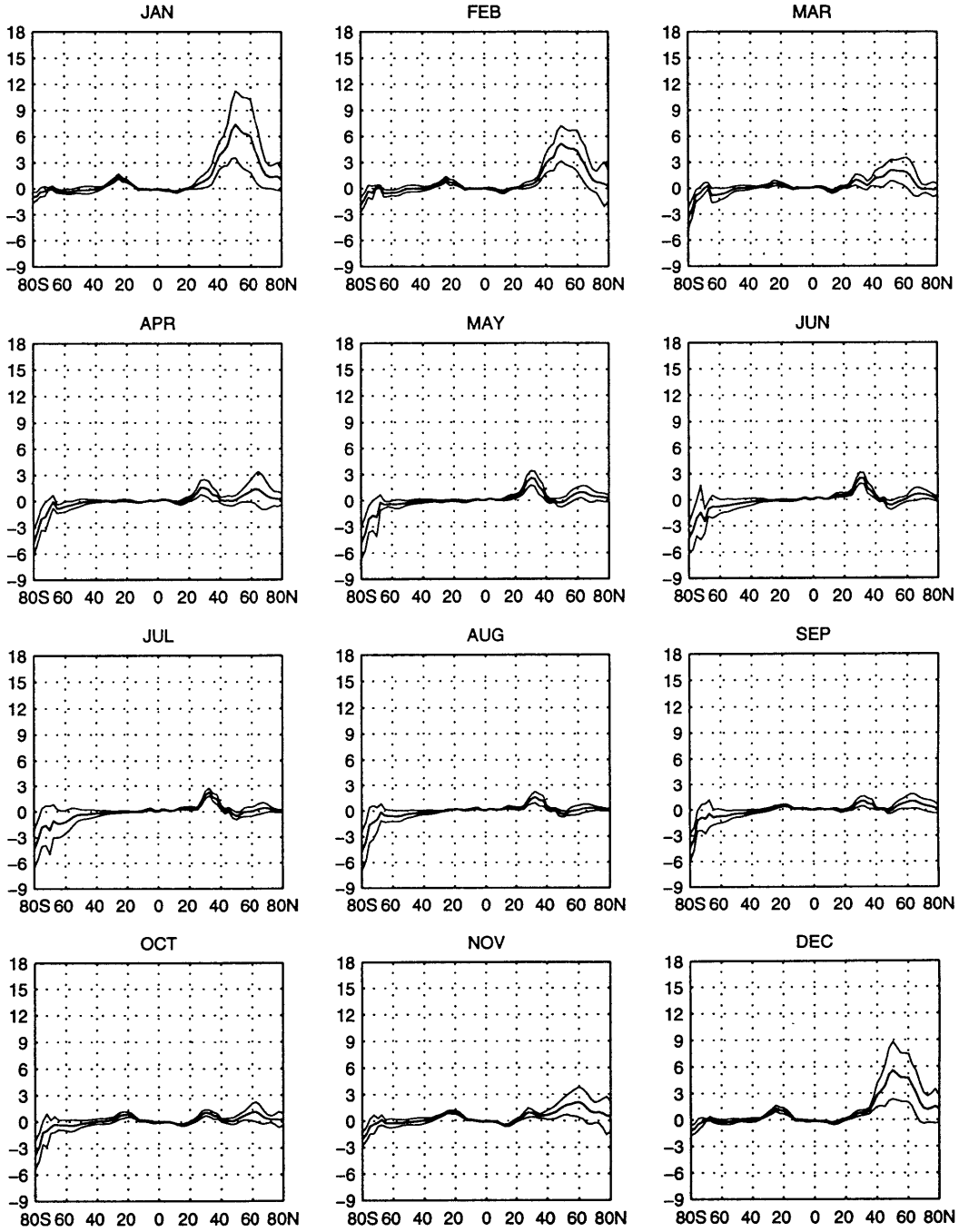

Figure B.4: As in Figure B.1 but for the sum of wavenumbers 4–72.

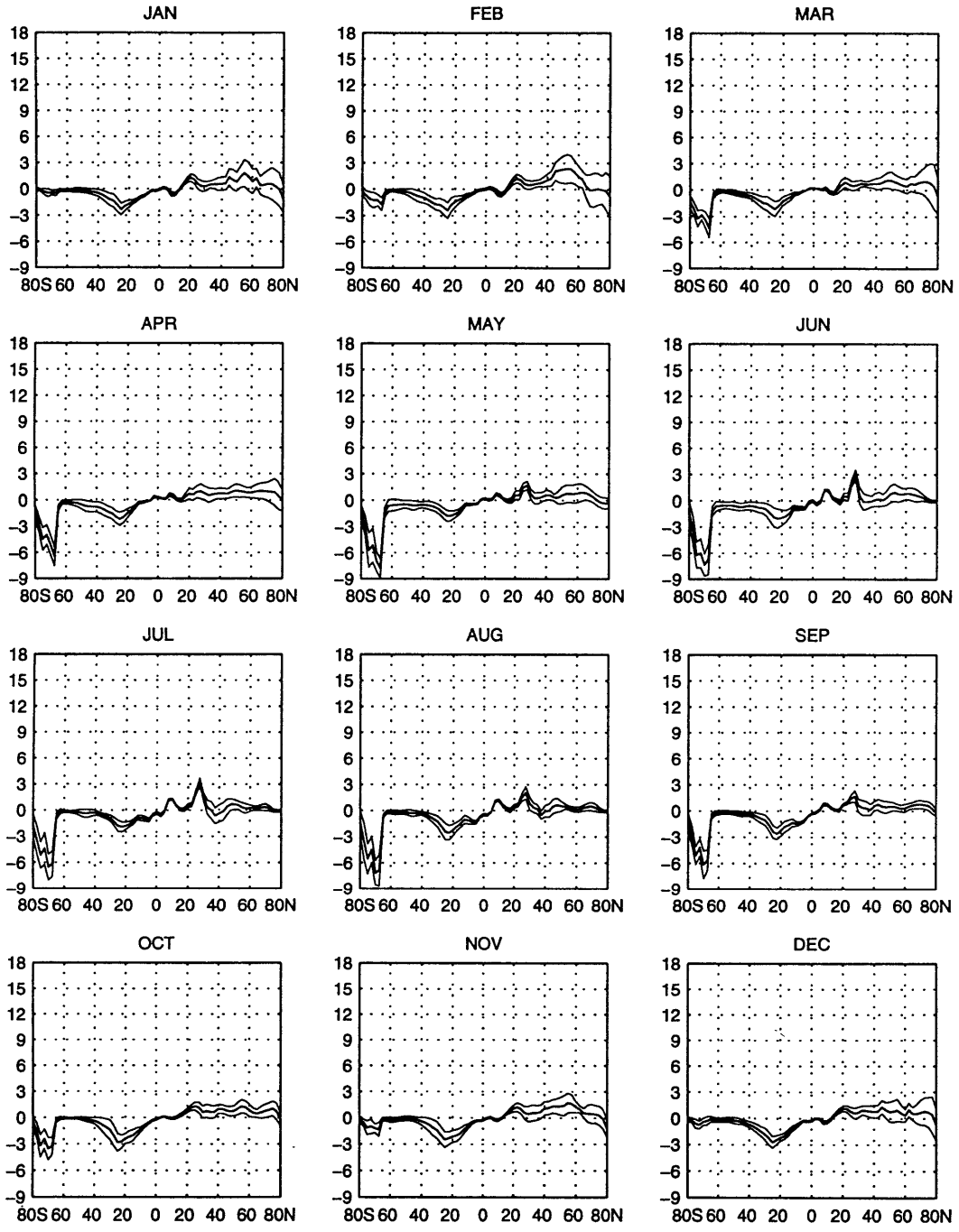

Figure B.5: The quasi-stationary northward transport of sensible heat by wavenumber 1 at 200 hPa in °C m s^{-1}. Heavy solid line is the 13 year average. Thin solid lines represent the interannual standard deviation.

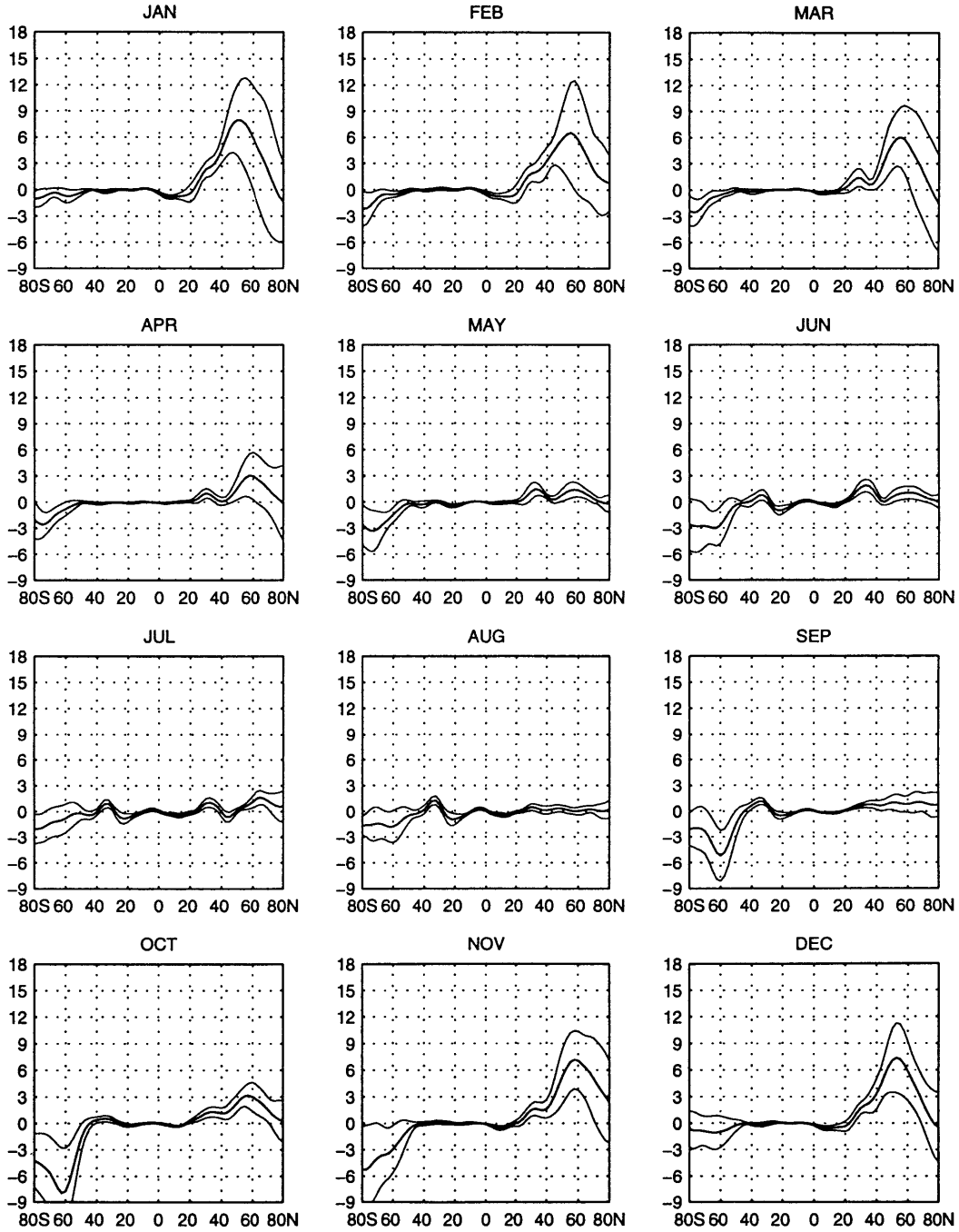

Figure B.6: As in Figure B.5 but for wavenumber 2.

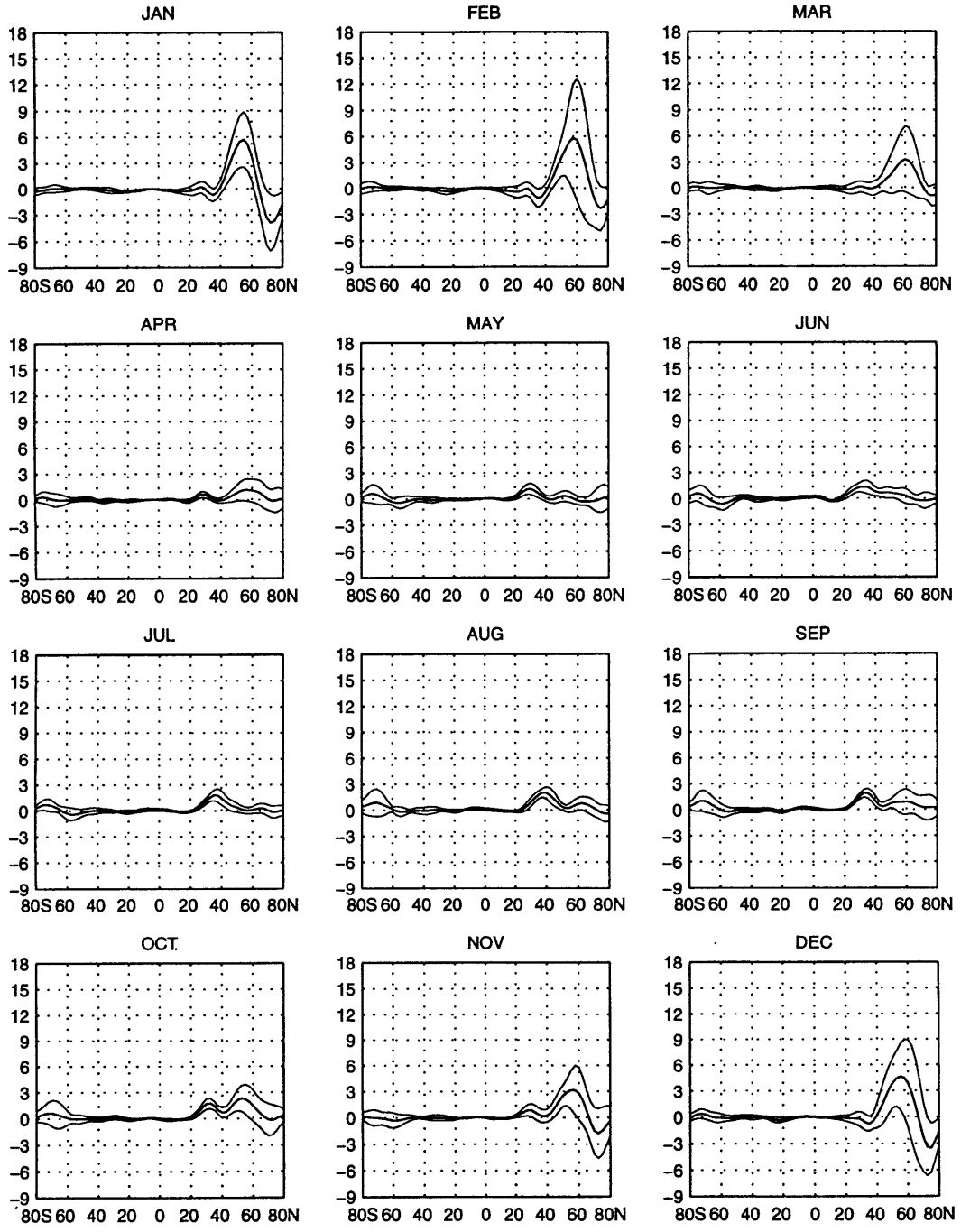

Figure B.7: As in Figure B.5 but for wavenumber 3.

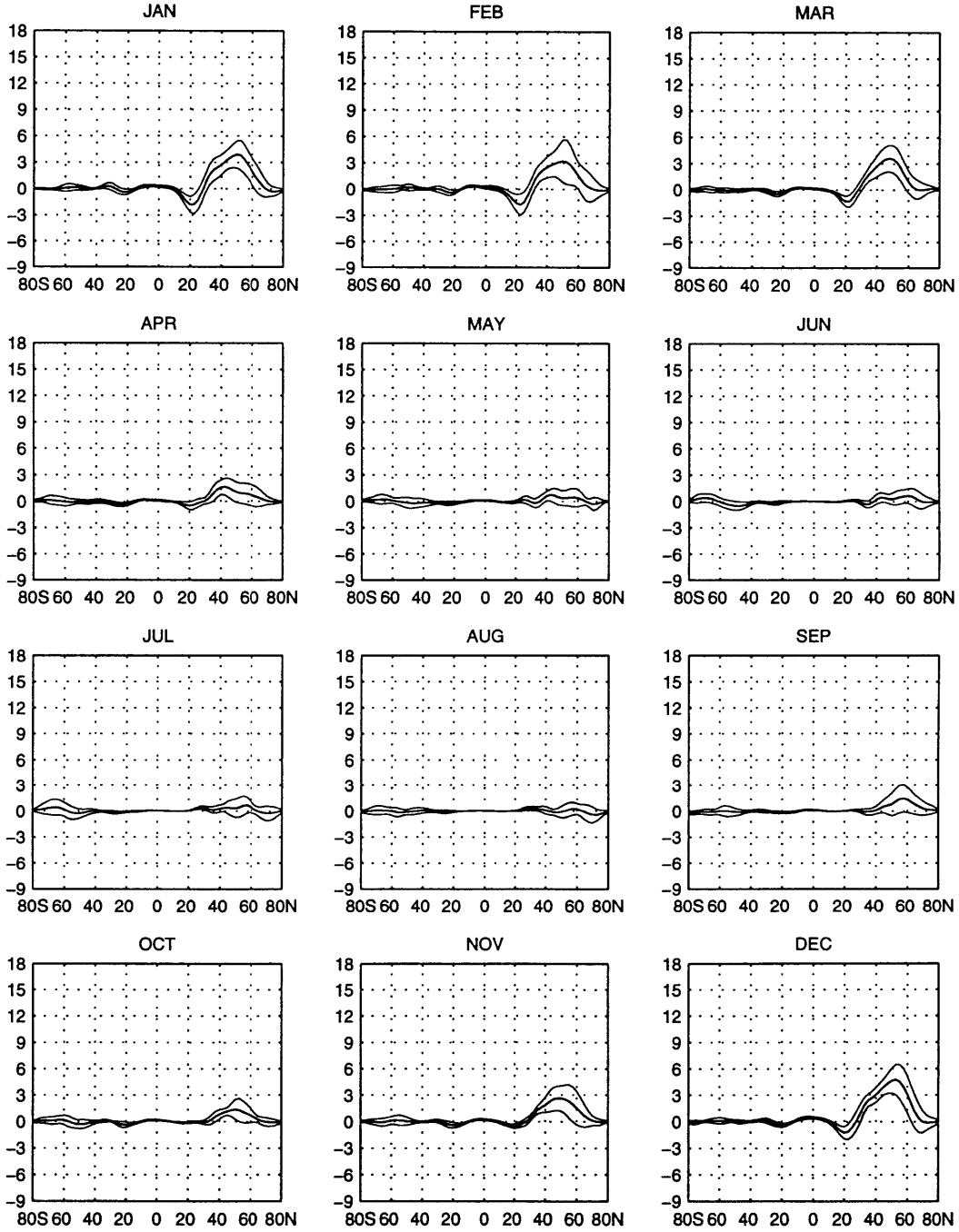

Figure B.8: As in Figure B.5 but for the sum of wavenumbers 4–72.

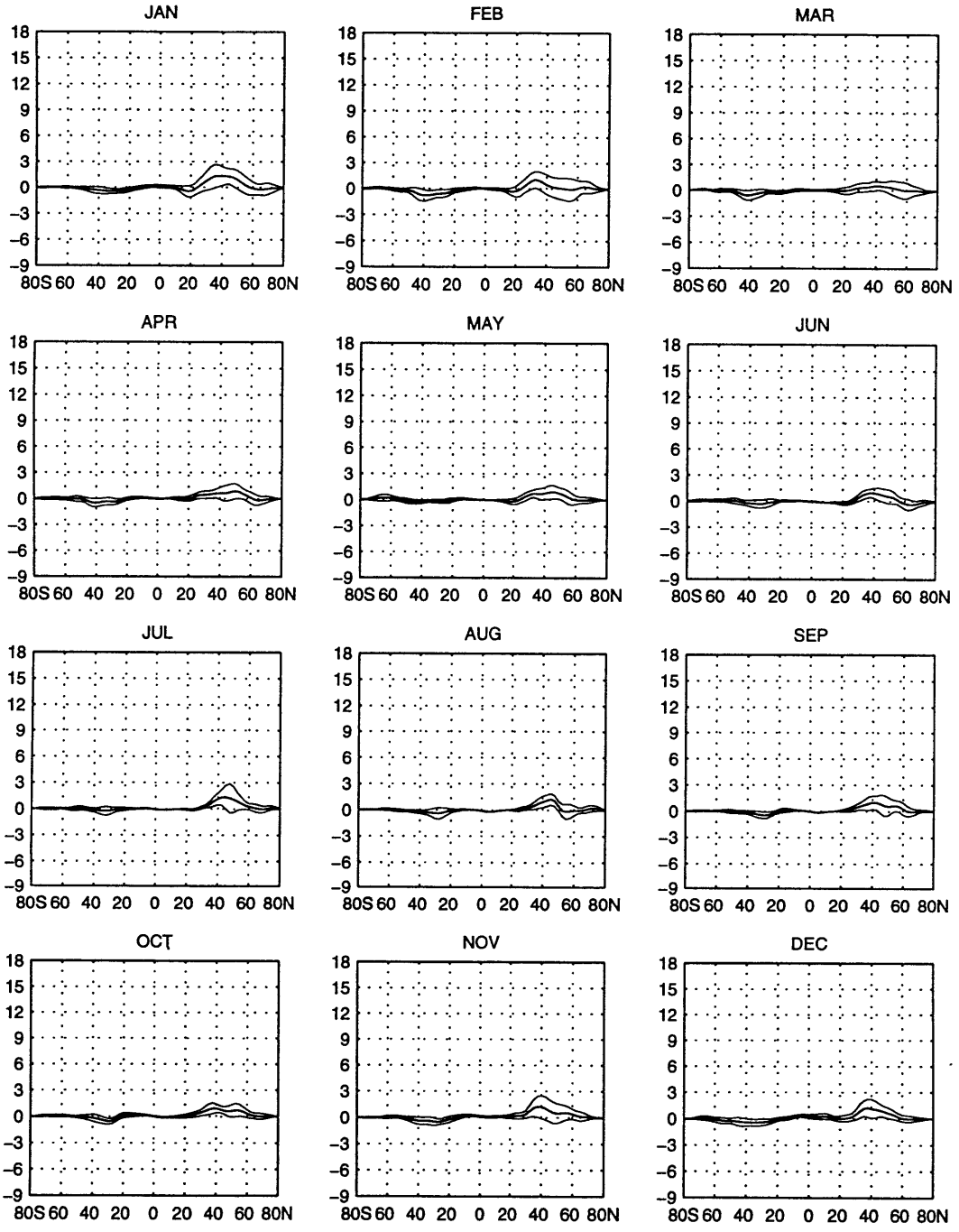

Figure B.9: As in Figure B.5 but at 10 hPa.

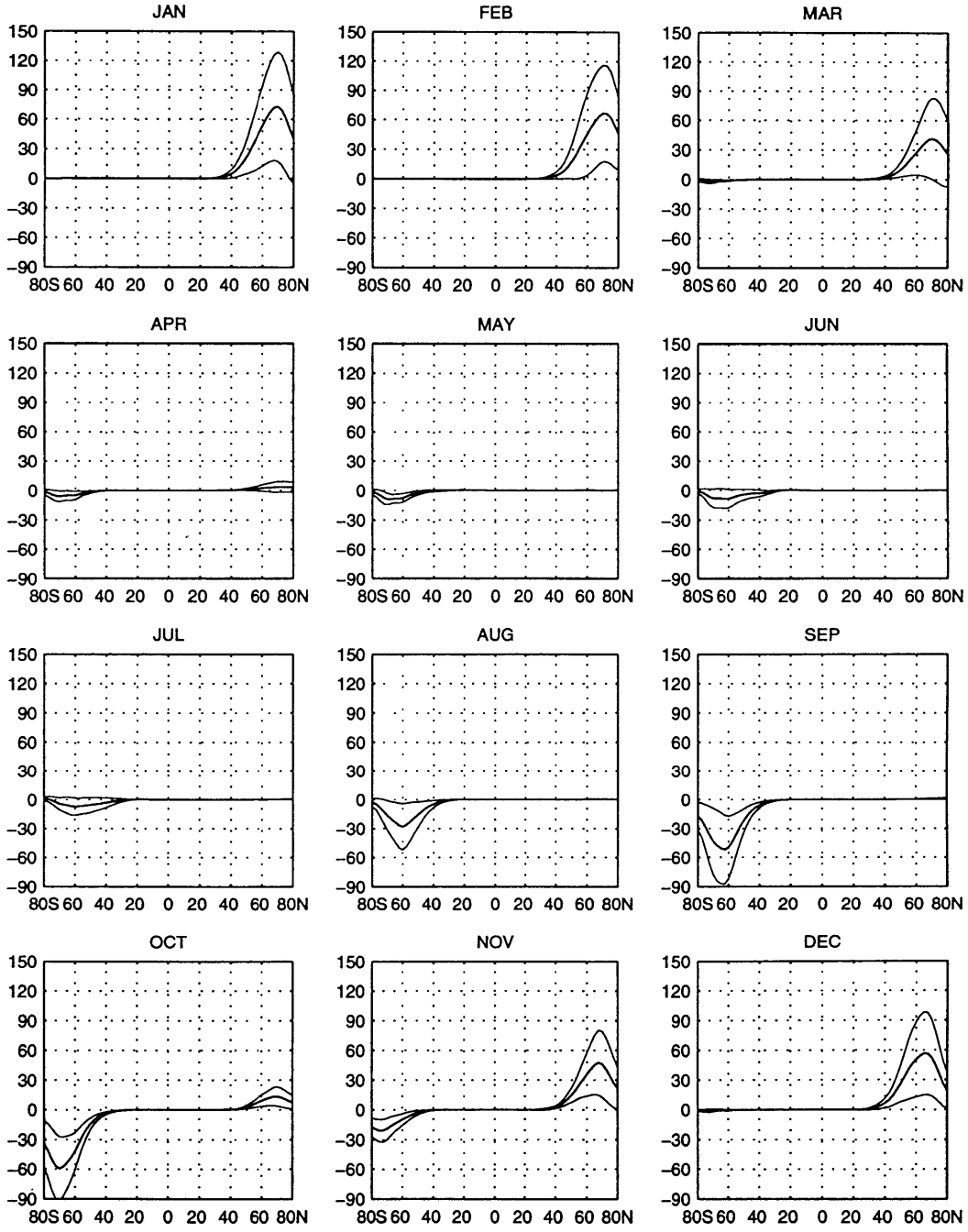

Figure B.10: As in Figure B.9 but for wavenumber 2.

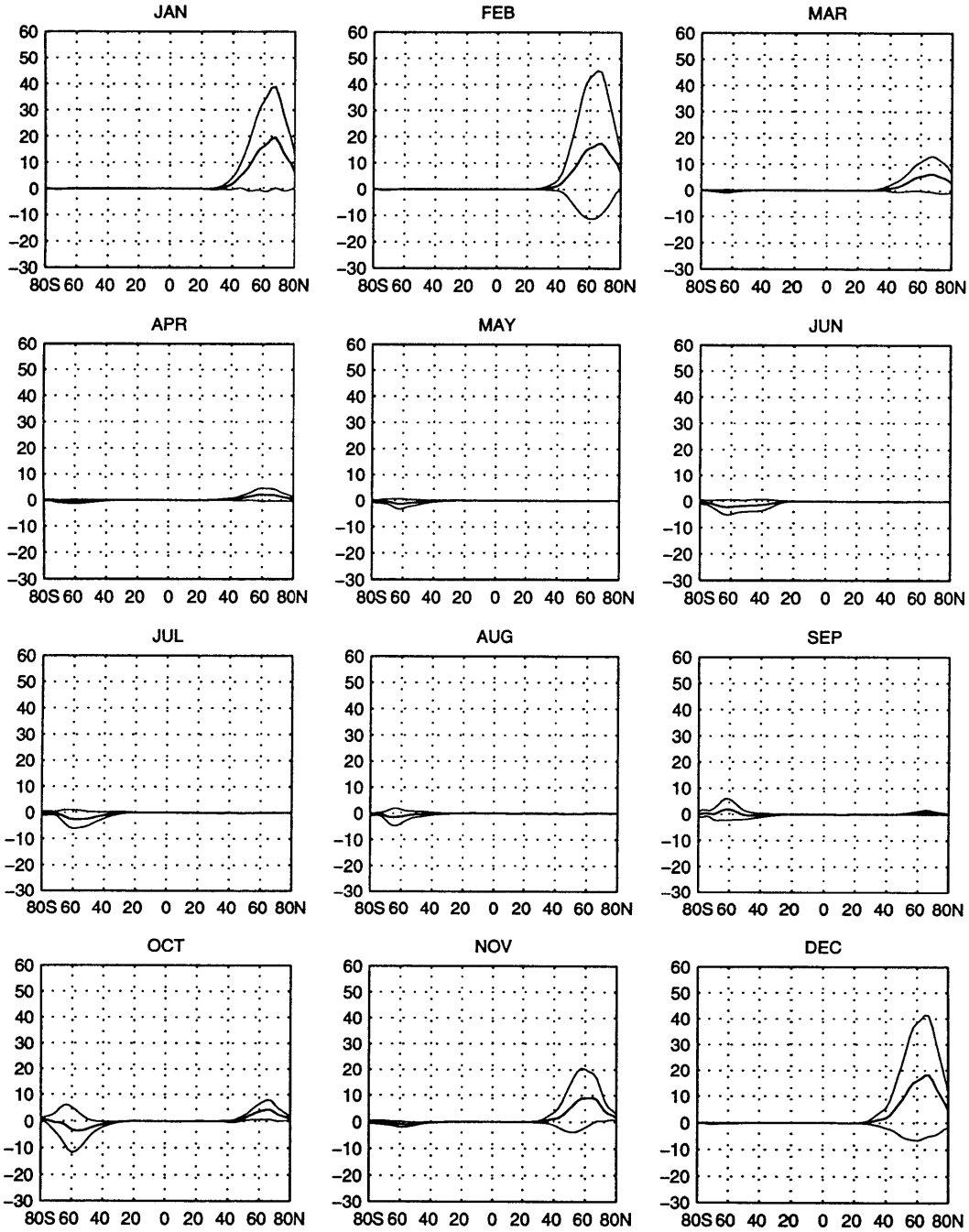

Figure B.11: As in Figure B.9 but for wavenumber 3.

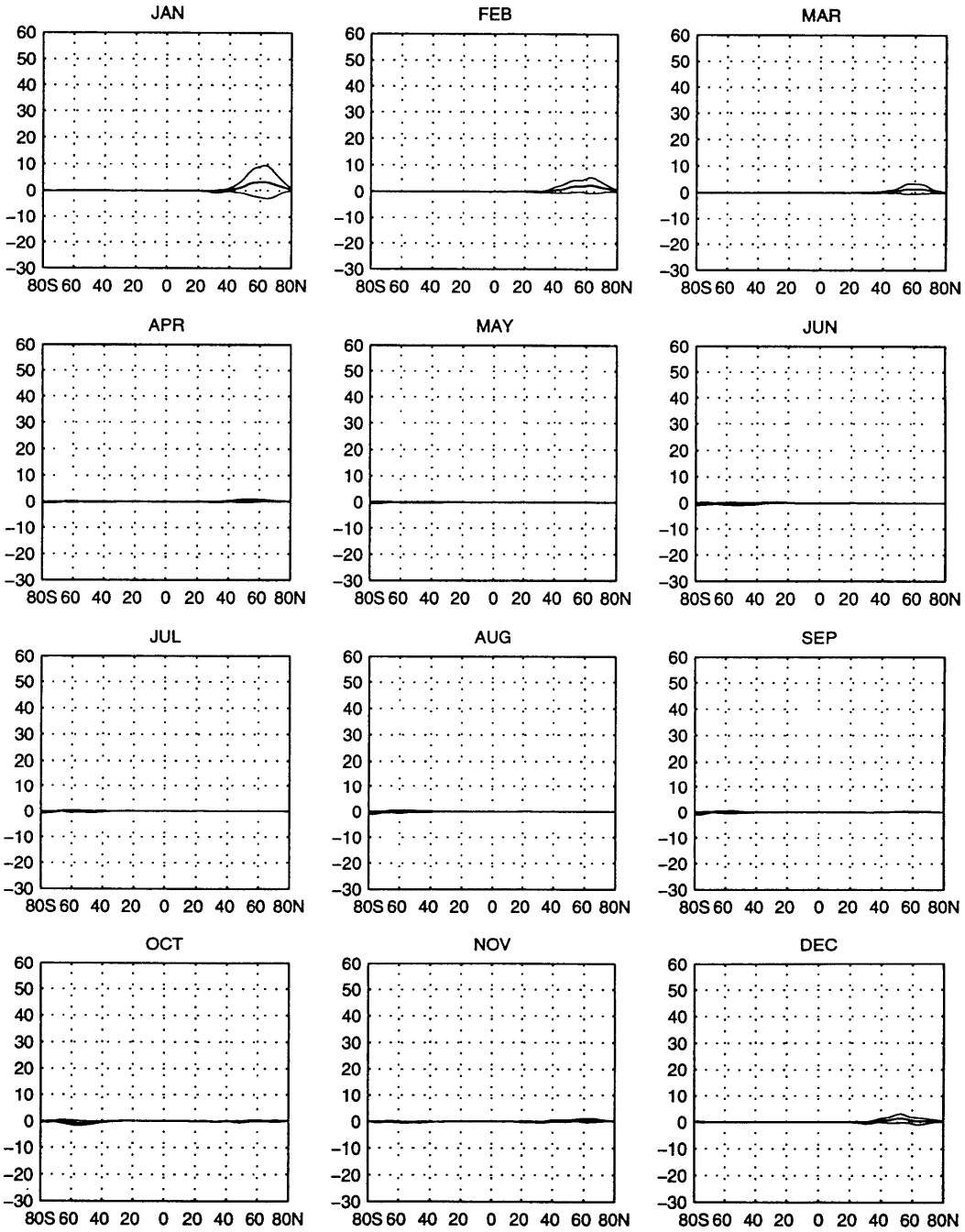

Figure B.12: The quasi-stationary northward transport of westerly momentum by wavenumber 1 at 200 hPa in $m^2\ s^{-2}$. Heavy solid line is the 13 year average. Thin solid lines represent the interannual standard deviation.

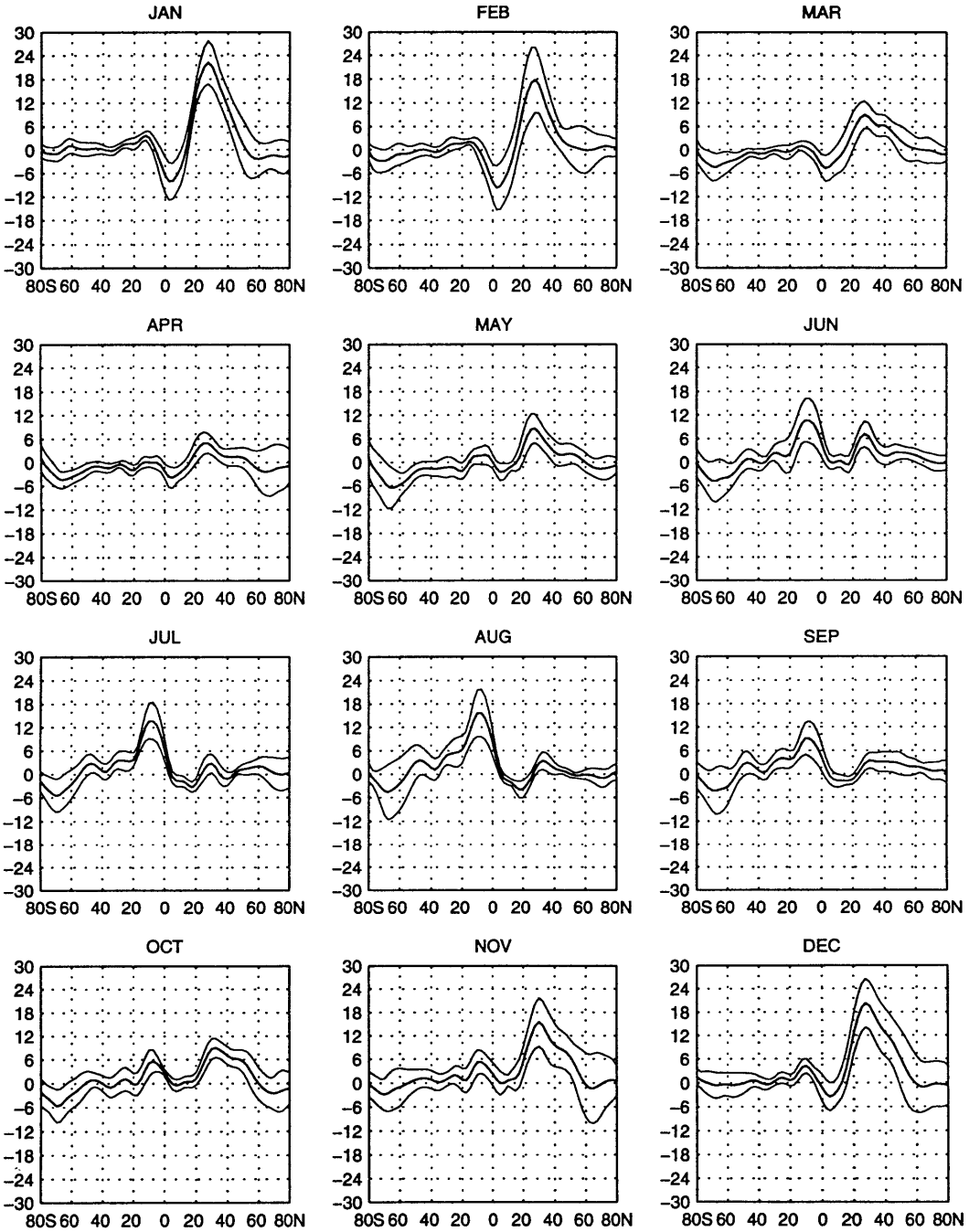

Figure B.13: As in Figure B.12 but for wavenumber 2.

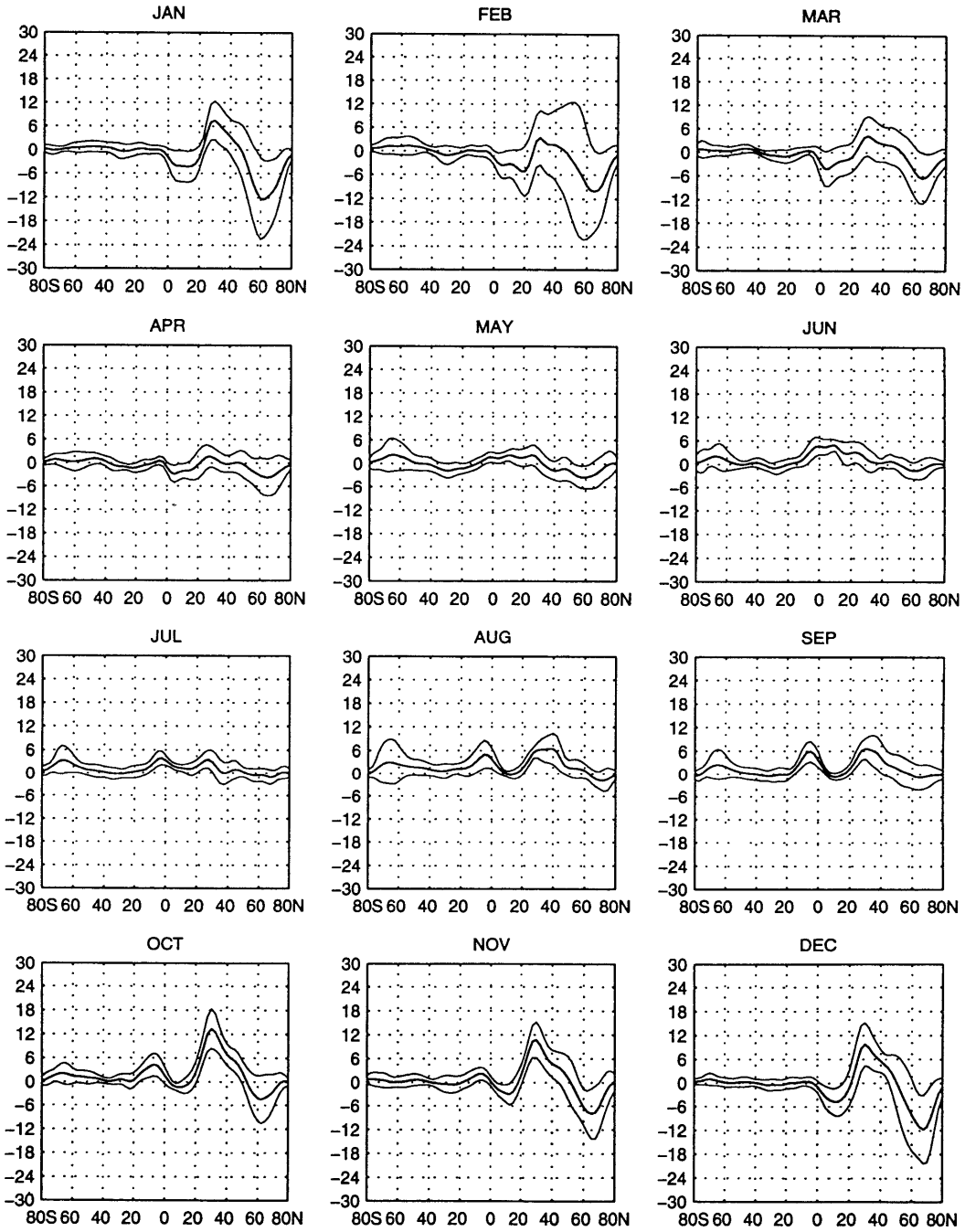

Figure B.14: As in Figure B.12 but for wavenumber 3.

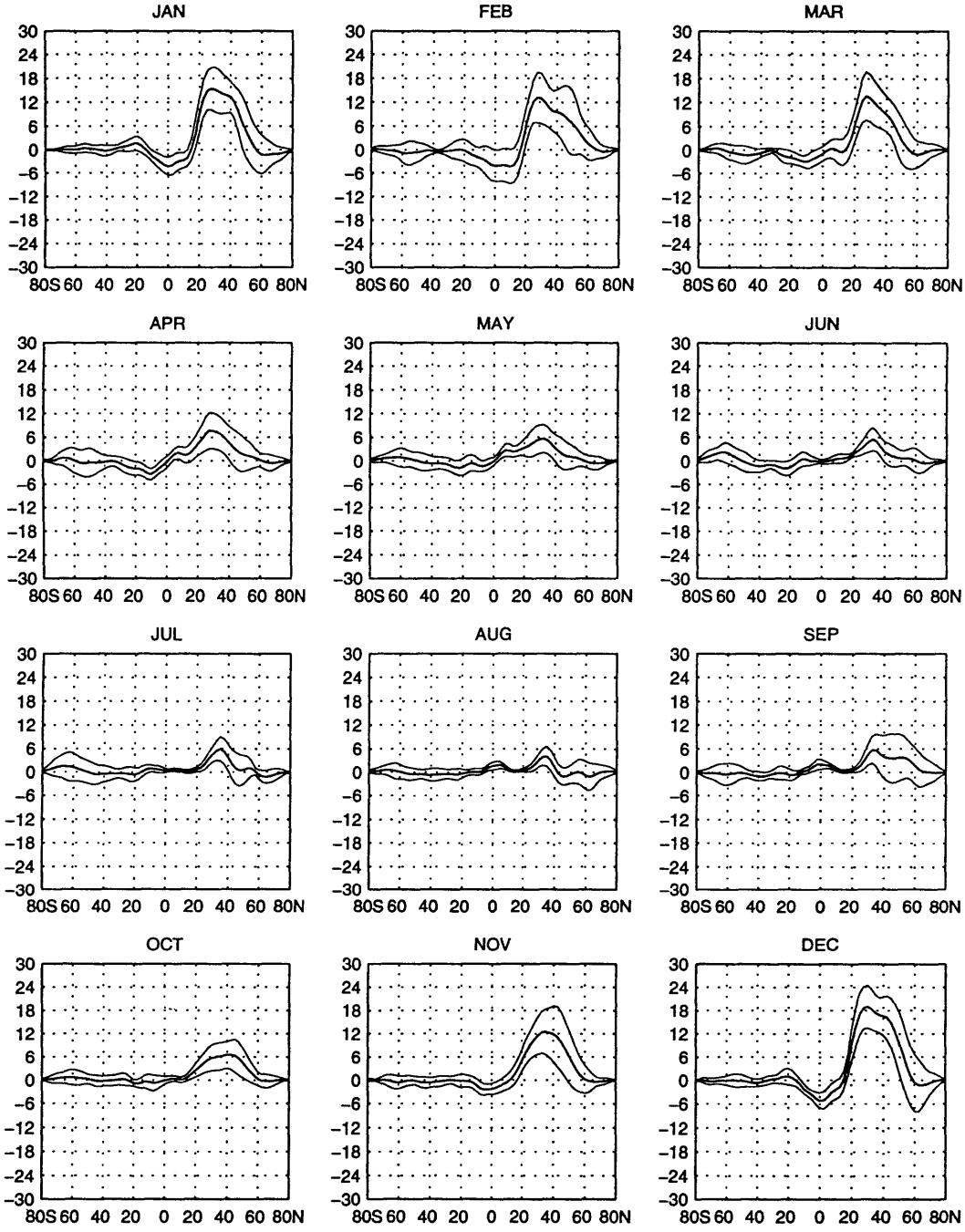

Figure B.15: As in Figure B.12 but for wavenumber 4.

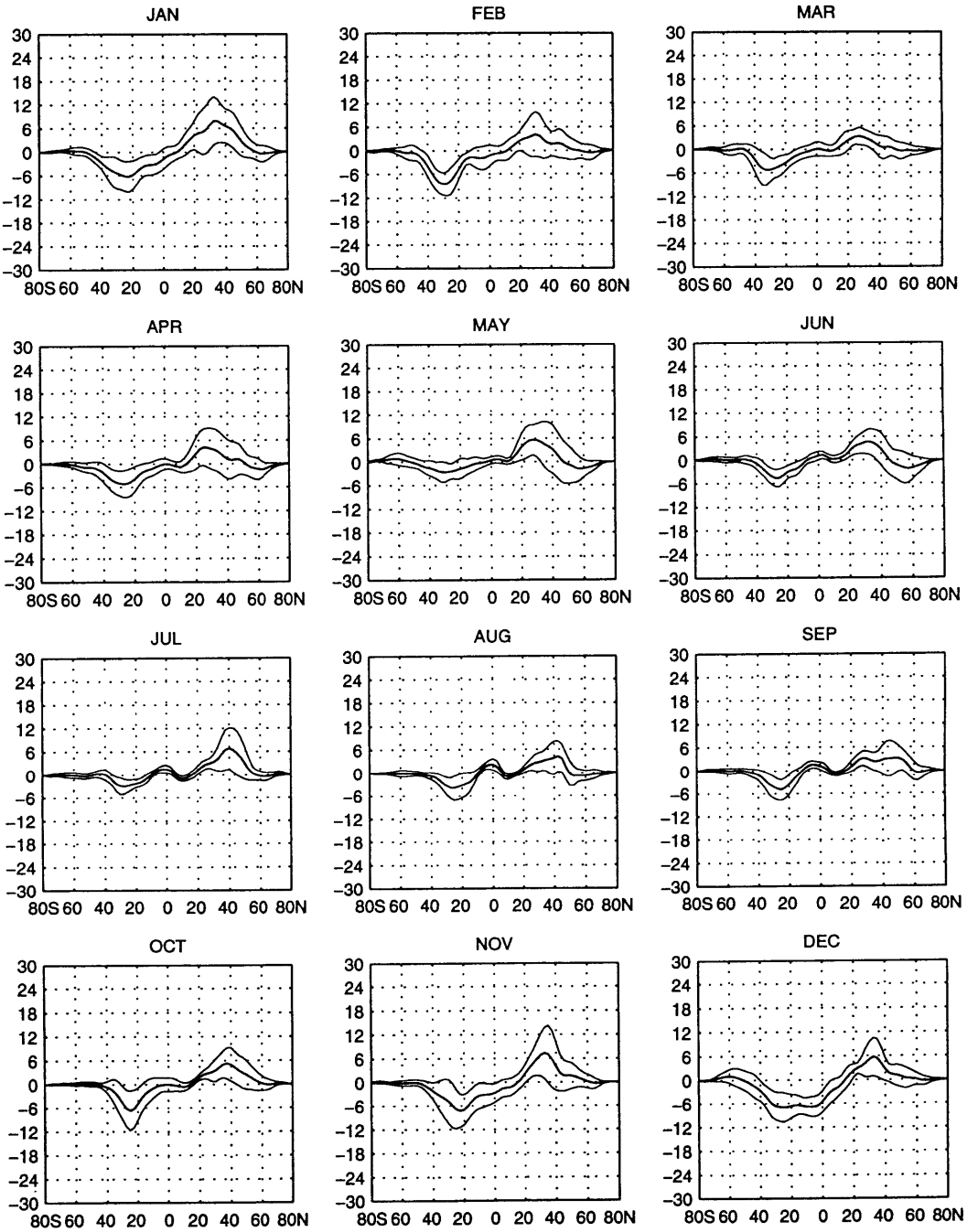

Figure B.16: As in Figure B.12 but at 10 hPa.

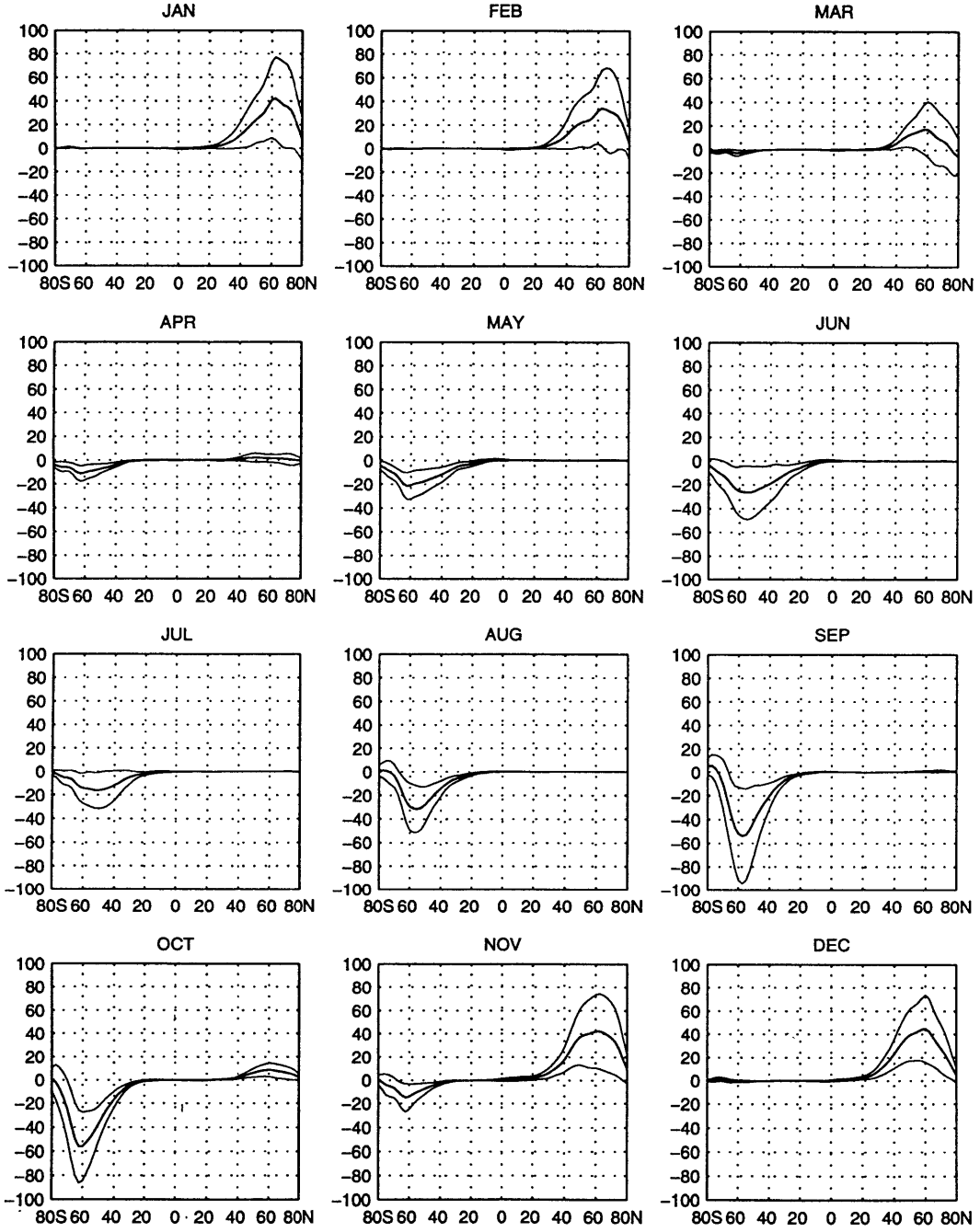

Figure B.17: As in Figure B.16 but for wavenumber 2.

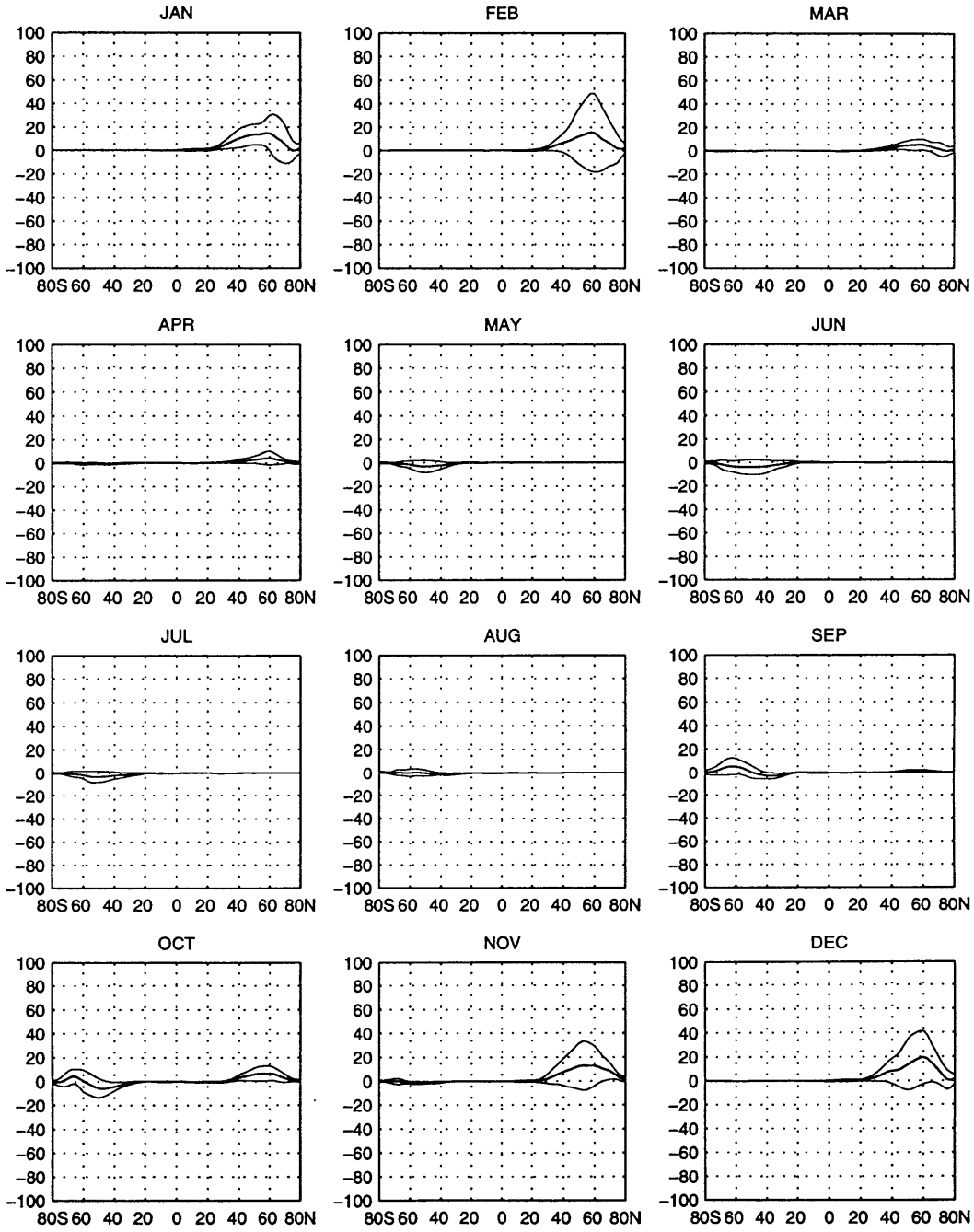

Figure B.18: As in Figure B.16 but for wavenumber 3.

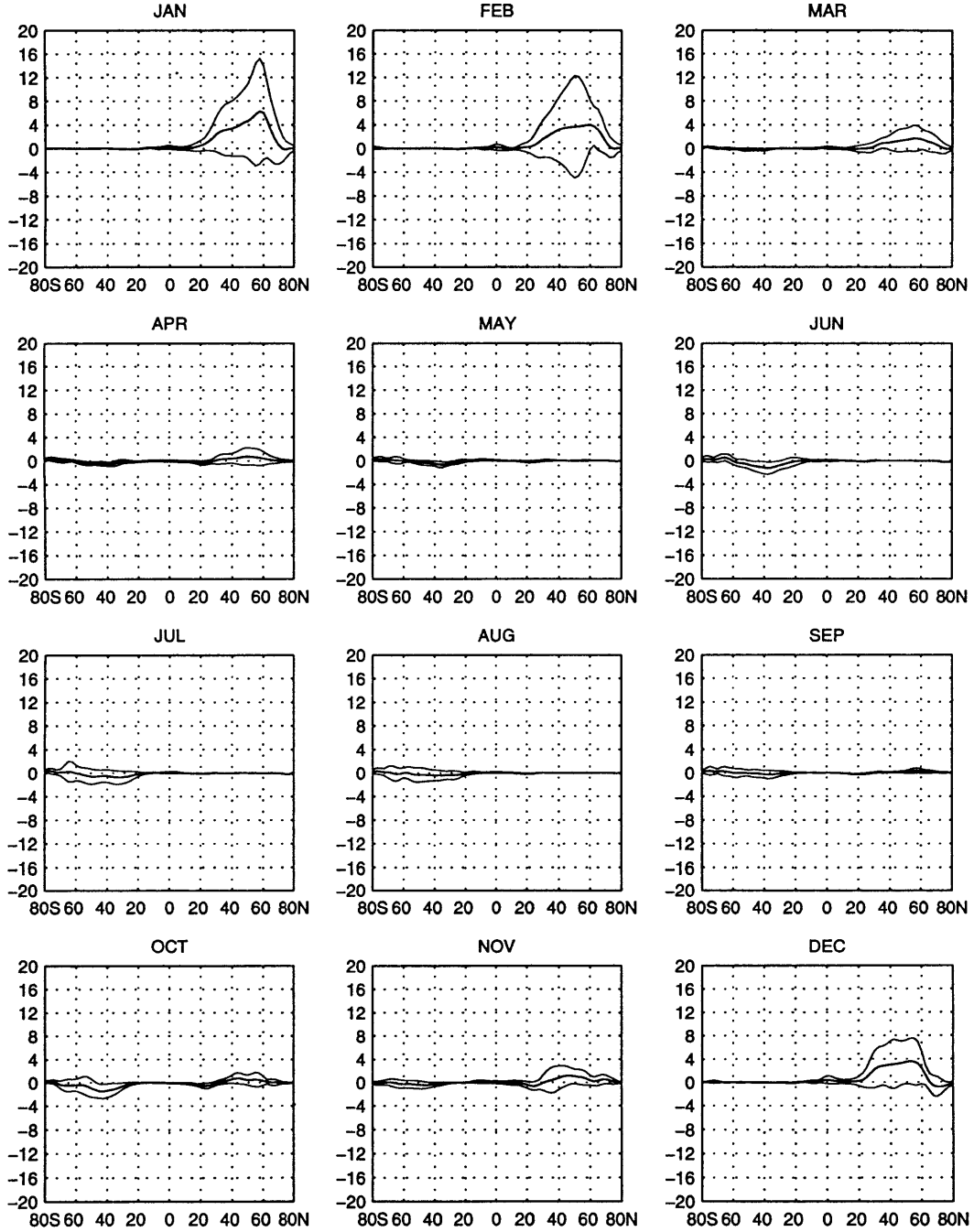

Figure B.19: The quasi-stationary northward transport of moisture by wavenumber 1 at 925 hPa in m s^{-1} g kg^{-1}. Heavy solid line is the 13 year average. Thin solid lines are plus or minus a standard deviation.

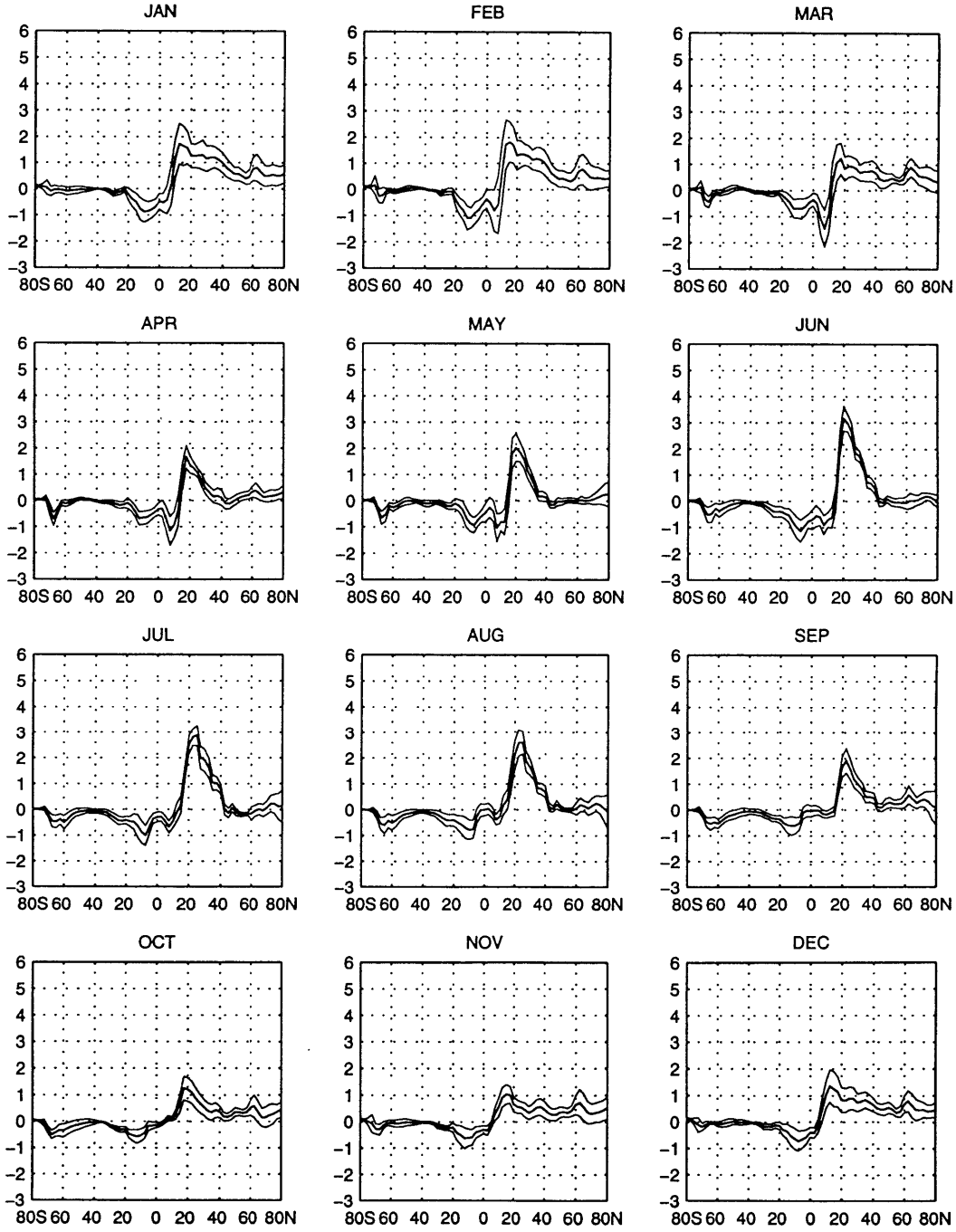

Figure B.20: As in Figure B.19 but for wavenumber 2.

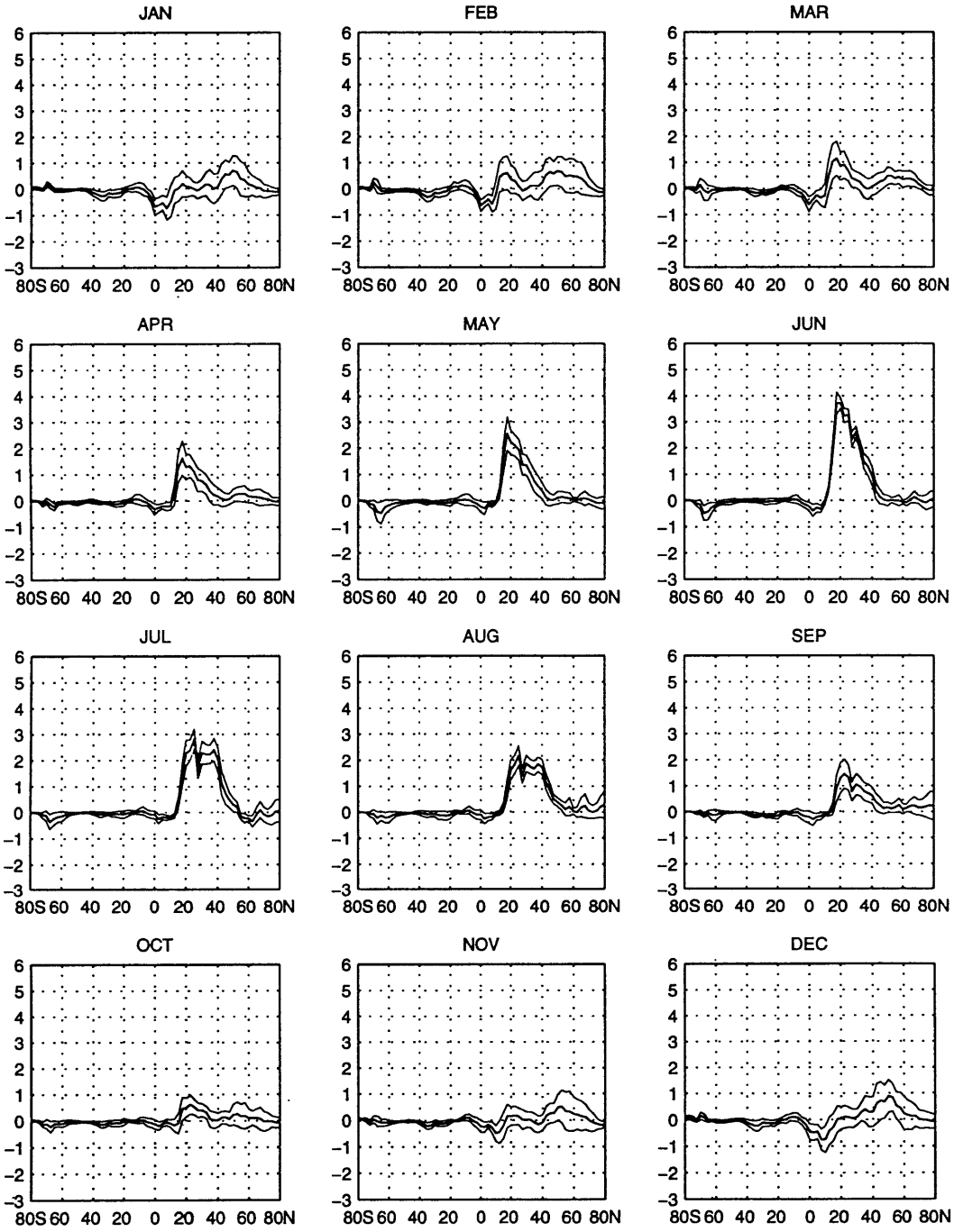

Figure B.21: As in Figure B.19 but for wavenumber 3.

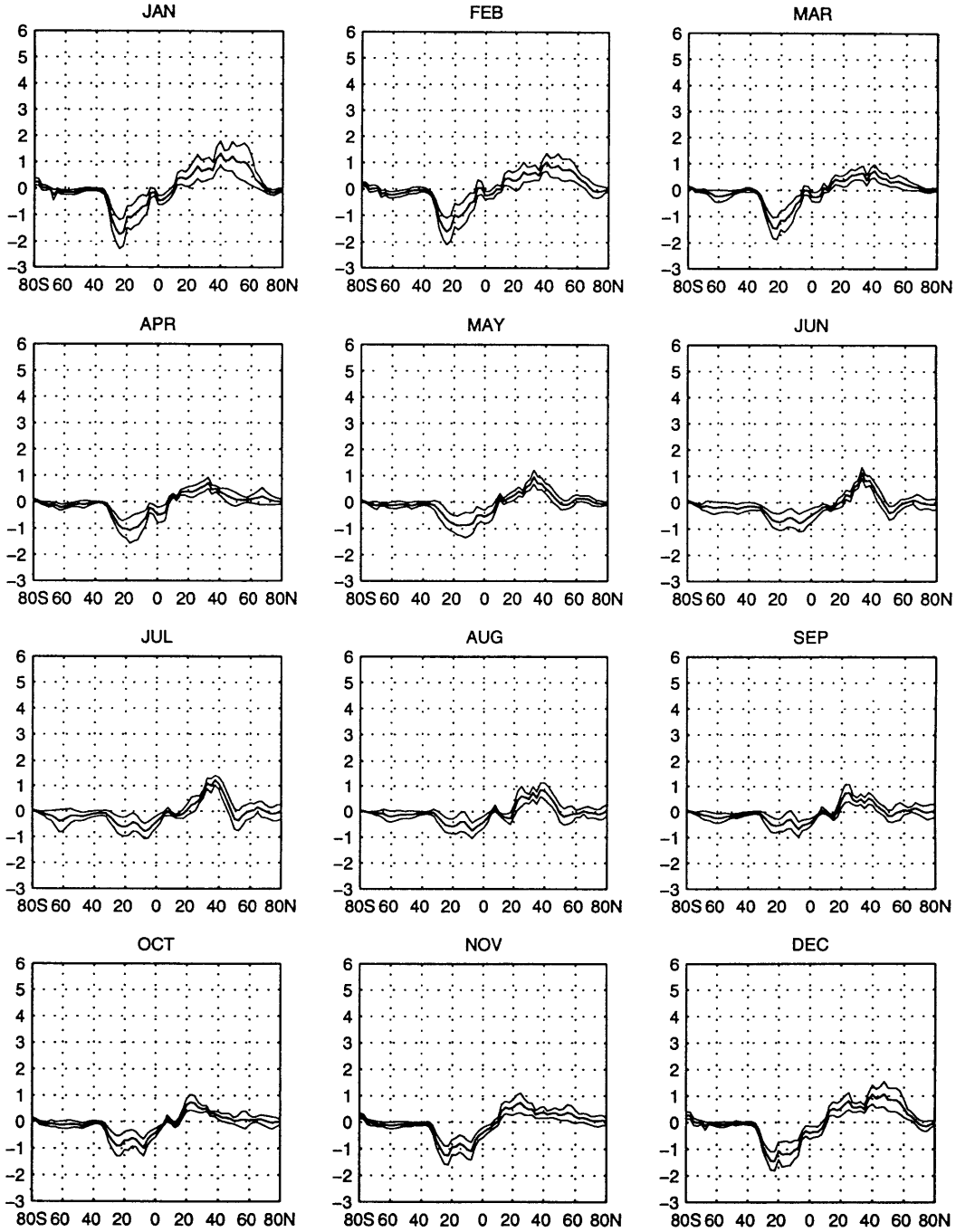

Figure B.22: As in Figure B.19 but for the sum of wavenumbers 4–72.

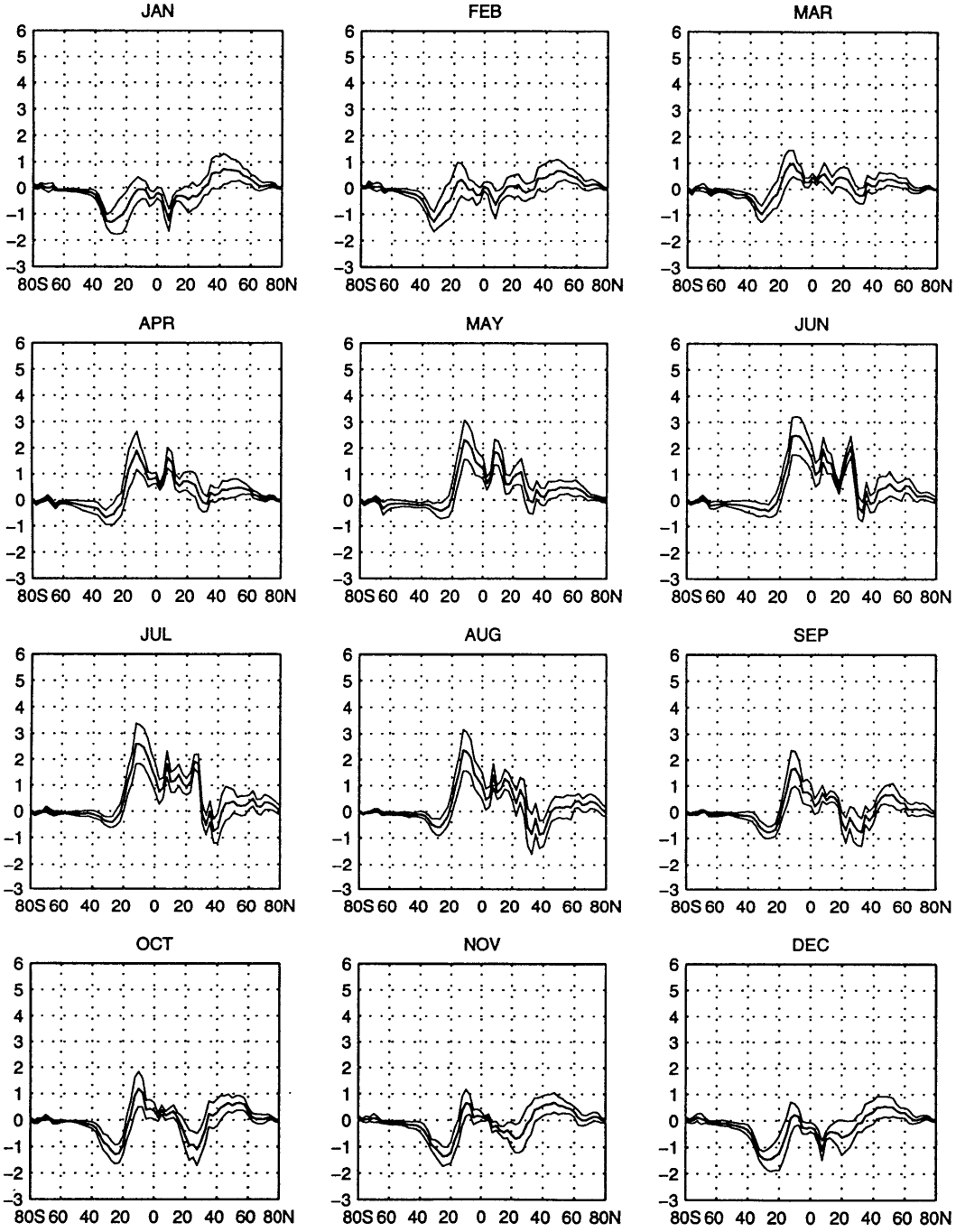

Appendix C

Influences on Eddy Propagation: Figures

The following appendix presents the figures discussed in Chapter 5.

Figure C.1: Cross-sections of the EP flux and it's divergence for January and July. Vertical axis in hPa. Contour interval is 2.0×10^{15} m^3. A horizontal arrow exactly 10° latitude in length represents a magnitude of 2.5 (0.5) $\times 10^{15}$ m^3 for January (July). The rescaling factor b is 64.7 kPa.

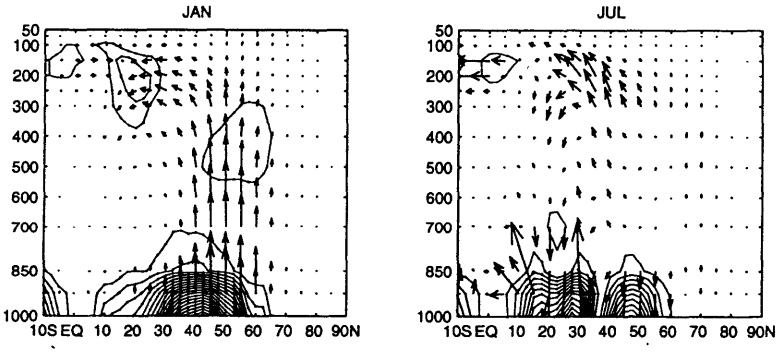

Figure C.2: Cross-sections of the EP flux and it's divergence from January to April for wavenumber 1. Vertical axis in hPa. Contour interval is 1.0×10^{15} m^3. A horizontal arrow exactly 10° latitude in length represents a magnitude of 1.0×10^{15} m^3. The rescaling factor b is 64.7 kPa.

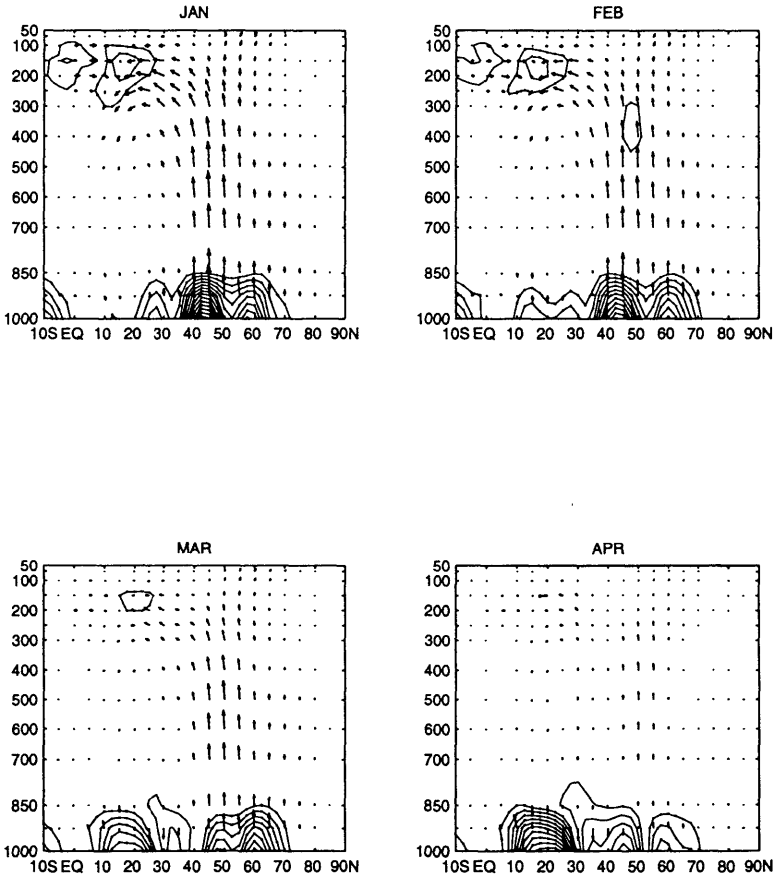

Figure C.3: As in Figure C.2 but from May to August.

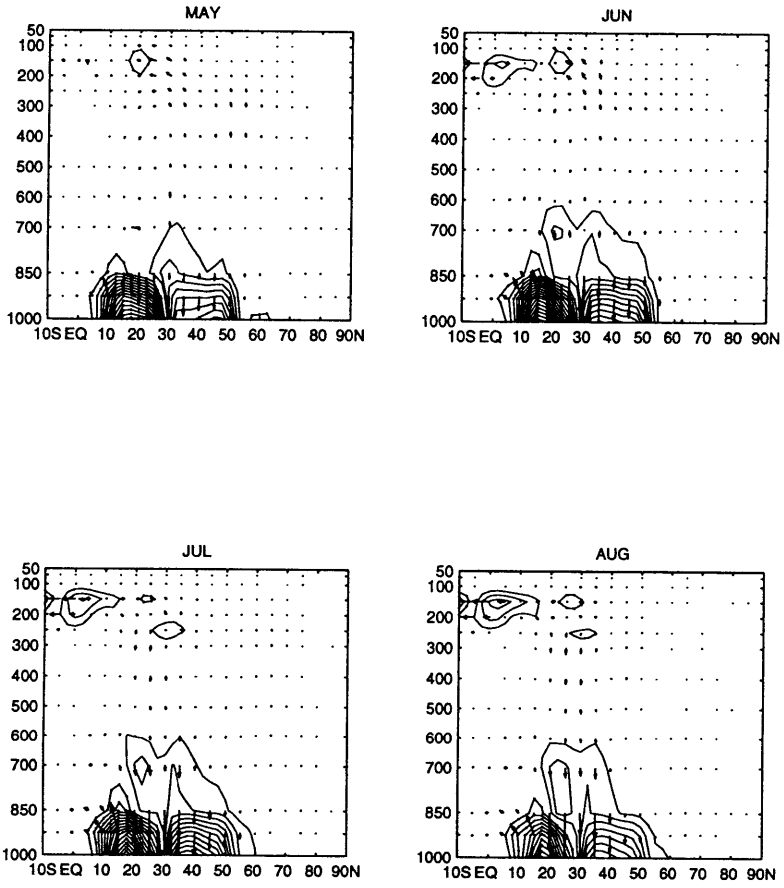

Figure C.4: As in Figure C.2 but from September to December.

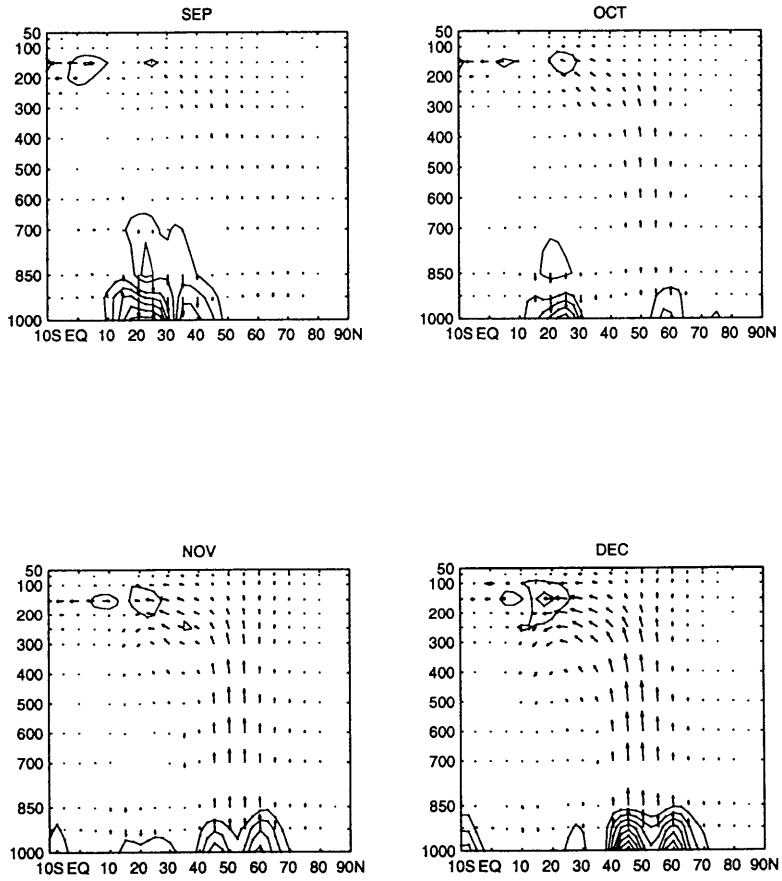

Figure C.5: As in Figure C.2 but for wavenumber 2.

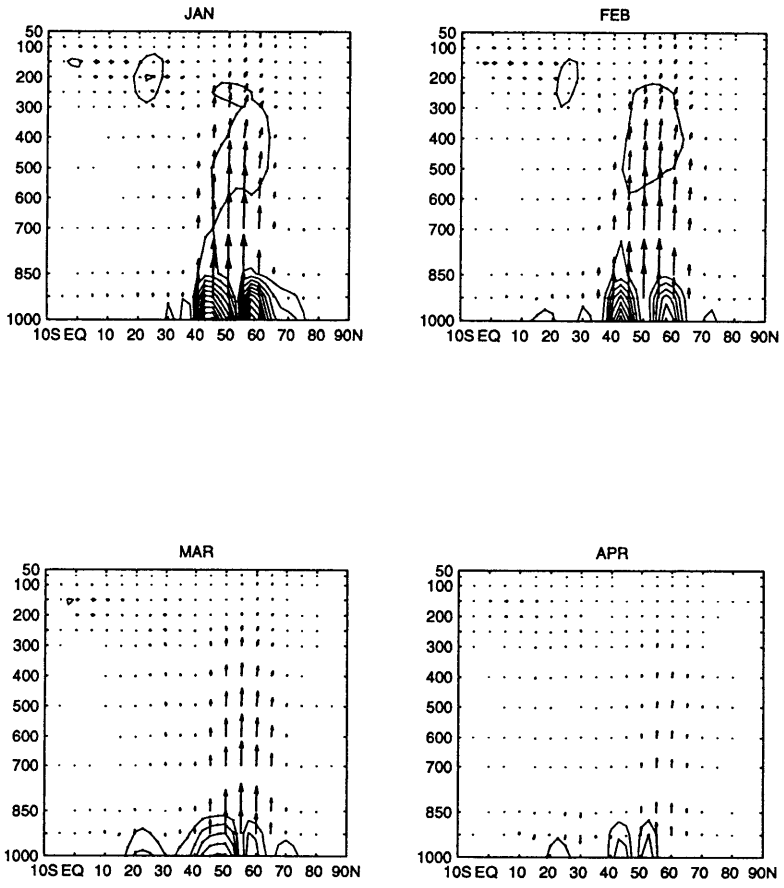

Figure C.6: As in Figure C.5 but from May to August.

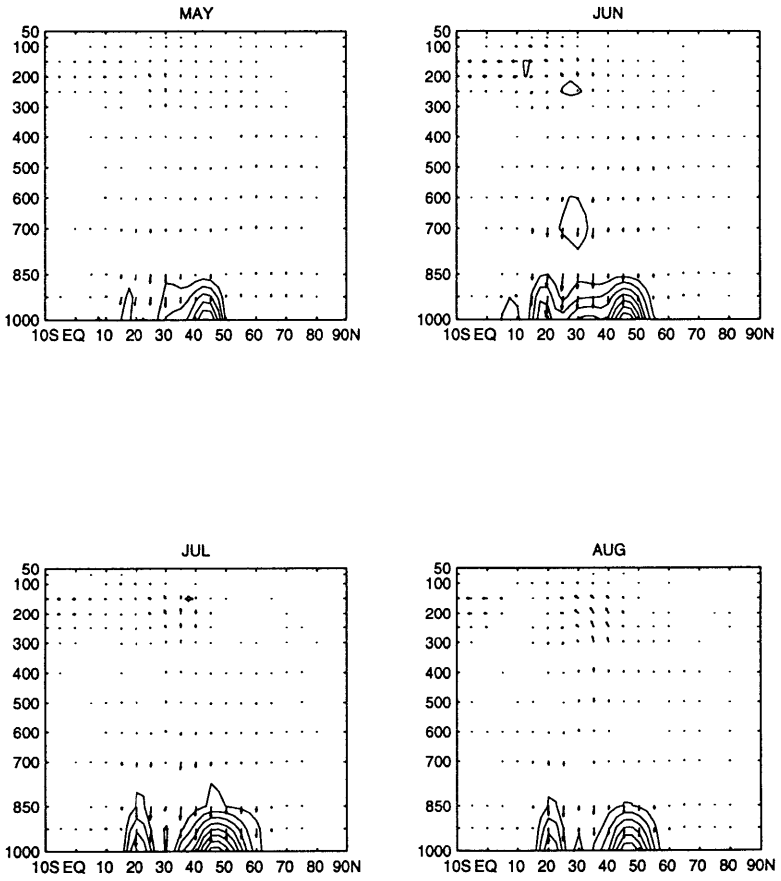

Figure C.7: As in Figure C.5 but from September to December.

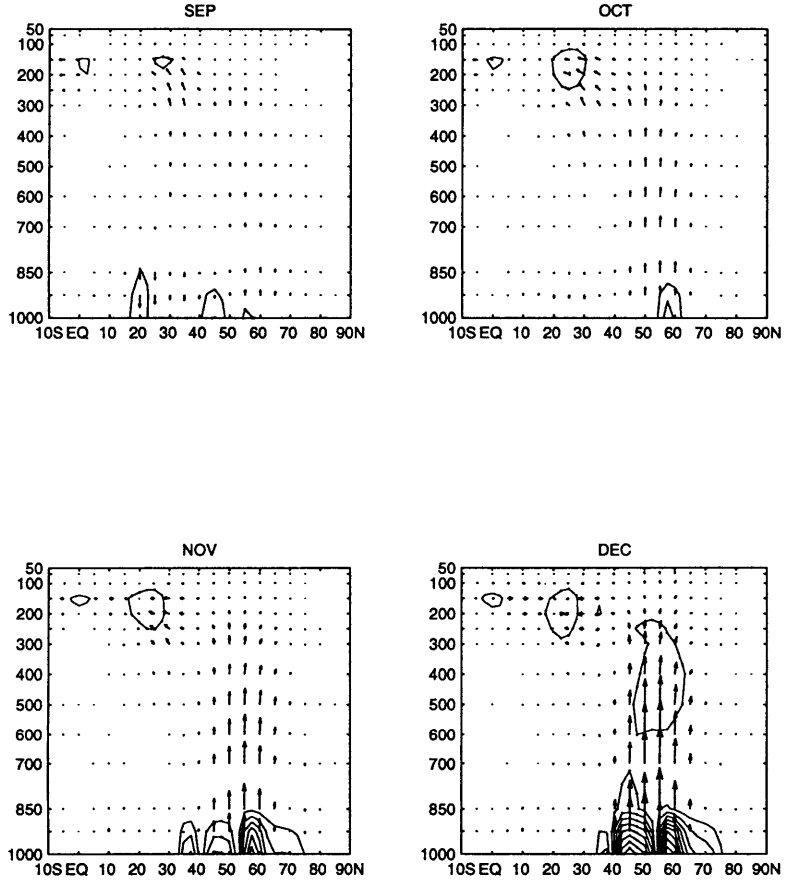

Figure C.8: As in Figure C.2 but for wavenumber 3.

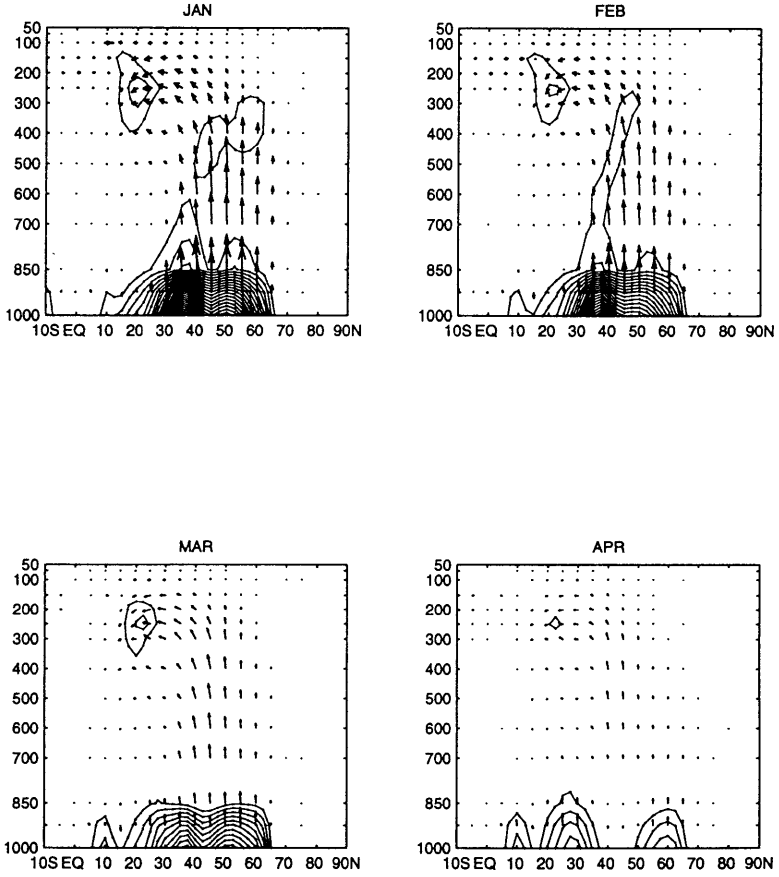

Figure C.9: As in Figure C.8 but from May to August.

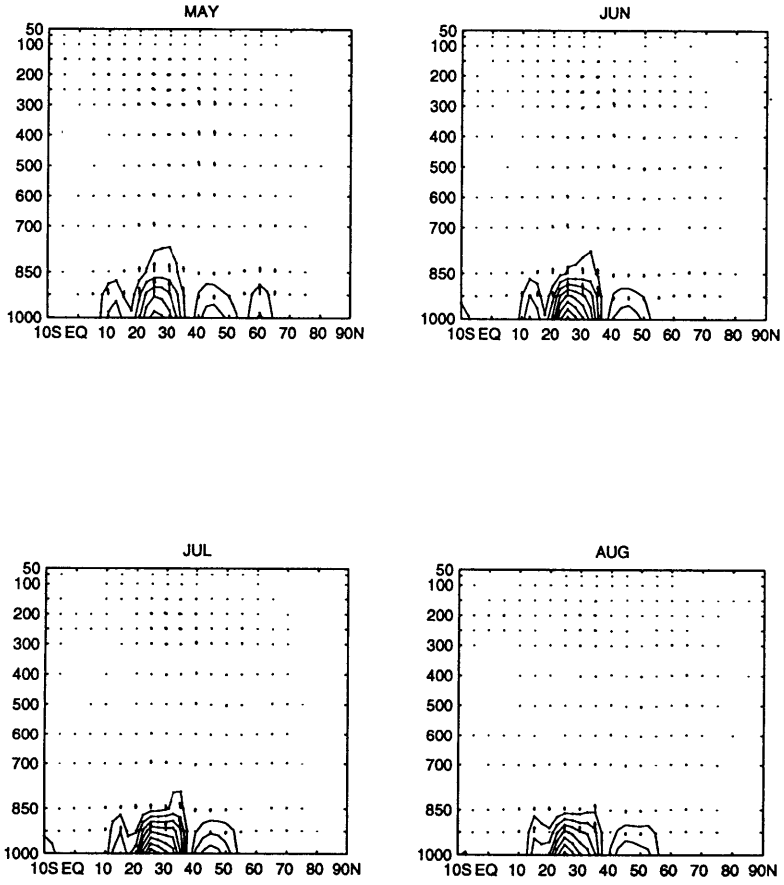

Figure C.10: As in Figure C.8 but from September to December.

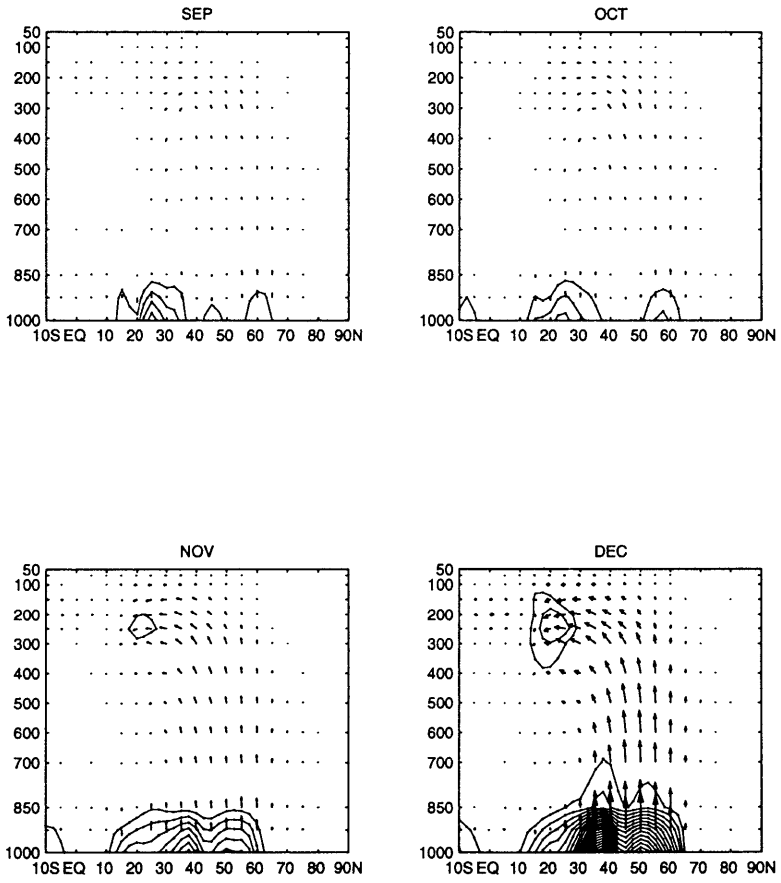

Figure C.11: EP cross-sections from 200 hPa to 5 hPa for wavenumbers 1 (top) and 2 (bottom). Contour interval is 1.0×10^{15} m^3. A horizontal arrow exactly 10° in latitude represents a magnitude of 2.0×10^{15} m^3. The rescaling factor b is 13.3 kPa.

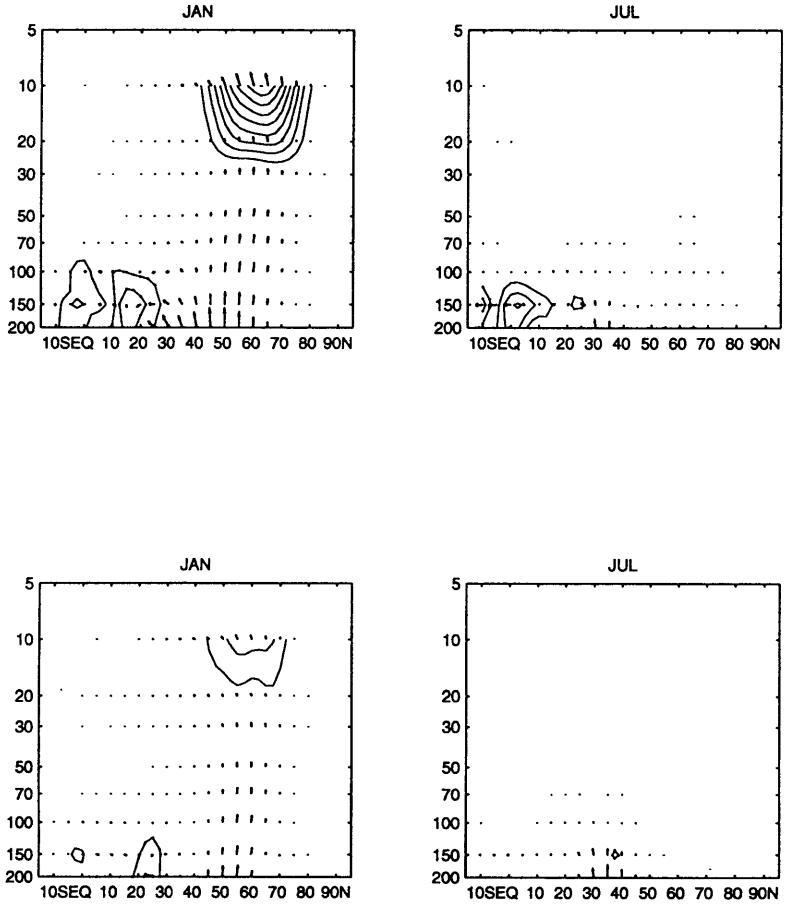

Figure C.12: Contours of the real part of $\tilde{Q}_k$ for wavenumbers 1, 2, and 3 during northern winter and for wavenumber 1 in summer. Contour interval is 10.

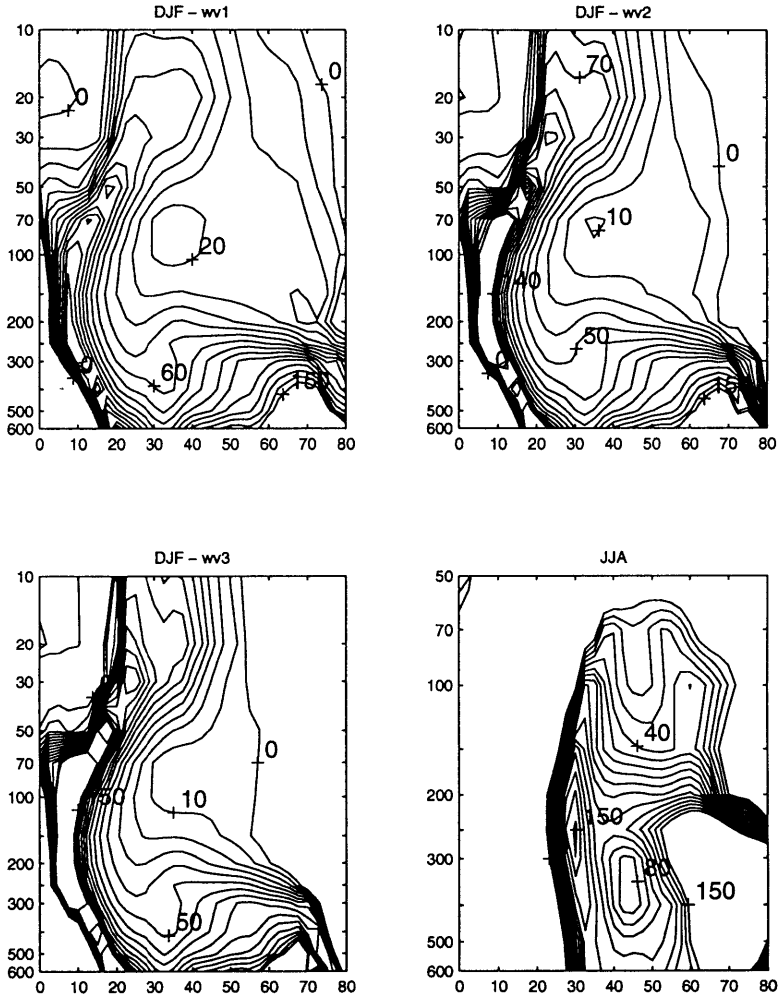

Figure C.13: EP cross-sections for wavenumber 1 in the southern hemisphere. Vertical axis in hPa. Contour interval is 1.0×10^{15} m^3. A horizontal arrow exactly 10° in latitude represents a magnitude of 0.5×10^{15} m^3. The rescaling factor b is 64.7 kPa.

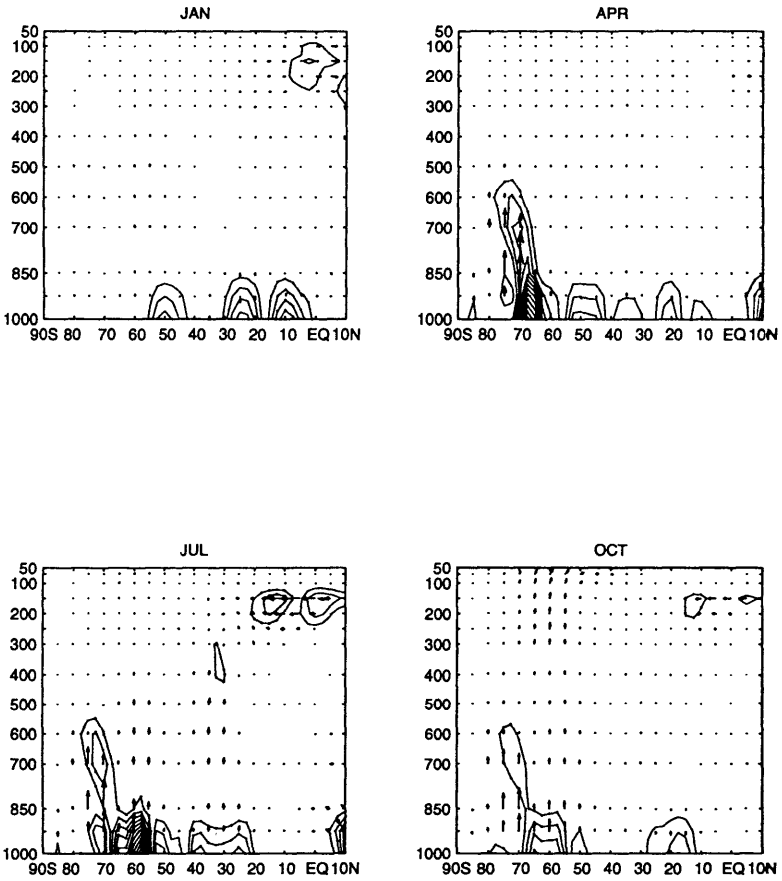

Figure C.14: As in Figure C.13 but for wavenumber 2.

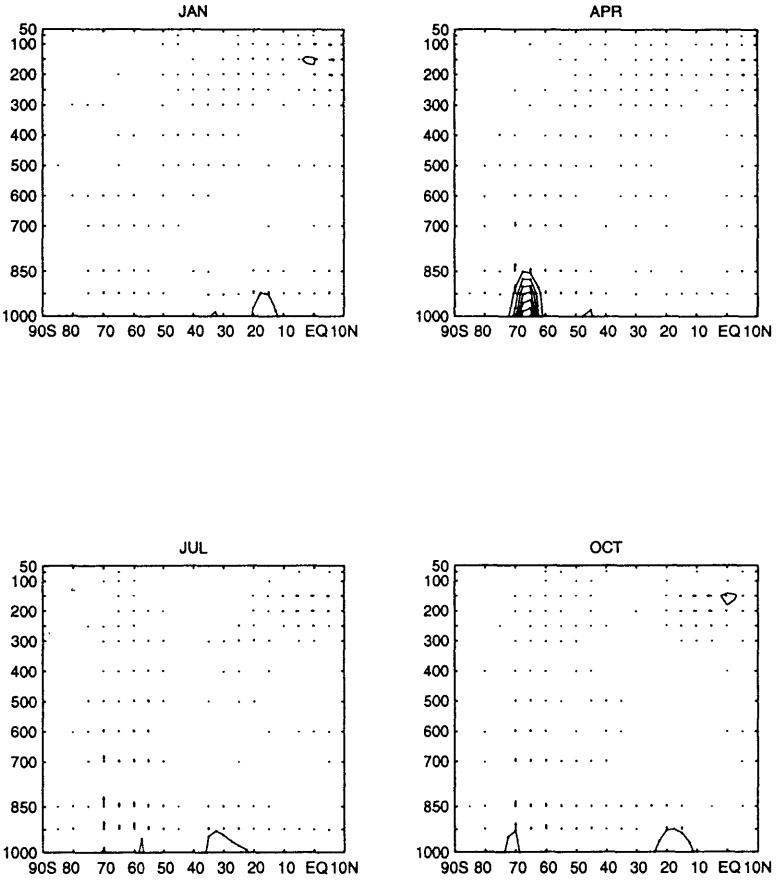

Figure C.15: EP cross-sections for wavenumbers 1 (left) and 2 (right) for the southern stratosphere. Contour interval is 1.0×10^{15} m^3. A horizontal arrow exactly 10° in latitude represents a magnitude of 2.0×10^{15} m^3. The rescaling factor b is 13.3 kPa.

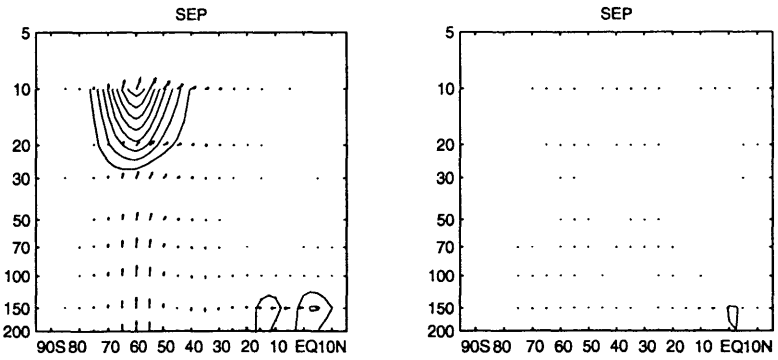

Figure C.16: Contour plots of the real part of $\tilde{Q}_k$ for the southern hemisphere. Contour interval is 10. Vertical axis in hPa.

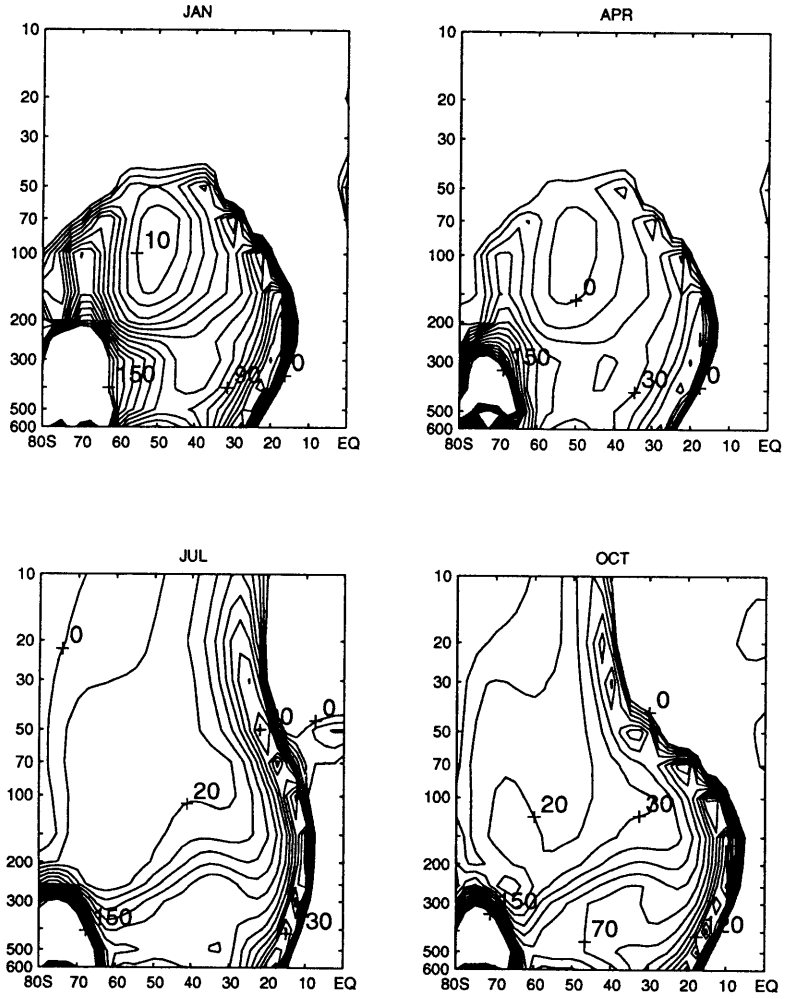

References

Branstator, G., 1995: Organization of storm track anomalies by recurring low-frequency circulation anomalies. *J. Atmos. Sci.* **52**, 207–226.

Butchart, N., S. A. Clough, T. N. Palmer, and P. J. Trevelyan, 1982: Simulations of an observed stratospheric warming with quasi-geostrophic refractive index as a model diagnostic. *Q. J. R. Meteor. Soc.* **108**, 475–502.

Charney, J. G. and A. Eliassen, 1949: A numerical method for predicting the perturbations of the middle latitude westerlies. *Tellus* **1**, 38–54.

Charney, J. G. and P. G. Drazin, 1961: Propagation of planetary-scale disturbances from the lower into the upper atmosphere. *J. Geophys. Res.* **66**, 83–109.

Chen, T.-C. and M.-Y. Yen, 1993: The effect of planetary-scale divergent circulation on the interannual variation of the summertime stationary eddies: the tropical easterly jet. *Tellus* **45A**, 15–27.

DaCamara, C. C., E. C. Kung, W. E. Baker, B.-C. Lee, and J. A. M. Corte-Real, 1991: Long-term analysis of planetary wave activities and blocking circulation in the northern hemisphere winter. *Contrib. Atmos. Phys.* **64**, 285–298.

Edmon, H. J., Jr., B. J. Hoskins, and M. E. McIntyre, 1980: Eliassen–Palm cross sections for the troposphere. *J. Atmos. Sci.* **37**, 2600–2616.

Findlater, J., 1969: A major low-level air current near the Indian Ocean during the northern summer. *Q. J. R. Meteor. Soc.* **95**, 362–380.

Fraedrich, K. and H. Böttger, 1978: Wavenumber–frequency analysis of the 500 mb geopotential at 50°N. *J. Atmos. Sci.* **35**, 745–750.

Geller, M. A., M.-F. Wu, and M. E. Gelman, 1983: Troposphere-Stratosphere (surface–55 km) monthly winter general circulation statistics for the northern hemisphere—four year averages. *J. Atmos. Sci.* **40**, 1334–1352.

Geller, M. A., M.-F. Wu, and M. E. Gelman, 1984: Troposphere-Stratosphere (surface–55 km) monthly winter general circulation statistics for the northern hemisphere—interannual variations. *J. Atmos. Sci.* **41**, 1726–1744.

Gleckler, P. J., D. A. Randall, G. Boer, R. Colman, M. Dix, V. Galin, M. Helfland, J. Kiehl, A. Kitoh, W. Lau, X.-Y. Liang, V. Lykossov, B. McAvaney, K. Miyakoda, S. Planton, and W. Stern, 1995: Cloud-radiative effects on implied oceanic energy transports as simulated by atmospheric general circulation models. *Geophys. Res. Lett.* **22**, 791–794.

Hantel, M., 1976: On the vertical eddy transports in the northern atmosphere, Pt. 1, Vertical eddy heat transport for summer and winter. *J. Geophys. Res.* **81**, 1577–1588.

Hastenrath, S., 1985: *Climate and Circulation of the Tropics.* D. Reidel Publishing Company, Dordrecht, Holland. 455 pp.

Hayashi, Y., 1982: Space-time spectral analysis and its application to atmospheric waves. *J. Met. Soc. Japan* **60**, 156–171.

Held, I., 1983: "Stationary and quasi-stationary eddies in the extratropical troposphere: Theory." In: *Large-scale dynamical processes in the atmosphere.* Eds., Hoskins, Brian J.;Pearce, Robert F., Academic Press, 1983, pp. 127–168.

Holopainen, E. O., 1970: An observational study of the energy balance of the stationary disturbances in the atmosphere. *Q. J. R. Meteor. Soc.* **96**, 626–644.

Holton, J. R., 1976: A semi-spectral numerical model for wave-mean flow interactions in the stratosphere: application to sudden stratospheric warmings. *J. Atmos. Sci.* **33**, 1639–1649.

Kalnay, E., M. Kanamitsu, R. Kistler, W. Collins, D. Deaven, L. Gandin, M. Iredell, S. Saha, G. White, J. Woollen, Y. Zhu, M. Chelliah, W. Ebisuzaki, W. Higgins, J. Janowiak, K. C. Mo, C. Ropelewski, J. Wang, A. Leetmaa, R. Reynolds, R. Jenne, and D. Joseph, 1996: The NCEP/NCAR 40-year reanalysis project. *Bull. Amer. Met. Soc.* **77**, 437–471.

Kanamitsu, M., R. E. Kistler, and R. W. Reynolds, 1997: NCEP/NCAR reanalysis and the use of satellite data. *Adv. Space Res.* **19**, 481–489.

Kao, S. K. and J. F. Sagendorf, 1970: The large–scale meridional transport of sensible heat in wavenumber frequency space. *Tellus* **22**, 172–185.

Karoly, D. J. and B. J. Hoskins, 1982: Three-dimensional propagation of planetary waves. *J. Met. Soc. Japan* **60**, 109–123.

Lau, N.-C., 1979: The observed structure of tropospheric stationary waves and the local balances of vorticity and heat. *J. Atmos. Sci.* **36**, 996–1016.

Matsuno, T., 1970: Vertical propagation of stationary planetary waves in the winter northern hemisphere. *J. Atmos. Sci.* **27**, 871–883.

Mechoso, C. R., D. L. Hartmann, and J. D. Farrara, 1985: Climatology and interannual variability of wave, mean-flow interaction in the southern hemisphere. *J. Atmos. Sci.* **42**, 2189–2206.

Mo, K. C. and R. W. Higgins, 1996: Large-scale atmospheric moisture transport as evaluated in the NCEP/NCAR and the NASA/DAO reanalyses. *J. Clim.* **9**, 1531–1544.

Mo, K. C., X. L. Wang, R. Kistler, M. Kanamitsu, and E. Kalnay, 1995: Impact of satellite data on the CDAS-Reanalysis system. *Mon. Weather Rev.* **123**, 124–139.

Newell, R. E., J. W. Kidson, D. G. Vincent, and G. J. Boer, 1972: *The General Circulation of the Tropical Atmosphere and Interactions with Extratropical Latitudes, Vol. 1.* MIT Press, Cambridge, MA. 258 pp.

Newell, R. E., J. W. Kidson, D. G. Vincent, and G. J. Boer, 1974: *The General Circulation of the Tropical Atmosphere and Interactions with Extratropical Latitudes, Vol. 2.* MIT Press, Cambridge, MA. 371 pp.

Oort, A. H., 1977: *Interannual Variability of Atmospheric Circulation Statistics.* NOAA Professional Paper 8, U. S. Government Printing Office, Washington, D. C., 76 pp.

Oort, A. H., 1983: *Global Atmospheric Circulation Statistics 1958–1973.* NOAA Professional Paper 14, U. S. Government Printing Office, Washington, D. C., 180 pp.

Oort, A. H. and J. P. Peixoto, 1974: The annual cycle of the energetics of the atmosphere on a planetary scale. *J. Geophys. Res.* **79**, 2705–2719.

Oort, A. H. and J. P. Peixoto, 1983: "Global angular momentum and energy balance requirements from observations." In: *Advances in Geophysics*, Vol. 25, Academic Press, New York, 1983, p.355–490.

Oort, A. H. and E. M. Rasmusson, 1971: *Atmospheric Circulation Statistics.* NOAA Professional Paper 5, U. S. Government Printing Office, Washington, D. C., 323 pp.

Paegle, J., 1989: Variable resolution global model based upon Fourier and finite-element representation. *Mon. Weather Rev.* **117**, 583–606.

Peixoto, J. P. and A. H. Oort, 1974: The annual distribution of atmospheric energy on a planetary scale. *J. Geophys. Res.* **79**, 2149–2159.

Peixoto, J. P. and A. H. Oort, 1992: *The Physics of Climate.* American Institute of Physics, New York, 520 pp.

Plumb, R. A., 1985: On the three-dimensional propagation of stationary waves. *J. Atmos. Sci.* **42**, 217–229.

Plumb, R. A., 1989: On the seasonal cycle of stratospheric planetary waves. *PAGEOPH* **130**, 233–242.

Pratt, R. W., 1979: A space–time spectral comparison of the NCAR and GFDL general circulation models to the atmosphere. *J. Atmos. Sci.* **36**, 1681–1691.

Quintanar, A. I. and C. R. Mechoso, 1995: Quasi-stationary waves in the southern hemisphere, Pt 1, Observational data. *J. Clim.* **8**, 2659–2672.

Randel, W. J. and I. M. Held, 1991: Phase speed spectra of transient eddy fluxes and critical layer absorption. *J. Atmos. Sci.* **48**, 688–697.

Rosen, R. D., D. A. Salstein, T. M. Eubanks, J. O. Dickey, and J. A. Steppe, 1984: An El Niño signal in atmospheric angular momentum and earth rotation. *Science* **225**, 411–414.

Rosen, R. D., D. A. Salstein, J. P. Peixoto, A. H. Oort, and N.-C. Lau, 1985: Circulation statistics derived from level III-b and station-based analyses during FGGE. *Mon. Weather Rev.* **113**, 65–88.

Smagorinsky, J., 1953: The dynamical influence of large-scale heat sources and sinks on the quasi-stationary mean motions of the atmosphere. *Q. J. R. Meteor. Soc.* **79**, 342–366.

Speth, P. and G. Frenzen, 1982: Variability in time of horizontal transports of heat and momentum by stationary eddies. *Contrib. Atmos. Phys.* **55**, 142–157.

Speth, P. and E. Kirk, 1981: One–year study of power spectra in wavenumber–frequency domain. *Contrib. Atmos. Phys.* **54**, 186–206.

Speth, P. and A. Osthaus, 1980: Global energy budget of the atmosphere, Pt. 3, Horizontal transports of sensible heat and momentum of stationary eddies and connected energy conversions throughout a 10–yr period (1967-1976). *Contrib. Atmos. Phys.* **53**, 389–413.

Starr, V. P., J. P. Peixoto, and N. E. Gaut, 1970: Momentum and zonal kinetic energy balance of the atmosphere from five years of hemispheric data. *Tellus* **22**, 251–274.

Trenberth, K. E., 1992: *Global analyses from ECMWF and atlas of 1000 to 10 mb circulation statistics.* NCAR Tech. Note NCAR/TN-373+STR, National Center for Atmospheric Research, Boulder, Colorado, 191 pp.

Trenberth, K. E. and A. Solomon, 1994: The global heat balance: heat transports in the atmosphere and ocean. *Clim. Dynam.* **10**, 107–134.

van Loon, H., 1979: Association between latitudinal temperature gradient and eddy transport, Pt. 1, Transport of sensible heat in winter. *Mon. Weather Rev.* **107**, 525–534.

van Loon, H. and J. Williams, 1980: Association between latitudinal temperature gradient and eddy transport, Pt. 2, Relationships between sensible heat transport by stationary waves and wind, pressure, and temperature in winter. *Mon. Weather Rev.* **108**, 604–614.

Whitaker, J. S. and R. M. Dole, 1995: Organization of storm tracks in zonally varying flows. *J. Atmos. Sci.* **52**, 1178–1191.

Yang, S. and W. J. Gutowski, 1994: GCM simulations of the three-dimensional propagation of stationary waves. *J. Clim.* **7**, 414–433.